CHALMERS
UNIVERSITY OF TECHNOLOGY

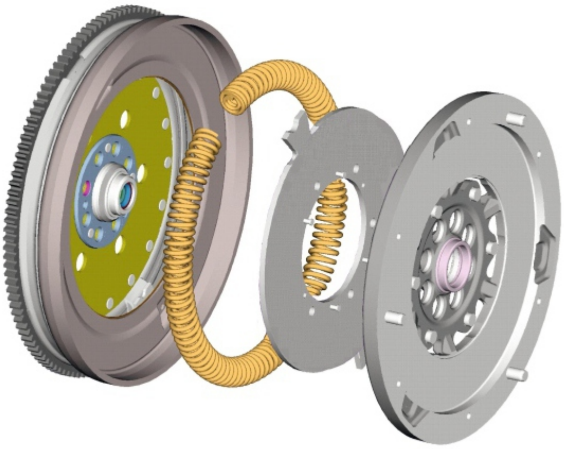

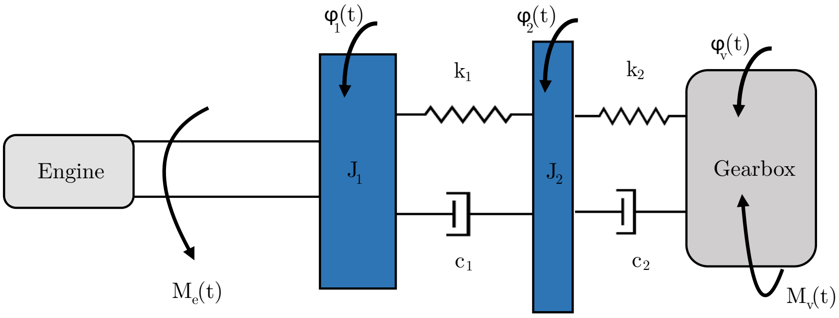
$\varphi_1(t)$
$\varphi_2(t)$
$\varphi_v(t)$
k_1
k_2
Engine
J_1
J_2
Gearbox
c_1
c_2
$M_e(t)$
$M_v(t)$

Dual Mass Flywheel for Torsional Vibrations Damping

Parametric study for application in heavy vehicle

GÉRÉMY BOURGOIS

Department of Applied Mechanics
CHALMERS UNIVERSITY OF TECHNOLOGY
Gothenburg, Sweden 2016

MASTER'S THESIS 2016:22

Dual Mass Flywheel for Torsional Vibrations Damping

Parametric study for application in heavy vehicle

GÉRÉMY BOURGOIS

CHALMERS
UNIVERSITY OF TECHNOLOGY

Department of Applied Mechanics
CHALMERS UNIVERSITY OF TECHNOLOGY
Gothenburg, Sweden 2016

Dual Mass Flywheel for Torsional Vibrations Damping

© GÉRÉMY BOURGOIS, 2016.

Supervisor: Viktor Berbyuk, Håkan Johansson, Lina Wramner
Examiner: Viktor Berbyuk

Master's Thesis 2016:22
Chalmers University of Technology
SE-412 96 Gothenburg
Telephone +46 31 772 1000

Cover: Dual Mass Flywheel [1], Volvo Truck [2], Engineering model of the Dual Mass flywheel.

Gothenburg, Sweden 2016

Dual Mass Flywheel for torsional vibrations damping
Parametric study for application in heavy vehicle.
Gérémy Bourgois
Division of Dynamics, Department of Applied Mechanics
Chalmers University of Technology

Abstract

TORSIONAL vibrations are produced due to the pulsating load from the cylinders. These vibrations can cause crankshaft cracking, excessive bearing wear or failure, broken accessory drives, slapping of belts. Currently, engine designers have to downsize and downspeed the engine in order to satisfy European requirements in terms of CO_2 emissions. These two actions make torsional vibrations more significant.

Different technologies are used to reduce these vibrations, one of them is the Dual Mass Flywheel (DMF). DMF is a complex system containing rotational inertia, torsional stiffness and damping properties. A simplified mathematical model (2 degrees of freedom) has been developed in order to show the positive effect of a DMF on the powertrain. This work will focus on heavy vehicles.

Two models have been made: one into Matlab and the other one in the open-source software Easydyn. The integration in Matlab is computed by a function based on an explicit Runge-Kutta formula, whereas EasyDyn uses the Newmark method. Both of them give similar results.

An optimization of the model has been realised into Matlab for the time and frequency domain. The optimization of the time domain is treated by local free-gradient method using two objective functions (OFs): variation of the output torque and estimation of the power losses. For the frequency domain two other OFs are used: Reduction of the maximum value of the amplitude frequency response of the secondary flywheel and Reduction of the area under the curve of this frequency response. The optimization leads to similar results: increasing inertia, decreasing stiffness. Damping should be increased if high resonance peaks should be reduced.

The effect of a more accurate torque expression on the output response is approached. At higher speeds (1500-2000 RPM), difference can be observed in the shape of the output responses, from the results obtained from the simplified input torque.

Keywords: Torsional Vibration, Dual Mass Flywheel, Objective function, Temporal domain, Frequency domain.

Preface and Acknowledgements

This thesis work is the final part of my Master of Mechanical Engineering. I had the opportunity to realize my thesis in the department of Applied Mechanics at Chalmers University of Technology, Gothenburg, Sweden.
This present document is the result of 4 months of work. The thesis work counts for 21 of 60 credits of my second year of the Master Program in Mechanical Engineering specialized in Design and Production at the Faculty of Engineering of the university of Mons.

First of all I would like to thank Prof. Viktor Berbyuk for agreeing my application and for his welcome in the department of Applied Mechanics.
It is a genuine pleasure to express my deep sense of thanks and gratitude to my three supervisors, Prof. Viktor Berbyuk, Dr. Hakan Johansson and M. Sc. Lina Wramner. I am highly indebted to them for their guidance and for the time they have devoted to my project.
Special thanks go to Prof. Georges Kouroussis who supervises me from the university of Mons.
I would like to express special gratitude towards my parents, my sister, my friends and especially my girlfriend, for their encouragement which help me to finalize this project.
Last but not the least I thank profusely all my friends who take the time to answer to my questions, in particular to Benoit Brackeveldt, Céline Cremer, Clément Dutoit, Sébastien Mercier, Hugo Simonetti and Jean-Louis Truffaut.

"None of us is as smart as all of us." KEN BLANCHARD

Gérémy Bourgois, Gothenburg, June 2016

Contents

List of Abbreviations and Notations **xiii**

List of Figures **xiv**

List of Tables **xvii**

1 Introduction **1**
1.1 Purpose and Goal 2
1.2 Delimitations 2
1.3 Outline of thesis 2

2 State of the art **3**
2.1 Conventional Flywheel 3
2.2 Conventional Dual Mass Flywheel 5
2.3 Hydrodynamic Torque Converter 6
2.4 Centrifugal Pendulum Vibration Absorbers (CPVAs) 7
2.5 Triple Mass Flywheel 8
2.6 Planetary gear Dual Mass flywheel 8
2.7 Electrorheological fluid vibration absorber 9
2.8 Magnetorheological fluid vibration absorber 10
2.9 Viscous Dampers 10
2.10 Torsional balancers 11
2.11 Power Split flywheel [3] 11

3 Dual Mass flywheel approach **15**
3.1 Engineering Model 15
3.2 Mathematical model 17
  3.2.1 Assumptions 17
  3.2.2 Parameters 17
  3.2.3 Solving strategy 18
3.3 Programming environment 19
3.4 Test cases 19
  3.4.1 Initial parameters 20
  3.4.2 Torsional vibration analysis 20
  3.4.3 Selection of objective functions 24
    3.4.3.1 Objective function 1 24

3.4.3.2 Objective function 2 24
3.5 Sensitivity analysis 24
3.5.1 Conclusion 26
3.6 Optimization 29
3.6.1 Implementation of the optimal values into the mathematical model 30
3.7 Frequency analysis 32
3.7.1 Sensitivity analysis of the eigenfrequencies 33
3.7.1.1 Eigenfrequencies values 33
3.7.1.2 Amplitude of the frequency response 34
3.7.1.3 Eigenfrequencies with the optimization of OF1 and OF2 36
3.7.2 Frequency resolution 37
3.7.2.1 Selection of objective functions 38
3.7.2.2 Optimization with $fminsearch$ 39
3.7.2.3 Comparison with the other optimizations 39
3.7.3 Dimensional analysis 40
3.7.3.1 Sensitivity analysis on the response of the secondary flywheel 44
3.7.3.2 Optimization of the dimensionless expression 45

4 Engine Dynamics **49**
4.1 Assumptions 49
4.2 Piston motions 49
4.3 Forces acting on the piston 50

Conclusion and Future Work **57**

Bibliography **1**

A Dimensional analysis Φ_1 case **I**

B Design parameters in dimensionless space **III**

C Matlab code **V**
C.1 Integration file V
C.1.1 Main V
C.1.2 Function used VIII
C.2 Optimization file IX
C.2.1 Main file IX
C.2.2 Function used IX
C.3 Real Torque expression XI

D EasyDyn model **XV**
D.1 General data of the studied mechanism XV
D.2 Complete kinematics calculed by CAGeM XV
D.3 Definition of external efforts XVII
D.4 Simulation XVIII

D.5 Visualization XVIII
D.6 User's MuPAD code XVIII

E Optimization results XXI
E.1 1500 RPM scenario XXI
E.2 2000 RPM scenario XXII

F Optimization results with a real expression of the Torque XXV
F.1 1500 RPM scenario XXV
F.2 2000 RPM scenario XXVI

List of Abbreviations and Notations

Abbreviations

DMF	Dual Mass flywheel
OF	Objective Function
DMTDVA	Dual Mass Torsional Dynamic Vibration Absorber
IFC	Inertial Functional Componant
RPM	Revolutions Per Minute
OF1	First Objective Function
OF2	Second Objective Function
DFT	Discrete Fourier Transform
PS	Power spectrum

Notations

$\varphi_{\mathbf{1}}$	Absolute angle of rotation the primary IFC	$[rad]$
$\varphi_{\mathbf{2}}$	Absolute angle of rotation the second IFC	$[rad]$
$\dot{\varphi_{\mathbf{1}}}$	Absolute angular speed of rotation the primary IFC	$[rad/s]$
$\dot{\varphi_{\mathbf{2}}}$	Absolute angular speed of rotation the secondary IFC	$[rad/s]$
$\ddot{\varphi_{\mathbf{1}}}$	Absolute angular acceleration of rotation the primary IFC	$[rad/s^2]$
$\ddot{\varphi_{\mathbf{2}}}$	Absolute angular acceleration of rotation the secondary IFC	$[rad/s^2]$
$\mathbf{J_1}$	Moment of inertia of the primary IFC	$[kg.m^2]$
$\mathbf{J_2}$	Moment of inertia of the secondary IFC	$[kg.m^2]$
$\mathbf{c_1}$	Torsional damping coefficient of the primary IFC	$[Nm.s/rad]$
$\mathbf{c_2}$	Torsional damping coefficient of the secondary IFC	$[Nm.s/rad]$
$\mathbf{k_1}$	Torsional stiffness coefficient of the primary IFC	$[Nm/rad]$
$\mathbf{k_2}$	Torsional stiffness coefficient of the secondary IFC	$[Nm/rad]$
$\mathbf{M_0}$	Mean engine torque	$[Nm]$
$\mathbf{M_1}$	Amplitude of the torque fluctuations	$[Nm]$
$\mathbf{M_e}$	Engine torque	$[Nm]$
$\varphi_{\mathbf{v}}$	Absolute angle of the gearbox input shaft	$[rad]$

$\mathbf{M_v}$	Gearbox input torque	$[Nm]$
$\omega_{\mathbf{e}}$	Angular velocity of the engine	$[rad/s]$
$\omega_{\mathbf{v}}$	Angular velocity of the gearbox side	$[rad/s]$
$\alpha_{\mathbf{1}}$	Phase shift angle of the primary torque	$[rad]$
$\mathbf{f_n}$	Eigenfrequency	[Hz]
$\omega_{\mathbf{k}}$	Pulsation	$[rad/s]$
$\xi_{\mathbf{k}}$	Damping rate	
$\mathbf{\Omega}$	Forcing frequency ratio	[-]
$\xi_{\mathbf{1}}$	Damping ratio 1	[-]
$\xi_{\mathbf{2}}$	Damping ratio 2	[-]
μ	Mass ratio	[-]
ψ	Frequency ratio	[-]
$\mathbf{l}$	Conrod length	[mm]
$\mathbf{r}$	Crank length	[mm]
$\mathbf{D}$	Bore diameter	[mm]

List of Figures

1.1 Downspeeding and downsizing of an engine. 1

2.1 Flywheel of a car engine 4
2.2 Comparison between the engine and the transmission torque with-/without flywheel for several cycles. 4
2.3 Benefits of a flywheel during a 4-stroke cycle. (1: Intake, 2: Compression, 3: Power, 4: Exhaust) 4
2.4 Dual mass flywheel- DMF [4] 5
2.5 Spring stop on dual mass flywheel [4] 6
2.6 Hydrodynamic Torque Converter [5] 6
2.7 DMF with CPVAs device [6] 7
2.8 Schematic figure of Triple Mass Flywheel [7] 8
2.9 Planetary gear Dual Mass flywheel concept [8] 9
2.10 Planetary gear Dual Mass flywheel: SACHS [9] 9
2.11 MR fluid property [10] 10
2.12 Viscous damper device [11] 11
2.13 Power split concept [3] 13

3.1 DMF from [1] 15
3.2 Spring-damper element DMF model 16
3.3 Difference between the angular displacement $\varphi_1 - \varphi_2$. 21
3.4 Difference between the angular velocity $\dot{\varphi}_1 - \dot{\varphi}_2$. 22
3.5 gearbox input torque 22
3.6 Angular displacement/velocity between the secondary flywheel and the gearbox. 22
3.8 Comparison of the gearbox input torque for different models. 23
3.7 Deflection angle between the flywheels ($\varphi_1 - \varphi_2$) using the Matlab model with different tolerances. 23
3.9 Time history of the deflection angle for different damping coefficient values. 25
3.10 Influence of c_1 on the OFs 26
3.11 Influence of c_2 on the OFs 27
3.12 Influence of J_1 on the OFs 27
3.13 Influence of J_2 on the OFs 27
3.14 Influence of k_1 on the OFs 28
3.15 Influence of the stiffness coefficient k_2 on the OFs. 28
3.16 Influence of the input frequency on the OFs. 28

3.17 Benefits of the optimization on the different deflection angles and their time derivatives. 31
3.18 Benefits of the optimization of the gearbox input torque. 31
3.19 Influence of inertia on the eigenfrequencies. 33
3.20 Influence of the stiffness. 34
3.21 Influence on the frequency response of the secondary flywheel 35
3.22 Influence on the frequency response of the secondary flywheel 36
3.23 Comparison between the time domain and the frequency domain. . . 39
3.24 Frequency response of the secondary flywheel. 40
3.25 Frequency response of the secondary flywheel. 43
3.26 Impact of the Dual Mass flywheel (normal and large scale). 43
3.27 Single Mass flywheel 44
3.28 Influence of the dimensionless parameters on the response of the secondary flywheel 45
3.29 Influence of ψ and ξ_1 on OF3 46
3.30 Influence of ψ and ξ_1 on OF4 46
3.31 Frequency response with optimal values deduced from OF3 and OF4 optimization. 47

4.1 Silder-crank mechanism 49
4.2 Crank angle evolution of the pressure inside a cylinder 52
4.3 Crank angle history of the torque for 3 different scenarios. 53
4.4 Torque produce by a 6-cylinder engine. 54
4.5 Time history of the deflection angle and its time derivative between the flywheels. 55
4.6 Time history of the deflection angle and its time derivative between the primary flywheel and the gearbox. 55
4.7 Time history of the gearbox input torque. 55
4.8 DFT diagram comparing the engine and the gearbox input torque. . . 56

D.1 Visualization via EasyAnim XVIII

E.1 Benefits of the optimization on the different deflection angles and their time derivatives. (1500 RPM scenario) XXI
E.2 Benefits of the optimization of the output torque (1500 RPM scenario).XXII
E.3 Benefits of the optimization on the different deflection angles and their time derivatives.(2000 RPM scenario) XXII
E.4 Benefits of the optimization of the output torque. (2000 RPM scenario)XXIII

F.1 Benefits of the optimization on the different deflection angles and their time derivatives. (1500 RPM scenario) XXV
F.2 Benefits of the optimization of the output torque (1500 RPM scenario).XXVI
F.3 Benefits of the optimization on the different deflection angles and their time derivatives. (1500 RPM scenario) XXVI
F.4 Benefits of the optimization of the output torque (20000 RPM scenario).XXVII

List of Tables

3.1 Optimization of OF1 for 3 different scenarios 30
3.2 Optimization of OF2 for 3 different scenarios 30
3.3 Eigenfrequencies obtained with the optimization 37
3.4 Optimization of OF4 with *fminsearch* 40
3.5 Values used for the example 43

4.1 Main characteristics of the piston 52

1

Introduction

In order to respect the environmental standard, engine manufacturers have to design new engines. The industries have to produce cars, trucks, tractors, etc., with low fuel consumption to minimize the CO_2 emission. The design of the new engine consists of downsizing and downspeeding it. As is shown in Figure 1.1, downsizing means that the number of cylinders are reduced while downspeeding means that the peak torque is obtained at lower speed.

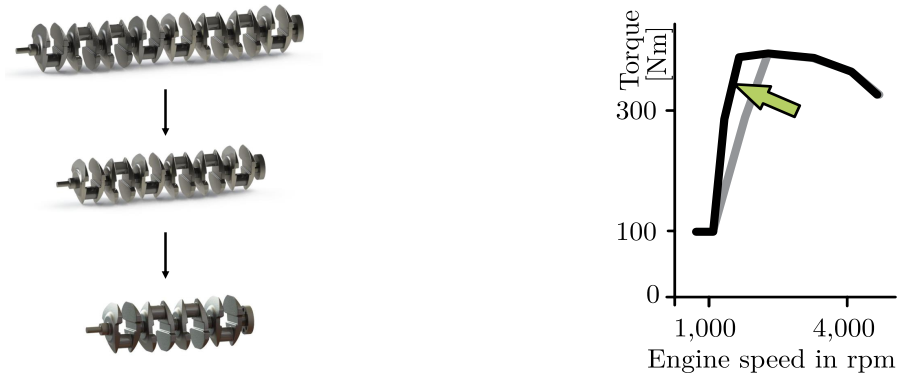

(a) Downsizing

(b) Downspeeding [12]

Figure 1.1 – Downspeeding and downsizing of an engine.

Unfortunately this new design will affect the crankshaft and the torsional vibrations become significant. The torsional vibrations come from the crankshaft. In fact, combustion generates an extremely rapid rise of pressure in the cylinder that results in a torque with peaks. The pressure applies a force on the top of the piston, which allows the crankshaft to turn. The pulsating load from the cylinders causes the vibrations. Various concepts of vibrations absorbers exist to reduce the output vibrations from the crankshaft. They will be described in the following chapter. One of them is called the Dual Mass flywheel (DMF). This vibration absorber is placed between the crankshaft and the gearbox. As its name indicates, it is composed of 2 flywheels which are connected to each other by at least one arc spring. Springs store energy and allow to provide a continuous motion. This device separates the engine (primary flywheel) to the gearbox (secondary flywheel). These torsional vibrations must be reduced because they impact the vehicle ride comfort directly but also the durability of parts. The interest of the Dual Mass flywheel is to reduce the torque fluctuations by moving the resonances so that they are not excited in the operating speed range.

1.1 Purpose and Goal

The main purpose of this thesis is to learn more about the Dual Mass flywheel concept. A state of the art of the different technologies used to reduce the torsional vibration is realized to develop the knowledge in the torsional vibration area. This work is focusing on heavy vehicles. The goal of this thesis can be summarized in the following points:

- Realize a state of the art of the torsional vibration concepts;
- Investigate the Dual Mass flywheel concept:
  - Create a model in Matlab for several different scenarios
  - Verify the model by using software EasyDyn
  - Optimize the DMF flywheel for different scenarios
  - Analyse the Dual Mass flywheel in frequency domain

1.2 Delimitations

The most important delimitations of this project are the following:

- The analysis will be restricted to 1-D
- Gravitational energy is assumed to be small compared to the kinetic energy and is neglected in the models
- Only torsional vibration will be treated
- The project is realized with numerical simulations. Measurements and experimentation are not included
- The non-linearity effects are not taken into account
- The input torque will be assumed as a simple sine function

1.3 Outline of thesis

The present document will begin with a state of the art of the different approaches which are used to reduce the torsional vibrations.

The second chapter will focus on one of these technologies: Dual Mass Flywheel. First of all, the engineering and mathematical model are presented. The output response is then analysed using two different softwares. A sensitive analysis of the different design parameters is performed. An optimization with the Matlab subroutine $fminsearch$ is then realized. Finally, a frequency domain study is carried out (in dimension and dimensionless cases).

The last chapter approaches the study of the engine dynamics which is included in the model in order to have a more realistic input data.

At the end, conclusion and future work are exposed.

2

State of the art

There are many torsional vibration absorbers, these can be classified into 3 categories of vibration reduction method:

- Active control: It is an active application of equal and opposite force to the forces imposed by external vibration. An active damper gives the best vibration reduction performance. Unfortunately, it is a high cost and it is based on a complex technology. An active absorber requires an external energy supply, it has also a lack or robustness and reliability.
- Semi-active control: It is a kind of active control but external power requirements are lower than full active control.
- Passive control: It dissipates energy through some kind of motion without needing an external power source. Usually it consists of a spring and damper. This absorber ensures a good cost effectiveness.

Engineers have designed several different vibration absorbers. There are various basic types of torsional vibration reduction devices: conventional Dual Mass Flywheel, planetary Dual Mass Flywheel, hydrodynamic torque converter, Dual Mass Flywheel with conventional centrifugal pendulum vibration absorbers. The main function is to isolate the transmission input from the vibration generated by the engine but vibration damper will also improve the noise behaviour of the vehicle and reduce fuel consumption.

2.1 Conventional Flywheel

A flywheel is an energy storage unit, composed of a mass which gives a greater moment of inertia to the global system. Figure 2.1 shows an example of an automobile engine flywheel. The amount energy stored in a flywheel is proportional to the square of its rotational speed. Flywheel stores energy when torque is applied by the energy source and restores energy when the energy source is not applying torque to it. In fact, the engine provides a discontinuous energy, the aim of the flywheel is to supply a continuous energy which is shown in Figure 2.2. Figure 2.3 shows these principles for a 4-stroke engine during 1 cycle.

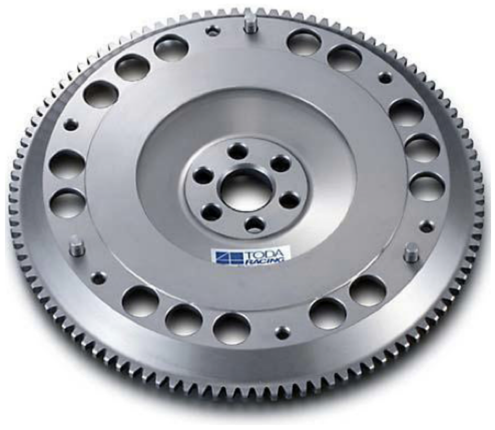

Figure 2.1 – Flywheel of a car engine

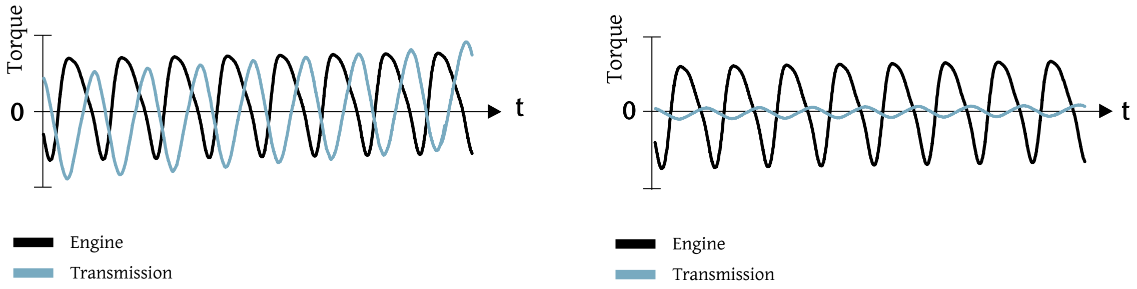

(a) Without a flywheel

(b) With a flywheel

Figure 2.2 – Comparison between the engine and the transmission torque with/without flywheel for several cycles.

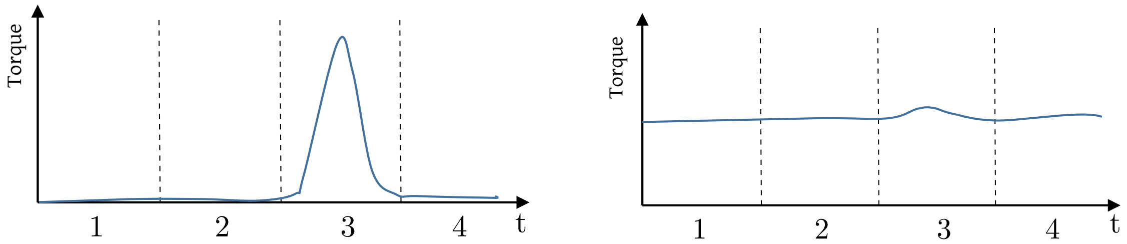

(a) Without a flywheel

(b) With a flywheel

Figure 2.3 – Benefits of a flywheel during a 4-stroke cycle. (1: Intake, 2: Compression, 3: Power, 4: Exhaust)

2.2 Conventional Dual Mass Flywheel

The Dual Mass Flywheel (DMF) is the most common conventional system. The DMF consist of two masses [4]:

- The primary flywheel
- The secondary flywheel

Figure 2.4 shows a typical DMF.

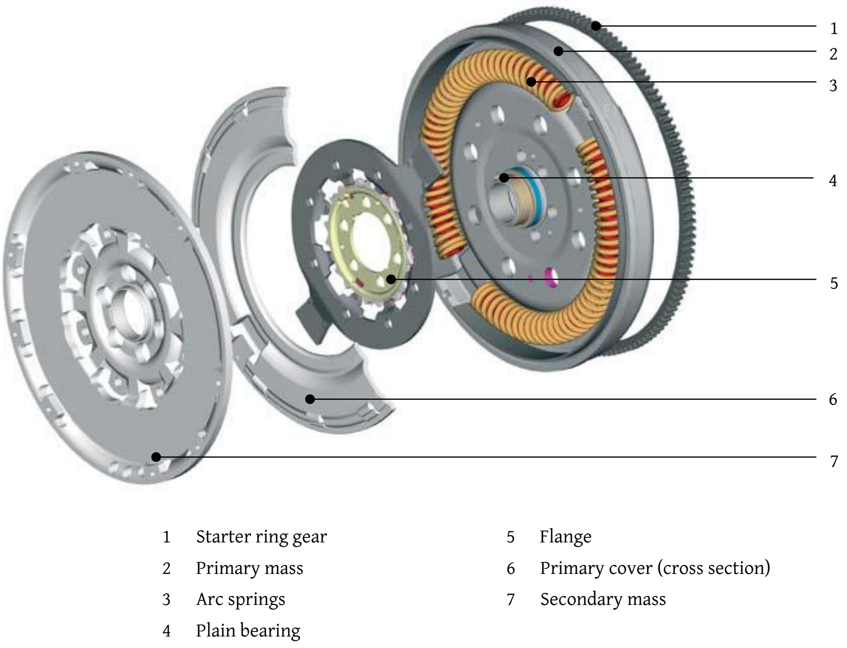

Figure 2.4 – Dual mass flywheel- DMF [4]

These masses are connected via a spring/damper device and supported by a bearing. The first mass is connected to the crankshaft of the engine and the second mass is connected to the transmission input. Thanks to bearing, these masses have an independent radial movement. The primary mass encloses a cavity which forms the arc spring channel. The spring/damper system is guiding into this arc spring channel, typically divided into two sections, separated by an arc spring stop which is represented in Figure 2.5. Grease is applied into the channel to reduce friction and increase the lifetime of arc springs.

Torque from the engine is transferred via the arc spring and the flange which is fixed to the secondary mass.

The secondary mass increases the moment of inertia and will decrease the vibration amplitude.

DMF is also equipped with vents which ensure heat dissipation.

Performances of the DMF are limited by the achievable torsional stiffness of the spring/damper device.

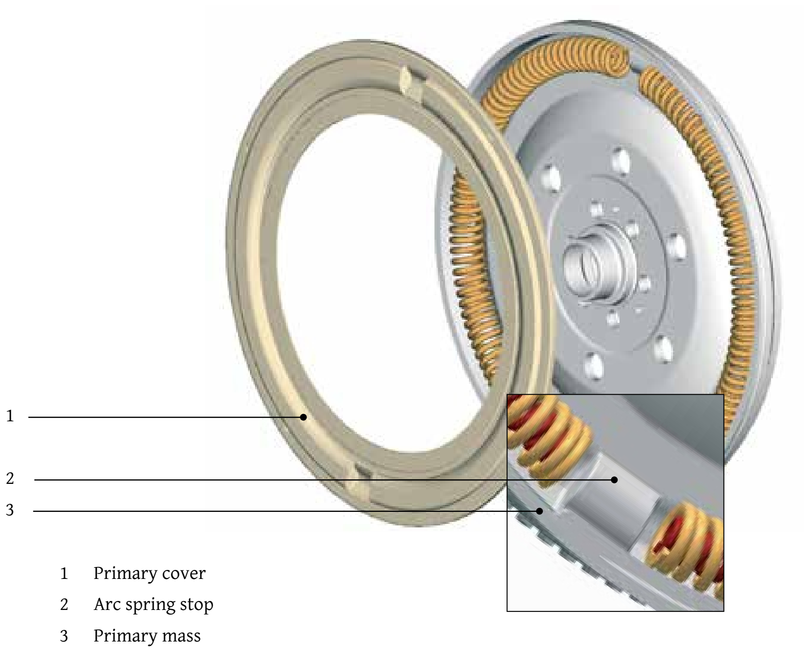

Figure 2.5 – Spring stop on dual mass flywheel [4]

2.3 Hydrodynamic Torque Converter

The hydrodynamic torque converter offers a way to reduce torsional vibrations for applications with automatic or continuously variable transmission. Figure 2.6 shows the hydrodynamic torque converter concept.

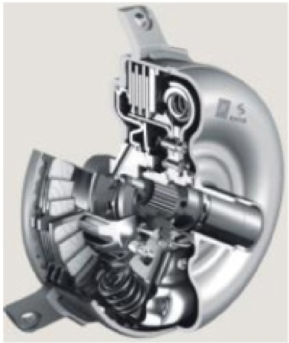

Figure 2.6 – Hydrodynamic Torque Converter [5]

This device is based on a fluid coupling which transfers torque from the engine side to the gearbox side. This hydrodynamic transfer has itself a damping effect but leads to dissipation of energy [5].

The hydrodynamic torque converter has the following properties [12]:

- A high-capacity torsional dampers
- A reduction of the rotating masses being accelerated

2.4 Centrifugal Pendulum Vibration Absorbers (CPVAs)

This device is composed of a series of pendulums suspended from a rotor such that they can oscillate in a plane perpendicular to the rotational axis [13]. During the torque fluctuations, masses will oscillate along specific paths relative to the axis of rotation of the crankshaft. In fact, pendulums will apply a centrifugal force which tends to increase the inertia of the flywheel. These paths have been the subject of many studies. CPVAs have the advantage that they stay tuned at all rotation speeds.

These devices were first used in aircraft engines or helicopter rotors, but they can now also be used in automotive industries.

Engineers also developed a DMF with CVPA flywheel, the CVPA is mounted on the secondary flywheel. These flywheels improve the performance of a conventional DMF.

Unfortunately, the efficiency of the pendulum can be assign by small manufacturing deviations. Furthermore, problems of Noise,Vibration and Hardness (NVH) can increase due to improper tuning of pendulum [5], [14]. A DMF with CVPA from the manufacturer LuK is shown in figure 2.7.

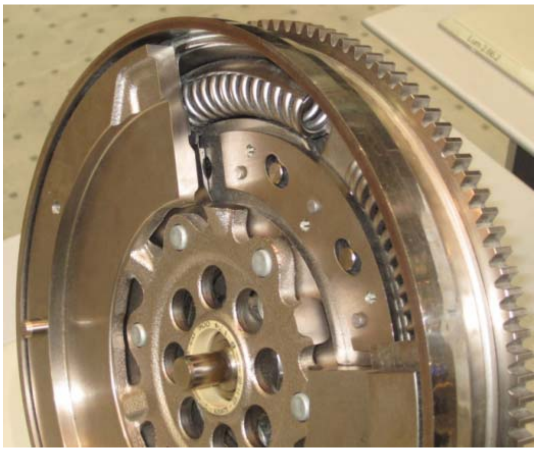

Figure 2.7 – DMF with CPVAs device [6]

2.5 Triple Mass Flywheel

This concept had been patented in Korea by Lee Hee Rak and Hur Man Dae in 2008 [14]. In 2014, one other kind of triple mass flywheel has been patented [7]. The flywheel is composed of 3 masses:

- A first mass is connected to the engine side and rotated via the engine torque.
- A second mass will offset torsional vibration of the engine transmitted to the first mass. Damping springs are placed between the first and the second mass, providing an elastic force against the relative rotational displacement between the first and second mass. There is a guide placed between the damping springs guiding the damping springs during extending/contracting.
- A third mass will offset torsional vibration of the engine transmitted to the second mass. A second damping spring is disposed between the third mass and the guide.

All of these elements are represented one Figure 2.8.

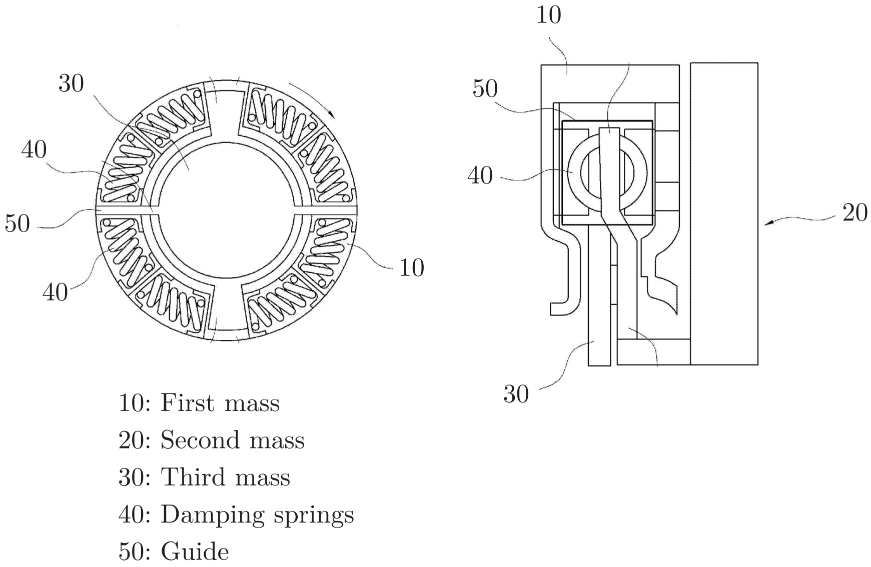

Figure 2.8 – Schematic figure of Triple Mass Flywheel [7]

2.6 Planetary gear Dual Mass flywheel

Planetary gear Dual Mass flywheel is similar to DMF: the primary mass is connected to the secondary mass via an arc spring damper unit but also via a planetary gear set. Figure 2.9 shows an example of this technology. The planetary gear directly connected to the primary side helps to create an anti-resonance in the transfer system behaviour. This system is manufactured by an German supplier ZF which called it "SACHS". Figure 2.10 represent the planetary gear dual mass flywheel "SACHS".

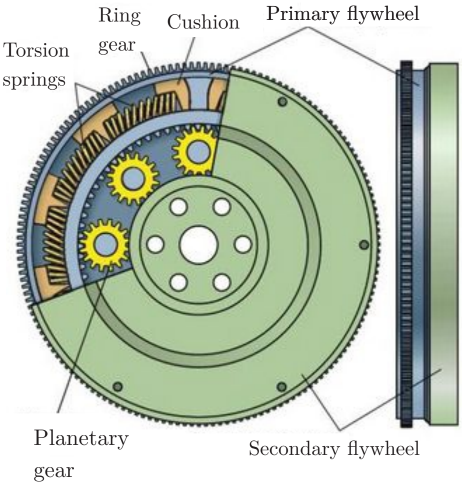

Figure 2.9 – Planetary gear Dual Mass flywheel concept [8]

Vibrational excitations with frequencies close to the anti-resonance frequency are reduced very well with these flywheels. For vibrations with other frequencies, the influence of the DMF transfer behaviour dominates according to [14], [5]. The planetary gear dual mass flywheel allows to reduce also noise.

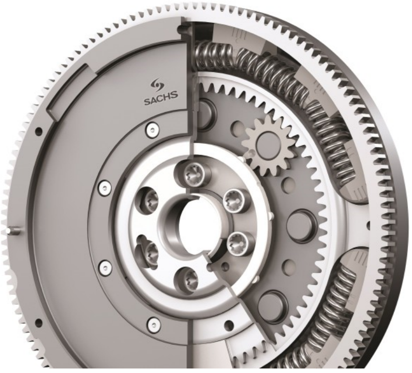

Figure 2.10 – Planetary gear Dual Mass flywheel: SACHS [9]

2.7 Electrorheological fluid vibration absorber

Electrorheolgical (ER) fluid is composed of tiny suspended particles into an isolating dielectric fluid. Their rheological behaviour is heavily influenced by the influence of an electrical field. ER fluid can play as an absorber role. These absorbers are advantageous only for frequencies close to resonance, the vibration dampening should be maximal close to the resonance frequency and minimal for frequency exceeding 1.4 times the fundamental frequency [15]. A passive absorber can not perform this property but the ER fluid can make an adaptable and flexible absorber. In fact, when frequency of the excitation force is close to the natural frequency of the system, the system absorber is increased by applying an electrical field.

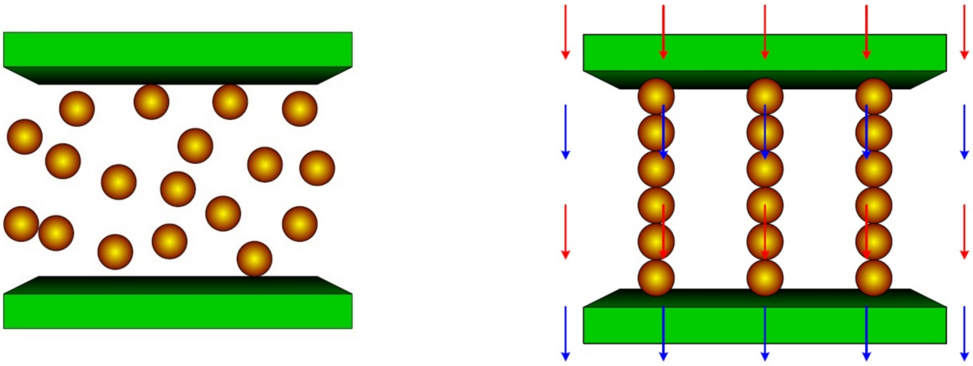

(a) Without Magnetic Field (b) With Magnetic Field

Figure 2.11 – MR fluid property [10]

On the other hand, when the frequency ratio exceeds 1.4, the system absorber is reduced to a minimum by not applying an electrical field.
Rheological behaviour of most ER fluid follows the Binhgam model when an electrical field is applied.

2.8 Magnetorheological fluid vibration absorber

Magnetorheological (MR) fluid is a smart fluid which can change their apparent viscosity under the influence of a magnetic field as Figure 2.11 shows.
When a MR fluid is subjected to a magnetic its apparent viscosity increases. MR fluid is also an example of semi-active damper. This technology allows very fast response speeds (order of a millisecond) [16].
Engineers are developing a variant of this absorber, they are studying a damper incorporating conventional centrifugal pendulum absorber and magnetorhelogical damper [17].

2.9 Viscous Dampers

A viscous dampers is composed of a housing containing the damper ring and a viscous fluid [18]. The viscous fluid such as silicon oil fills the backlash between the both parts (flywheel and housing). Figure 2.12 shows a viscous damper.
The viscous fluid dissipates vibration energy in the form of heat. The overheating is a prominent preoccupation, it can completely destroy the damper and cause problems in the whole system [19]. Adjusting the internal backlash allows to tune damping characteristics. Unfortunately, these dampers are designed to protect the engine crankshaft and not necessarily the driven machinery. Dampers need to be located at an anti-node of the crankshaft mode.
Viscous dampers have a limited service life, require periodic checks and maintenance. As an order of magnitude, viscous dampers should be replaced every 25000 hours of service [11].

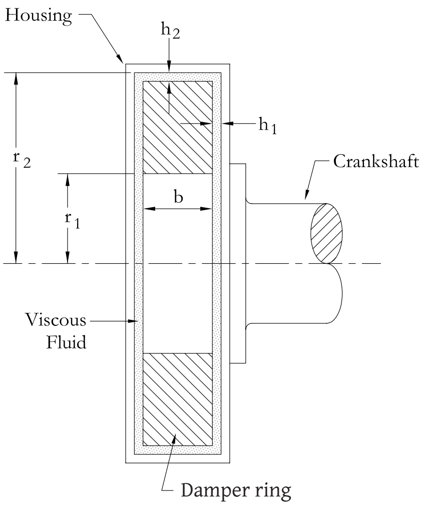

Figure 2.12 – Viscous damper device [11]

2.10 Torsional balancers

A damper can be placed on the front end of the crankshaft opposite to the flywheel. This wheel is called torsional balancer. It is generally composed of different pieces. The damper is simply another mass and a spring tuned to a single frequency [20], [21].

2.11 Power Split flywheel [3]

The power split flywheel is similar to the planetary gear dual mass flywheel.
A torsional vibration can be reduced by a power split device. The input torque is split in two torque transmission path, the power splitting will cause a phase shift between these paths. At the end of this device, torque from different paths are superposed in a coupling arrangement.

The input torque is split into a first transmission path and a second transmission path. The first path is composed of a phase shifter arrangement. This device generates a phase shift between torsional vibrations which are transmitted to the coupling arrangement via the first torque transmission path. The phase shifter is an oscillatory system which allows the shift, in ideal case, 180° starting from the resonant frequency. It comprises a primary mass to which a cover plate is screwed. The primary mass is connected via a two-spring arrangement to a secondary side of the oscillatory system. The secondary side can rotate with respect to the primary side. Several coil springs of a first step connect the primary side to a hub disk. Further several coil springs of a second step connect this hub disk to output-side cover plates. The output-side cover plates are in turn screwed to the ring gear carrier. Together, they form the secondary side of the oscillatory system.

An input-side ring gear is also screwed to the ring gear carrier. Then, the torque from the path 1 is transmitted to the output-side ring gear via a planet gear.

Regarding to Figure 2.13 and the previous explanation, the path A is composed of these following parts:

- Primary mass (1)
- Springs (2)
- Hub disk (3)
- Springs (4)
- Output-side cover plates (5)
- Ring gear carrier (6)
- Input-side ring gear (7)
- Planet gear (8)
- Output-side ring gear (9)
- Secondary flywheel (10)

Regarding the second path, the planet carrier is directly screwed on the primary mass. Several rotatable planet gears are secured to this planet carrier by means of bearings. The planet gear has two sets of teeth with different outer diameters. The ouput-side toothing has a smaller diameter than the input-side toothing.
The torque is transmitted to the output-side gear via the output-side toothing.

Regarding to Figure 2.13 and the previous explanation, the path B is composed of these following parts:

- Primary mass (1)
- Planet gear carrier (11)
- Planet gear (8)
- Output-side ring gear (9)
- Secondary flywheel (10)

The different torque transmission paths are superposed in a coupling arrangement to form the output torque. Thanks to the phase shift in the first path, the alternating torques erase each other mutually. Finally, the output torque is a constant torque. All of these elements are represented on Figure 2.13.

However, in a conventional power splitting system, this principle works only for one speed of the system.
To expand the cancellation point to an speed range, another device can be added on the secondary side of the oscillatory system. Via this device, changing the speed of the system changes the effective mass moment of inertia of the secondary side. This technology uses the centrifugal force, it is composed of a central element and several concentric mass rings which are supported so as to be rotatable relative to one another and the central element.

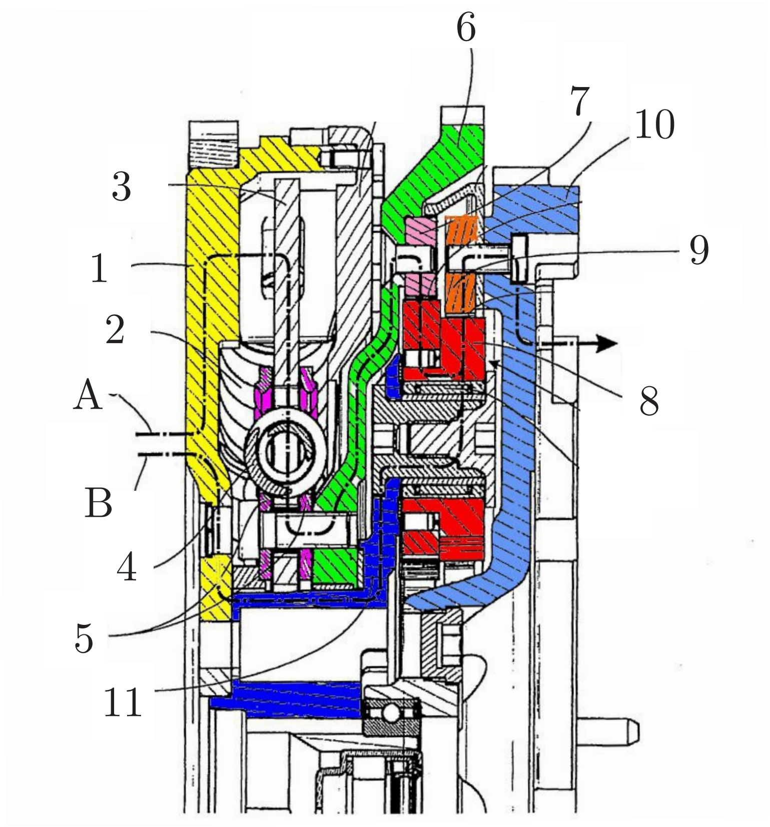
6
7
10
3
9
1
2
8
A
B
4
5
11

Figure 2.13 – Power split concept [3]

3

Dual Mass flywheel approach

ACCORDING the previous chapter, many approaches are composed of 2 inertias: Dual Mass flywheel, Centrifugal Pendulum Vibration Absorbers, Planetary gear Dual Mass Flywheel, Power Split flywheel. The concept of the DMF will be the subject is this work. In fact, the DMF model could thus be adapted to these other approaches in a future work.

An engineering model will be developed from which the mathematical model will be deduced. Three different cases will be treated. Different output properties will be analysed:

- Time history of the deflection angle between both flywheels and its time derivative
- Time history of the deflection angle between the secondary flywheel and the gearbox input shaft and its time derivative
- Time history of the gearbox input torque

A sensitive analysis and an optimization are also realised. Finally a study of the frequency domain is approached.

3.1 Engineering Model

As mentioned previously, and shown in Figure 3.1 the dual mass flywheel is composed of:

- A primary flywheel (1)
- A spring (2)
- A flange (3)
- A secondary flywheel (4)

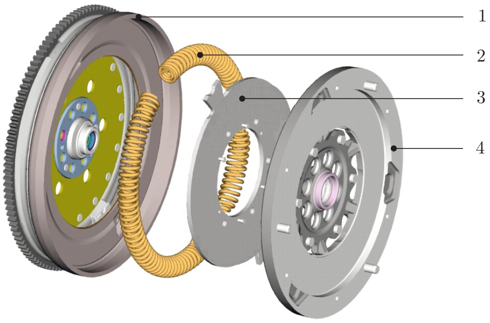

Figure 3.1 – DMF from [1]

The flange is screwed to the secondary flywheel. The flange and the flywheel will thus be assumed as one part. The primary and the secondary flywheel will be considered as disks of inertia J_1 and J_2 respectively.
These 2 flywheels are connected to each other by a torsional spring and a torsional damper. The Dual Mass flywheel is affected by a torque M_e(t), the engine torque. A counter torque is opposite to the engine torque and applied on the rear end of the driveline.
In order to be more general, we will call this system a Dual Mass Torsional Vibration Dynamic absorber (DMTVDA).

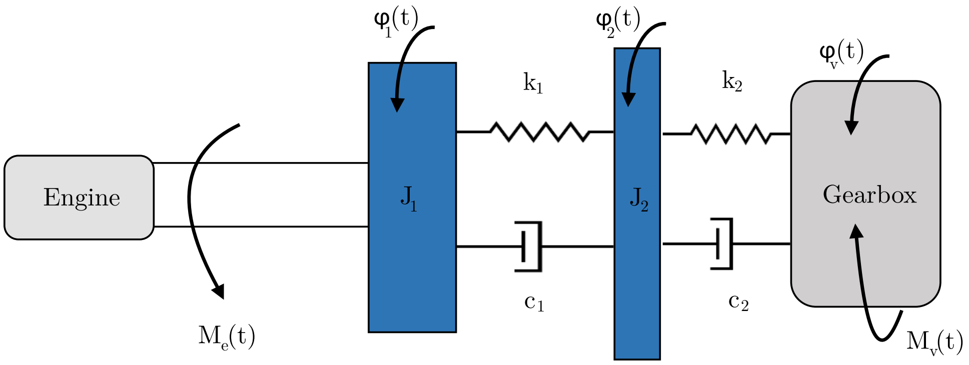

Figure 3.2 – Spring-damper element DMF model

Figure 3.2 shows a DMTVDA model, where:

- $M_e(t)$ is the torque at the rear end of the crankshaft of the engine acting upon the shaft of the DMTVDA.
- $\varphi_1(t)$ is the absolute angle of rotation of the first Inertial Functional Component (IFC) of DMTVDA.
- $\dot{\varphi}_1(t) = \dfrac{d\varphi_1(t)}{dt}$ is the absolute angular speed of rotation of the first IFC of DMTVDA.
- $\ddot{\varphi}_1(t) = \dfrac{d^2\varphi_1(t)}{dt^2}$ is the absolute angular acceleration of the first IFC of DMTVDA.
- $\varphi_2(t)$ is the absolute angle of rotation of the second IFC of DMTVDA.
- $\dot{\varphi}_2(t) = \dfrac{d\varphi_2(t)}{dt}$ is the absolute angular speed of rotation of the second IFC of DMTVDA.
- $\ddot{\varphi}_2(t) = \dfrac{d^2\varphi_2(t)}{dt^2}$ is the absolute angular acceleration of the second IFC of DMTVDA.
- $\varphi_v(t)$ is the absolute angle of rotation of the gearbox input shaft.
- $\dot{\varphi}_v$ is the absolute angular speed of rotation of the gearbox input shaft.
- k_1 is the torsional stiffness coefficient for the shaft between the first and the second IFC.
- c_1 is the torsional damping coefficient for the shaft between the first and the second IFC.
- k_2 is the torsional stiffness coefficient of the output shaft of the DMTVDA.
- c_2 is the torsional damping coefficient of the output shaft of the DMTVDA.
- $M_v(t)$ is the gearbox input torque.

3.2 Mathematical model

Using the free body diagram, the following equations of motion can be deduced:

$$J_1\ddot{\varphi}_1 + c_1(\dot{\varphi}_1 - \dot{\varphi}_2) + k_1(\varphi_1 - \varphi_2) = M_e(t) \tag{3.1}$$

$$J_2\ddot{\varphi}_2 + c_1(\dot{\varphi}_2 - \dot{\varphi}_1) + k_1(\varphi_2 - \varphi_1) + c_2(\dot{\varphi}_2 - \dot{\varphi}_v) + k_2(\varphi_2 - \varphi_v) = 0 \tag{3.2}$$

where $c_2(\dot{\varphi}_2 - \dot{\varphi}_v) + k_2(\varphi_2 - \varphi_v)$ is gearbox input torque $M_v(t)$.
These equations can be written in matrix form:

$$\begin{bmatrix} J_1 & 0 \\ 0 & J_2 \end{bmatrix} \begin{pmatrix} \ddot{\varphi}_1 \\ \ddot{\varphi}_2 \end{pmatrix} + \begin{bmatrix} c_1 & -c_1 \\ -c_1 & c_1 + c_2 \end{bmatrix} \begin{pmatrix} \dot{\varphi}_1 \\ \dot{\varphi}_2 \end{pmatrix} + \begin{bmatrix} k_1 & -k_1 \\ -k_1 & k_1 + k_2 \end{bmatrix} \begin{pmatrix} \varphi_1 \\ \varphi_2 \end{pmatrix} = \begin{pmatrix} M_e(t) \\ k_2\varphi_v + c_2\dot{\varphi}_v \end{pmatrix} \tag{3.3}$$

Appendix B shows that this equation can be expressed by using dimensionless design parameters.

3.2.1 Assumptions

The limitations are the following:

- The model will consider the Dual Mass flywheel and the output shaft joined to the gearbox
- A six-cylinder truck engine will be considered
- The engine torque will be assumed as a sum of a constant torque and a sine function:
  $M_e(t) = M_0 + M_1 \times sin(\omega_e t + \alpha_1)$
- The angular displacement and velocity of the gearbox side can be given by:
  $\varphi_v = \omega_v t$ and $\dot{\varphi}_v = \omega_v$. It means that there are no vibrations at gearbox side.

3.2.2 Parameters

The system parameters are:

- J_1, J_2
- k_1, k_2
- c_1, c_2
- ω_e, ω_v
- α_1
- M_0, M_1

3.2.3 Solving strategy

The equation system can be easily solved by ODE45 function using Matlab. But ODE45 requires a first-order differential equation [22].
It is necessary to rewrite the previous matrix equation 3.3 in the form of:

$$\dot{y}(t) = Ay(t) + Bf(t) \tag{3.4}$$

where:

- $y(t) = \begin{bmatrix} y_1 & y_2 & y_3 & y_4 \end{bmatrix}^T$
  - $y_1 = \varphi_1$
  - $y_2 = \varphi_2$
  - $y_3 = \dot{\varphi}_1$
  - $y_4 = \dot{\varphi}_2$
- $f(t) = \begin{bmatrix} 0 & 0 & M_e(t) & k_2\varphi_v + c_2\dot{\varphi}_v \end{bmatrix}^T$

The following equations can be obtained:

$$\begin{cases} \dot{y_1} = y_3 \\ \dot{y_2} = y_4 \\ J_1\dot{y_3} + c_1(y_3 - y_4) + k_1(y_1 - y_2) = M_e(t) \\ J_2\dot{y_4} + c_1(y_4 - y_3) + k_1(y_2 - y_1) + c_2(y_4 - \dot{\varphi}_v) + k_2(y_2 - \varphi_v) = 0 \end{cases} \tag{3.5}$$

Equation 3.4 can be obtained where:

$$A = \begin{pmatrix} 0 & I \\ -M^{-1}K & -M^{-1}C \end{pmatrix} \tag{3.6}$$

$$B = \begin{pmatrix} 0 & 0 \\ 0 & M^{-1} \end{pmatrix} \tag{3.7}$$

where

- 0 is a 2 × 2 zero matrix
- I is a 2 × 2 identity matrix

The resolution requires an initial vector of the parameters. In order to avoid a long transient time, the initial angular velocity $\dot{\varphi}_{1_0}$ and $\dot{\varphi}_{2_0}$ are imposed at the value of $\dot{\varphi}_v = \omega_v$, the angular displacements will be imposed to be zero. The initial vector y_0 is thus equal to: $y_0 = \begin{bmatrix} 0 & 0 & \omega_v & \omega_v \end{bmatrix}^T$.

3.3 Programming environment

Two different softwares have been used:

- Matlab
- EasyDyn

Matlab (*Mat*rix *Lab*oratory) [23], it is a commercial software which is used for numerical calculations. Matlab allows matrix manipulations, plotting curves, etc.

EasyDyn [24] is an open-source program which is used to study a multi-body dynamic system. It can predict how the mechanical system moves under the influence of forces.

EasyDyn comprises two main components:

- A C++ library for the simulation of problems represented as a second-order differential equations form
- CAGeM which generates the kinematics of a multibody system from the position matrices

Two different environments (Matlab and EasyDyn) allow the verification of output results and assure the consistency of the results. In this way, a comparison will be performed. In this work, the Matlab code integrates the system using the ODE45 function, while EasyDyn uses the Newmark method.

3.4 Test cases

Different test cases will be studied which will try to approach a dual mass flywheel of a truck engine. The speed range usually used in the truck engine studies extends from 900 RPM to 2000 RPM. A 4-stroke 6-cylinder engine is commonly mounted in the trucks. The number of cylinder affects the excitation frequency. The load from each cylinder will have a cycle corresponding to two crankshaft revolutions. During one crankshaft revolution half the cylinders will fire. This means that the main excitation frequency will correspond to the engine speed times one half of the number of cylinder.

As reminder, the engine torque is represented by:

$$M_e(t) = M_0 + M_1 \times sin(\omega_e t + \alpha_1) \tag{3.8}$$

Good assumptions for M_0 and M_1 are 300 and 500 Nm, respectively. In order to have a sufficient scope, three different cases will be studied:

1. A simulation at a low speed: 900 RPM which corresponds to 15 Hz.
2. A simulation at medium speed: 1500 RPM which corresponds to 25 Hz.
3. A simulation at high speed: 2000 RPM which corresponds to 33.333 Hz.

Therefore, these different frequencies will be multiplied by three and the following engine torques will be used:

$$M_{e_1}(t) = 300 + 500 \times sin(45 \times 2\pi t) \tag{3.9}$$

$$M_{e_2}(t) = 300 + 500 \times sin(75 \times 2\pi t) \tag{3.10}$$

$$M_{e_3}(t) = 300 + 500 \times sin(100 \times 2\pi t) \tag{3.11}$$

To perform the simulation the velocity from the gearbox side has to be imposed. An acceptable value is to use one third of the engine speed. ω_v in the expression of the angular velocity from the gearbox side, $\dot{\varphi}_v = \omega_v$, will thus be assumed as equal to $\frac{\omega_e}{3}$. We could demonstrate that the mean engine torque does not affect the torque variations, the same could be said for ω_v.

3.4.1 Initial parameters

The initial values of the design parameters have to be imposed. According to a master's thesis [25], the following values will be assumed as initial values:

- $J_1 = 1.8\ kg.m^2$
- $J_2 = 0.6\ kg.m^2$
- $c_1 = 30\ Nms/rad$
- $c_2 = 1\ Nms/rad$
- $k_1 = 20\ 000 Nm/rad$
- $k_2 = 11\ 000 Nm/rad$

3.4.2 Torsional vibration analysis

In the interest of analysing the torsional vibrations, different measures will be compared:

- Time history of the deflection angle between both flywheels and its time derivative
- Time history of the deflection angle between the secondary flywheel and the gearbox input shaft and its time derivative
- Time history of the gearbox input torque

This information has been obtained by using the Matlab code which is placed in Appendix C. The integration with ODE45 can not be used with its standard parameters. In fact, the standard value of the relative tolerance is 1×10^{-3} which does not offer enough accuracy in our case. A tolerance value of 1×10^{-5} has been imposed. Figure 3.7 shows the impact of this tolerance on the returned values by ODE45. Peaks appear on the chart of time history of the deflection angle between the primary and secondary flywheel with a poor tolerance. They disappear with a better tolerance.

From Figures 3.3 to 3.6 we can observe that with an increase of the velocity, the fluctuation of the different parameters is going down.
For the first scenario, we can see from Figures 3.4 and 3.6 that the peak to peak value for the difference between the angular displacement of the first and secondary flywheel is around 0.016 rad while the peak to peak value of the deflection angle between the secondary flywheel and the gearbox input shaft is around 0.009 rad. Moreover, the time derivative of the deflection angle between the secondary flywheel and the gearbox input shaft is twice as small as the time derivative of the deflection angle between the flywheels. The perturbations are thus reduced at the output of the Dual Mass flywheel.

The engine torque has an oscillation amplitude of 500 Nm. We can see all the benefits of the dual mass flywheel: the gearbox input torque has a very small oscillation amplitude:

- 100 Nm for the first scenario
- 7 Nm for the second scenario
- 3 Nm for the third scenario

Figures from 3.3 to 3.5 also compare the output functions from the Matlab Model to the output functions obtained by EasyDyn. As a reminder, Easydyn use the Newmark integration. Notice that the Newmark integration uses a tolerance of 1×10^{-4} which is sufficient to obtain good results without noise.
All the details concerning the EasyDyn model are placed at Appendix D.
As regards the gearbox input torque and the angular displacement/velocity, similar results are obtained: the average and the peak-to-peak values of the 3 different scenarios show good agreement. Moreover, no time offset can be observed between those two models which shows the accuracy of the results.

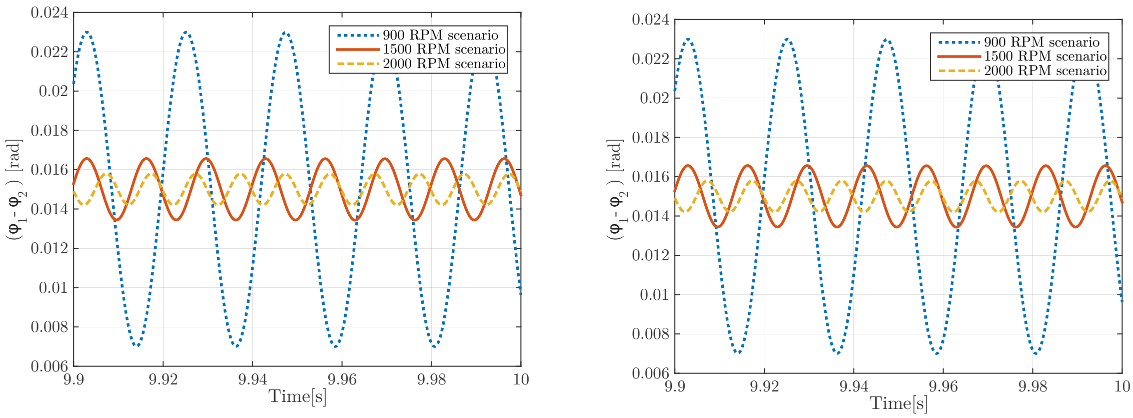

(a) Matlab model

(b) EasyDyn model

Figure 3.3 – Difference between the angular displacement $\varphi_1 - \varphi_2$.

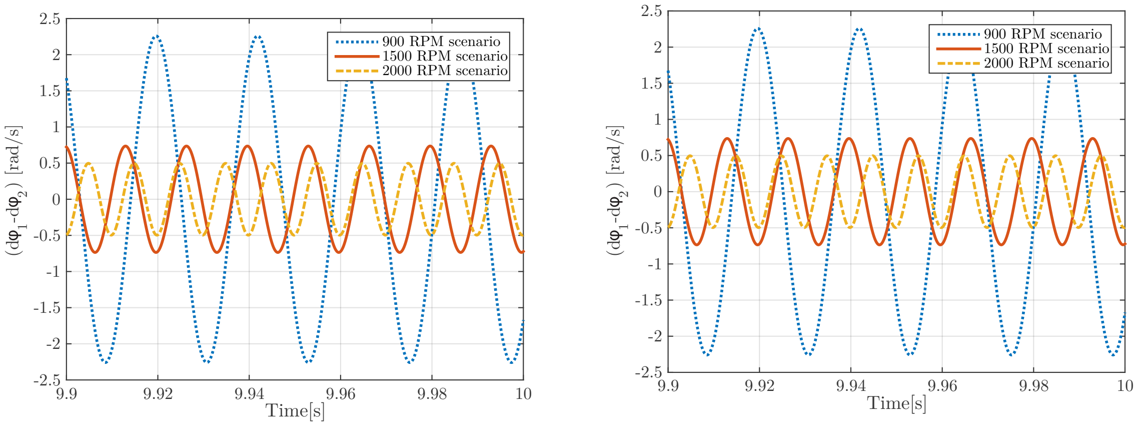

(a) Matlab model

(b) EasyDyn model

Figure 3.4 – Difference between the angular velocity $\dot{\varphi}_1 - \dot{\varphi}_2$.

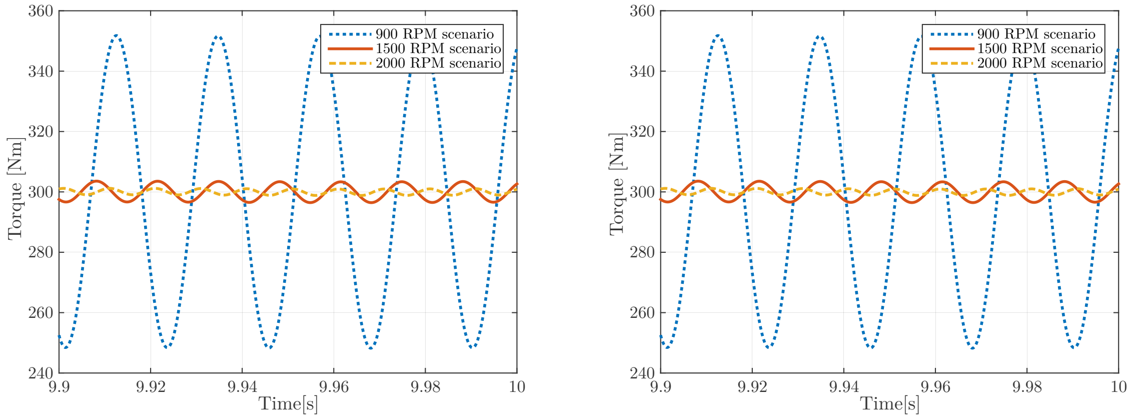

(a) Matlab model

(b) EasyDyn model

Figure 3.5 – gearbox input torque

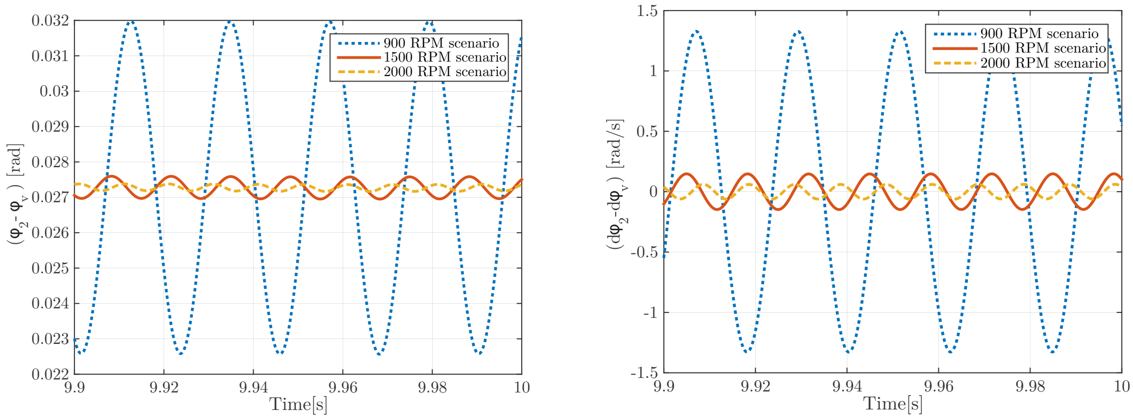

(a) $\varphi_v - \varphi_2$

(b) $\dot{\varphi}_v - \dot{\varphi}_2$

Figure 3.6 – Angular displacement/velocity between the secondary flywheel and the gearbox.

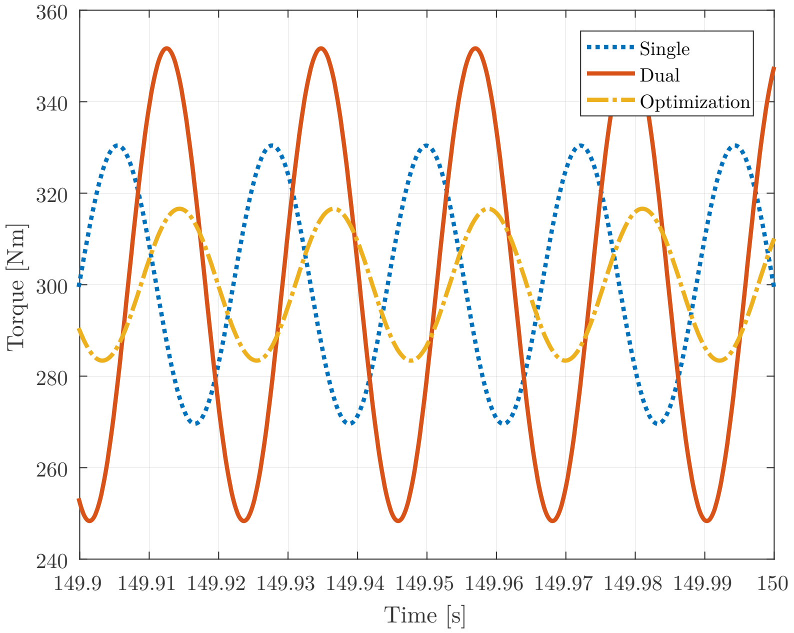

Figure 3.8 – Comparison of the gearbox input torque for different models.

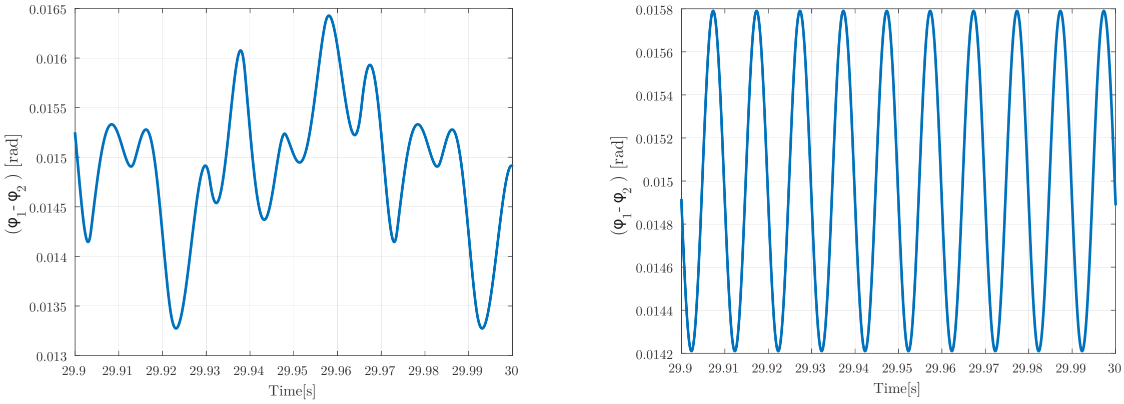

(a) With the default tolerance (1×10^{-3})

(b) With a tolerance of (1×10^{-5})

Figure 3.7 – Deflection angle between the flywheels $(\varphi_1 - \varphi_2)$ using the Matlab model with different tolerances.

Nevertheless, a right value of the stiffness and the damper coefficients has to be chosen. A wrong value of them can cause bad output properties.
If the Dual Mass flywheel is replaced by a Single Mass flywheel, Figure 3.8 can show that the initial example does not have as nice output properties as we expected.
In fact, if the dual mass flywheel is replaced by a single mass flywheel, we can observe that the torque fluctuations are lower by using only one mass. For this comparison, all the inertia from the second flywheel is moved to the first one assuming the same properties of the gearbox input shaft (c_2 and k_2).
Fortunately, Figure 3.8 also shows that it is possible to obtain better properties by using right value of the design parameters.

3.4.3 Selection of objective functions

As the previous figures show the gearbox input torque fluctuations are well reduced, but it might be possible to obtain better output properties. In order to optimize the DMTDVA, objective functions (OFs) are chosen, they will depend on:

- the following design parameters:
  - J_1, J_2, k_1, k_2, c_1, c_2
- a given set of Engine Operational Scenarios (EOS):
  - $M_{e_1}(t)$, $M_{e_2}(t)$, $M_{e_3}(t)$
- the output angular velocity:
  - ω_v

The objective functions will be measured once the transient time is established. Notice that the transient time increases with the increase of the inertia (J_1, J_2) and the primary stiffness coefficient (k_1) while it decreases with the increase of the secondary stiffness coefficient (k_2) and the damping coefficients (c_1, c_2).

3.4.3.1 Objective function 1

The main purpose of the DMTDVA is to reduce variation of the gearbox input torque. The first OF, called OF1 is:

$$OF1 = \sqrt{\frac{1}{N-1}\sum_{i=1}^{N}(M_v(i) - M_{v_{mean}})^2} \tag{3.12}$$

It is the corrected sample standard deviation. In fact, the standard deviation is a measure which quantifies the dispersion of a set of data. That way, the smaller OF1, the better the torque fluctuations are reduced.

3.4.3.2 Objective function 2

By reducing vibration, some energy is lost, in the interest of quantifying this energy, the following objective function, called OF2 is introduced:

$$OF2 = mean\left(\frac{1}{2}c_1(\dot{\varphi}_2 - \dot{\varphi}_1)^2 + \frac{1}{2}c_2(\dot{\varphi}_2 - \dot{\varphi}_v)^2\right) \tag{3.13}$$

This function will thus take into account the losses coming from the dampers.

3.5 Sensitivity analysis

In this section, the influence of the design parameters on the OFs mentioned previously will be studied.

This analysis has been performed for the three scenarios. That way, the influence of the engine speed can also be considered.

At first glance, we can notice that the parameters for a high engine speed do not affect the losses. The shape of the curve for the 900 RPM scenario differs from the other curves.

The curves of the variation of the damping coefficients c_1 and c_2 have the same global curves for the different scenarios. However, a low engine speed will have a bigger negative impact on the torque fluctuation.
As the previous torsional vibration analysis shows, torque fluctuations decrease with the increase in the engine speed. In fact, the curve from the third scenario is situated below the second scenario which is below the first one.
Finally, from the sensitivity analysis of the design parameters, the following observations can be made:

- **Damping coefficients**: Figures 3.10 outline that the increase in c_1 will decrease the torque fluctuations. The gearbox input torque depends on the deflection angle and its time derivative between the secondary flywheel and the gearbox side. The design parameters c_2 and k_2 are fixed. The increase of c_1 increases the deflection angle between the flywheels while the transient time is reduced. The deflection angle between the secondary flywheel and the gearbox input shaft has the same behaviour as the other deflection angle. Figure 3.9 shows this effect for a value of c_1=0 Nm.s/rad and c_1=38 Nm.s/rad.

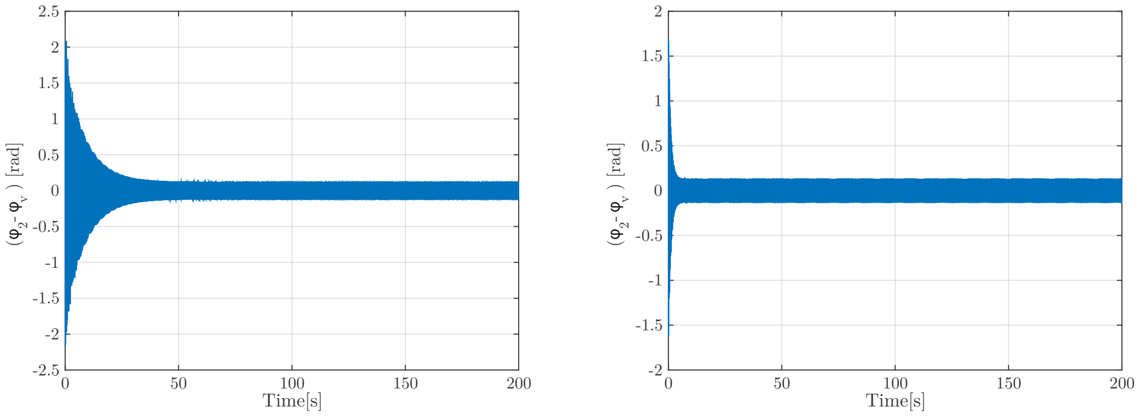

(a) for c_1=0 Nm.s/rad

(b) for c_1=38 Nm.s/rad

Figure 3.9 – Time history of the deflection angle for different damping coefficient values.

That way, torque fluctuations are increased. Notice that the opposite effect appears in the first scenario. In fact, the frequency of the first scenario (45 Hz) is close to an eigenfrequency of the system. Eigenfrequencies are outlined later in this document.
Figure 3.10 shows increasing c_1 will produce bigger losses. Actually the loss expression directly depends on c_1.
Increasing c_2 increases the torque fluctuations. In fact, the gearbox input torque directly depends on c_2: the increase in c_2 returns a higher value of the first part of the gearbox input torque ($c_2(\dot{\varphi}_2 - \dot{\varphi}_v)$) while the second part ($k_2(\varphi_2 - \varphi_v)$) changes lightly.

- **Inertia**: Figures 3.12 and 3.13, we can observe that for low values of J_1 there is a drop of the torque fluctuation. But for higher value, the torque fluctuation tends to zero. Similar results are obtained for the secondary inertia J_2.

One peak is observed for the first scenario (900 RPM) at each inertia.
The peaks occur for a value of 0.3 and 0.5 $kg.m^2$ for the primary and secondary flywheel, respectively. They come from the eigenfrequencies which are studied in Section 3.7.

- **Stiffness coefficients**: Figures 3.14 and 3.15 show the influence of the stiffness parameters. The shape of the curves are again similar to both parameters. A peak occurs for a value close to 3 $\times 10^4$ Nm/rad for the first scenario. For the other scenarios the increase in k_1 and k_2 will slightly affect the torque fluctuation and the losses. Figures also show that the lower the stiffness value, the better output properties. Nevertheless, there is a physical limit. If the stiffness decreases, the motion between the 2 flywheels will increase and lead to a large-sized flywheel. In fact, it is not conceivable to have completely compressed springs which lead to undesirable bump. For this reason, manufacturers use two-step springs which are composed of 2 springs with different stiffness.

From these figures we can see that the excitation frequency affects the properties of the system. Figure 3.16 shows the impact of the input frequency on the OFs. Two peaks appear on the chart, they correspond to the eigenfrequencies of the mechanical system which are:

- $f_{n1} = 9.3$ Hz
- $f_{n2} = 38.8$ Hz

This chart shows the interest to avoid the eigenfrequencies which occur more torque fluctuations and more losses.
The charts can not be explained more with the time domain information but the study of the frequency domain will clarify them.

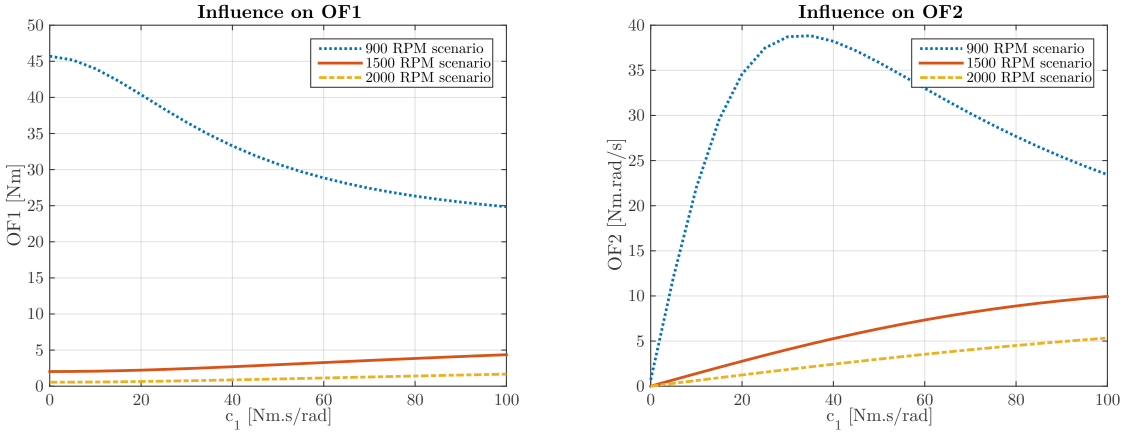

Figure 3.10 – Influence of c_1 on the OFs

3.5.1 Conclusion

Some curves have a peak which is linked to the eigenfrequencies. The frequency analysis will be realised later.

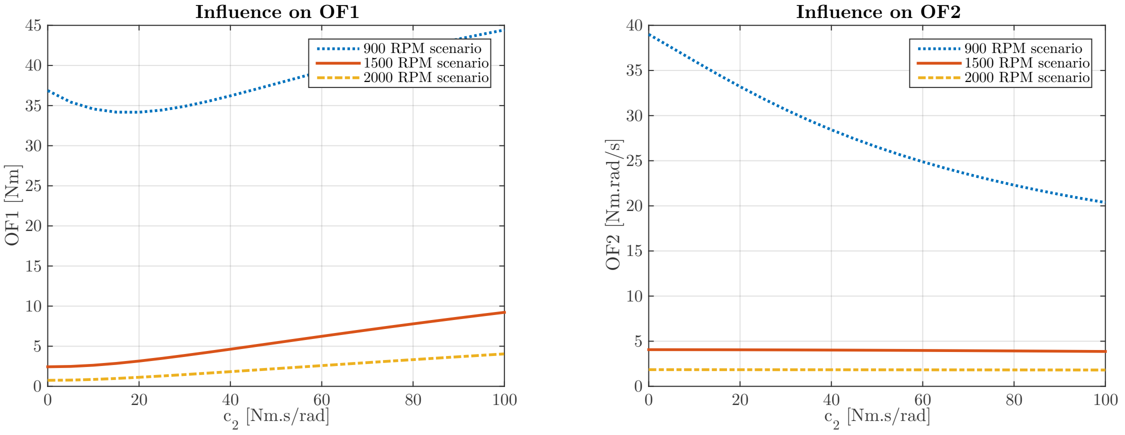

Figure 3.11 – Influence of c_2 on the OFs

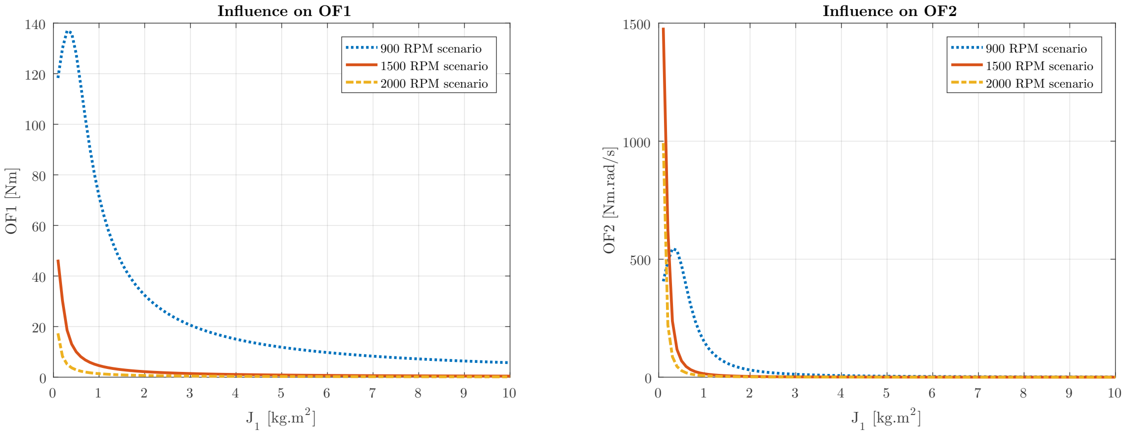

Figure 3.12 – Influence of J_1 on the OFs

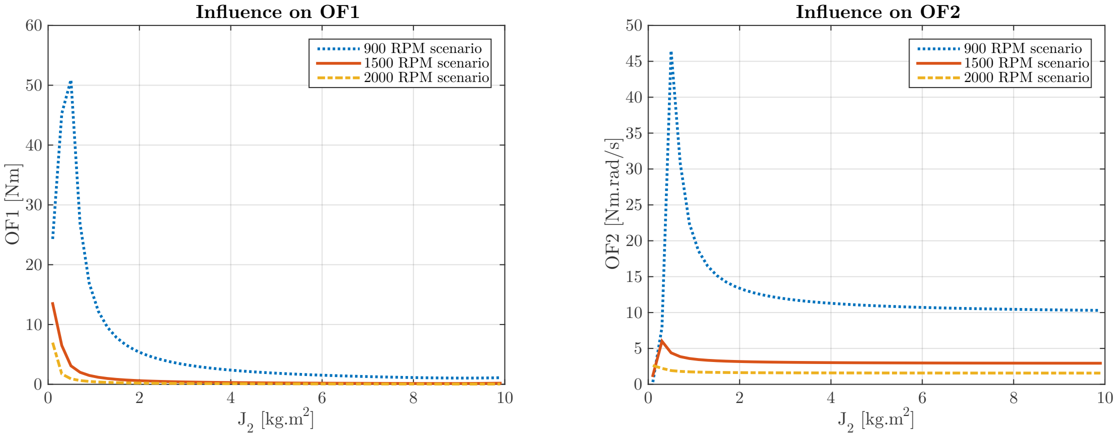

Figure 3.13 – Influence of J_2 on the OFs

In general, to reduce the torque fluctuations we can act on the followings actions:

- Decreasing the damping and stiffness coefficients
- Increasing the inertias

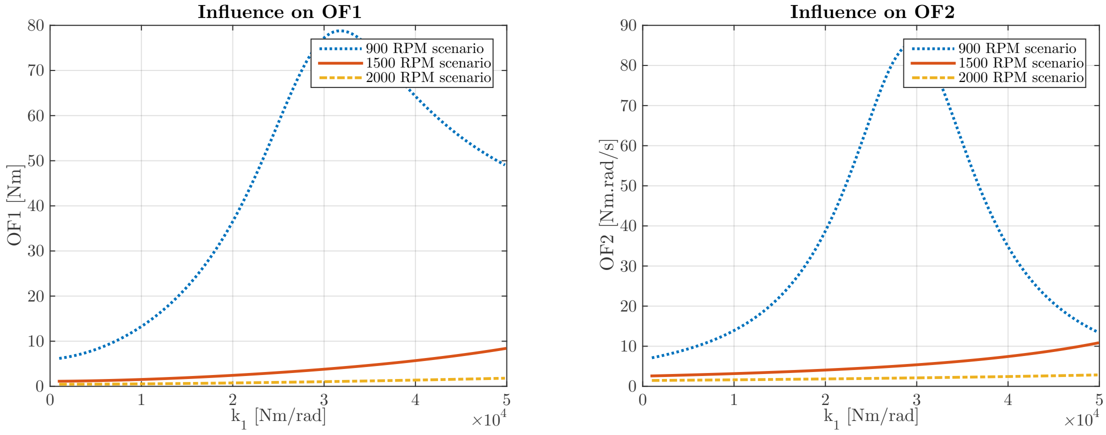

Figure 3.14 – Influence of k_1 on the OFs

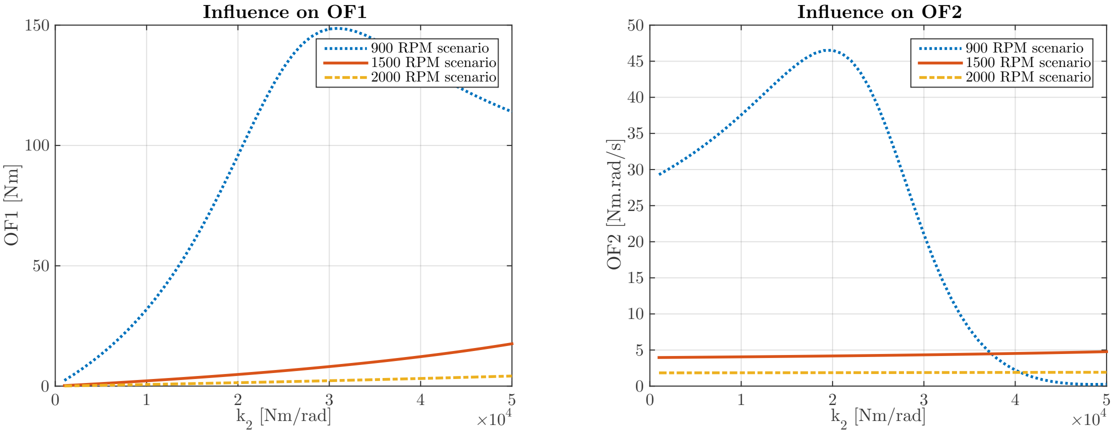

Figure 3.15 – Influence of the stiffness coefficient k_2 on the OFs.

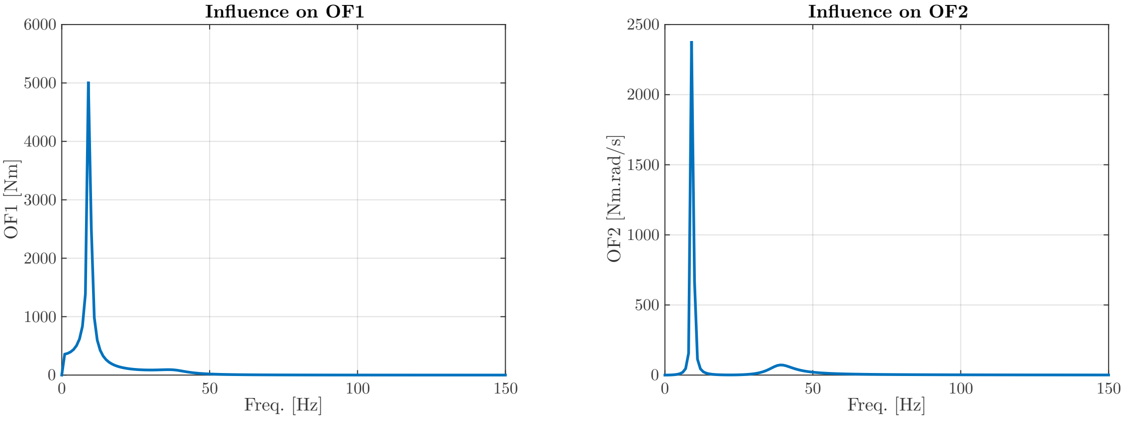

Figure 3.16 – Influence of the input frequency on the OFs.

Optimization with the $fminsearch$ function of Matlab has been realized in the following section. The optimization should confirm the previous conclusions.

3.6 Optimization

We have seen that for some values of the design parameters, the gearbox input torque fluctuations and the losses have a less significant impact. This section will try to optimize the DMTDVA. Optimization of the both previous OFs has been performed using the $fminsearch$ function of Matlab. $fminsearch$ will search the local extrema of an objective function of several variables. This function is based on the simplex method of Lagarias [26]. For further information the reader can be referred to [27].
$fminsearch$ function requires:

- A function to optimize
- Initial values of the parameters used in this function

It is necessary to use bounds in order to avoid physically non-understandable values. Lower and upper bounds are added to this function.
The functions to optimize are being the OFs.
The initial values used are the values used in the previous simulations (according to [25]):

- $J_1 = 1.8\ kg.m^2$
- $J_2 = 0.6\ kg.m^2$
- $c_1 = 30\ Nms/rad$
- $c_2 = 1\ Nms/rad$
- $k_1 = 20\ 000 Nm/rad$
- $k_2 = 11\ 000 Nm/rad$

With regard to the lower and upper bounds, a reasonable range is to use +/- 50 % on these initial values. In this way, the software can not return negative values, too high or too low values which ensure that the system is realistic.
Optimization has been performed for 3 input frequencies: 45 Hz, 75 Hz and 100 Hz.

The different results of the optimization are shown in Table 3.1 and 3.2 for OF1 and OF2 respectively. We can see that each optimization returns approximately the same result. That way, an optimization of OF1 provides an optimization of OF2 and vice versa.
The upper bounds of the inertia are reached. In fact, increasing the inertia improves the properties. But the inertia can not be too large, since there is a limited amount of available space.
The lower bounds of the stiffness are also reached. But a torsional spring with a too low stiffness is not possible for the reasons mentioned above. Apart from the choice of the optimal value of c_2, the results of the optimization are in agreement with the previous sensitivity analysis. In fact, the optimal value c_2 is not the upper bounds as we could expect. It is important to remind that $fminsearch$ is a local method. Note also that $fminsearch$ provides a better optimization that $fmincon$ for our problem. $fmincon$ is also a local method but it is a gradient methods.

		J_1 $[kg.m^2]$	J_2 $[kg.m^2]$	k_1 [Nm/rad]	k_2 [Nm/rad]	c_1 [Nms/rad]	c_2 [Nms/rad]	OF1 [Nm]	OF2 [Nm.rad/s]
Lower bounds		0.9	0.3	1.00E+04	5.5E+03	15	0.5		
Initial values		1.8	0.6	2.00E+04	1.10E+04	30	1	900 RPM 36.54 1500 RPM 2.44 2000 RPM 0.77	900 RPM 38.72 1500 RPM 4.07 2000 RPM 1.85
Upper bounds		2.7	0.9	3.00E+04	1.65E+04	45	1.5		
Returned Values	900 RPM	2.7	0.9	1.0E+04	5.5E+03	15	0.88	1.83	2.47
	1500 RPM	2.7	0.9	1.0E+04	5.5E+03	15	1.44	0.22	0.67
	2000 RPM	2.7	0.9	1.0E+04	5.5E+03	15	1.5	0.08	0.35

Table 3.1 – Optimization of OF1 for 3 different scenarios

		J_1 $[kg.m^2]$	J_2 $[kg.m^2]$	k_1 [Nm/rad]	k_2 [Nm/rad]	c_1 [Nms/rad]	c_2 [Nms/rad]	OF1 [Nm]	OF2 [Nm.rad/s]
Lower bounds		0.9	0.3	1.00E+04	5.5E+03	15	0.5		
Initial values		1.8	0.6	2.00E+04	1.10E+04	30	1	900 RPM 36.54 1500 RPM 2.44 2000 RPM 0.77	900 RPM 38.72 1500 RPM 4.07 2000 RPM 1.85
Upper bounds		2.7	0.9	3.00E+04	1.65E+04	45	1.5		
Returned Values	900 RPM	2.7	0.9	1.00E+04	5.5E+03	15	0.5	1.83	2.47
	1500 RPM	2.7	0.9	1.00E+04	5.5E+03	15	1.29	0.22	0.67
	2000 RPM	2.7	0.9	1.00E+04	5.5E+03	15	1.5	0.08	0.35

Table 3.2 – Optimization of OF2 for 3 different scenarios

3.6.1 Implementation of the optimal values into the mathematical model

The first objective function has the objective of reducing the torque fluctuations. Figures 3.17 and 3.18 illustrate the benefits of the optimization for the first scenario. In fact, these figures show that the fluctuations of the angular displacement, the angular velocity and the gearbox input torque are reduced.
The torque fluctuations are well reduced as well as the fluctuations of angular displacement/velocity. All the time, a mechanical part is subjected to fatigue. That way, the optimization will reduce this phenomenon. By reducing the vibrations, the driving comfort is also improved. Figures also show that a phase shift occurs between the initial and optimal case due to the reduction of the damping coefficients. Figures 3.17 (a) and (c) shows that another average value of the deflection angles is obtained. In fact, the optimization reduces the values of the stiffness coefficients. A modification of the stiffness properties leads to a modification of the equilibrium position of the dual mass flywheel. Figure 3.18 shows that for the initial case the peak-to-peak amplitude value is 103.4 Nm, the optimization reduce it until 5.2 Nm. The torque fluctuations are thus reduced by a factor of 20. Similar results are obtained for the second and third scenario. Appendix E exposes these different results.

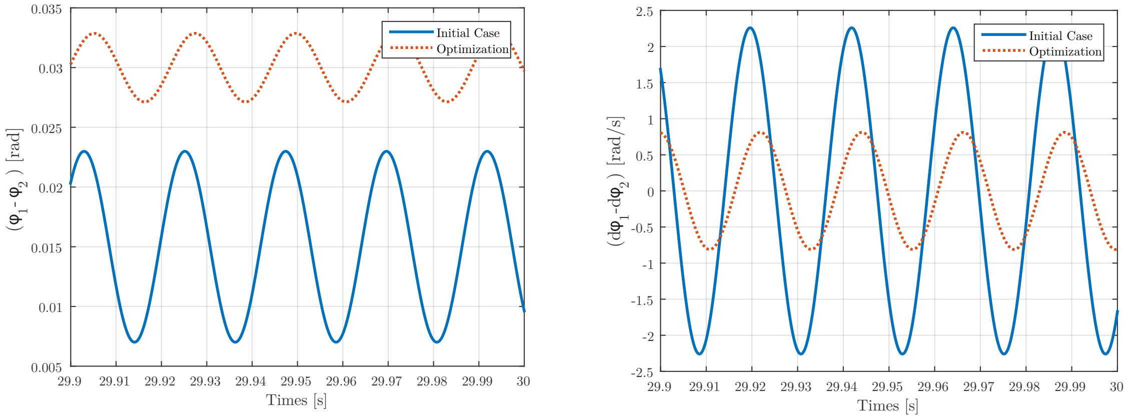

(a) $\varphi_1 - \varphi_2$ (b) $\dot{\varphi}_1 - \dot{\varphi}_2$

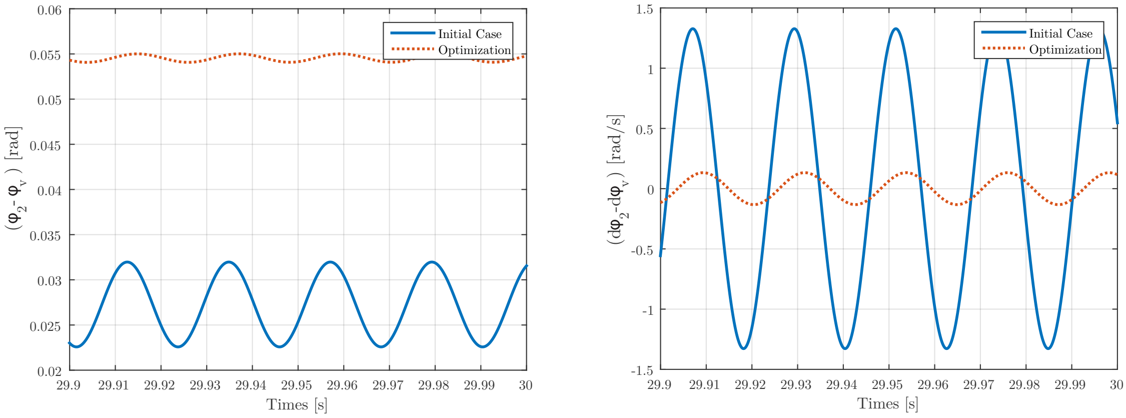

(c) $\varphi_2 - \varphi_v$ (d) $\dot{\varphi}_2 - \dot{\varphi}_v$

Figure 3.17 – Benefits of the optimization on the different deflection angles and their time derivatives.

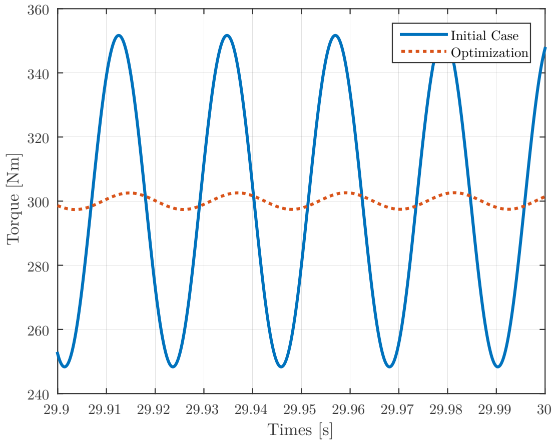

Figure 3.18 – Benefits of the optimization of the gearbox input torque.

3.7 Frequency analysis

The system has 2 degrees of freedom, 2 eigenvalues are thus expected. If a proportional damping is assumed, it means that $[C] = \alpha[M] + \beta[K]$. The characteristic equation is:

$$det(\lambda^2[M] + \lambda[C] + [K]) = 0 \tag{3.14}$$

The roots of this equation can be given as:

$$\lambda_k = -\xi_k \omega_k + j\omega_k \sqrt{1 - \xi_k^2} \tag{3.15}$$

with:

- $\omega_k = \sqrt{Im^2(\lambda_k) + Re^2(\lambda_k)}$ (the pulsation)
- $\xi_k = \dfrac{-Re(\lambda_k)}{Im^2(\lambda_k) + Re^2(\lambda_k)}$ (the damping rate)

The degree of freedom of the system is 2, 2 × 2 pairs of poles λ_k will be obtained. From these poles, the pulsations and the damping rate can be deduced.

For the different cases of study, the same inertia, damping and stiffness matrix are used and thus the same eigenvalues will be obtained:

- $\omega_{n1} = 58.6291$ rad/s which corresponds to $f_{n1} = 9.3Hz$
- $\omega_{n2} = 243.4370$ rad/s which corresponds to $f_{n1} = 38.8Hz$

These frequencies are below the excitations frequencies (45 Hz to 100 Hz). We have to ensure that values from the optimization do not move them inside the range from 45 Hz to 100 Hz.

3.7.1 Sensitivity analysis of the eigenfrequencies

3.7.1.1 Eigenfrequencies values

This subsection will show the influence of the design parameters on the eigenfrequencies. Each parameters will be varied one by one. It is necessary to impose one value on the other parameters, when one is varied. The imposed values are the same as the previous.

- **Inertia:** The increase in the inertia will decrease the value of the eigenfrequencies. Figure 3.19 shows that the decrease of the secondary inertia has a bigger impact on the eigenfrequencies than the primary inertia. One explanation of that is that when J_1 is taken as a variable, the fixed value of J_2 is 0.6 $kg.m^2$ while for the variation of J_2 the fixed value of J_1 is bigger (1.8 $kg.m^2$). For low values of inertia, there is an exponential decrease of the frequencies with the increase in the inertia. After a value of 6 $kg.m^2$, the second eigenfrequency is no longer affected while the first eigenfrequency is steadily decreasing.
- **Stiffness coefficient:** Figure 3.20 shows the influence of the stiffness coefficients, k_1 and k_2 on the eigenfrequencies. The increase of stiffness will increase the value of the eigenfrequencies. The second eigenfrequency is more affected by the stiffness than the second one. The attentive reader can also remark that if k_1 is equal to 3E+04 Nm/rad, an eigenfrequency appears at 45 HZ which explains the peak that we obtain at Figure 3.14 for the first scenario which corresponds to 45 Hz.

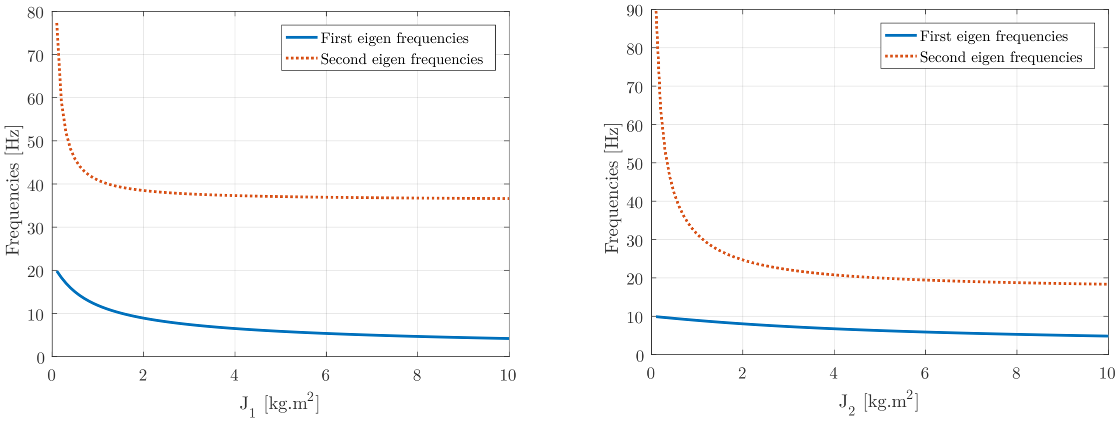

(a) Influence of inertia of the primary flywheel, J_1

(b) Influence of inertia of the secondary flywheel, J_2

Figure 3.19 – Influence of inertia on the eigenfrequencies.

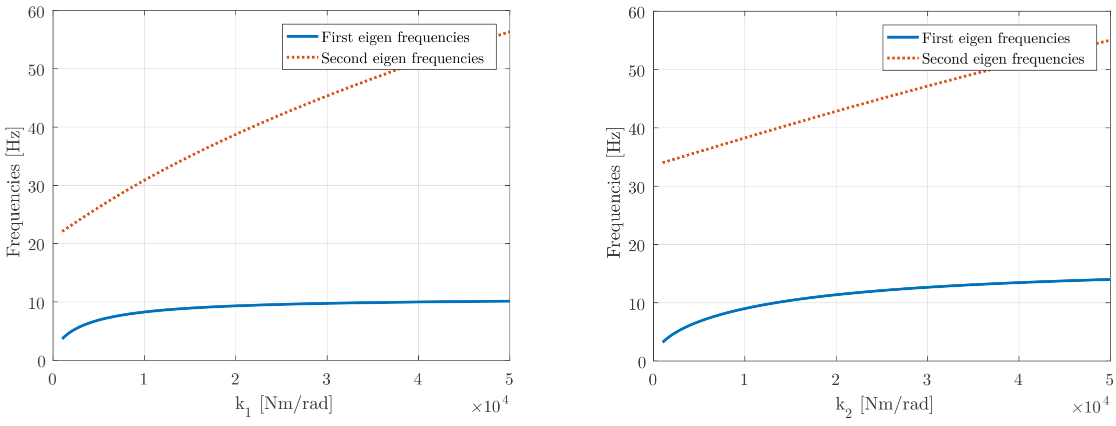

(a) Influence of the stiffness between the flywheels, k_1

(b) Influence of the stiffness of the output shaft, k_2

Figure 3.20 – Influence of the stiffness.

From Figures 3.19 and 3.20, we can deduce that the eigenfrequencies are affected by the stiffness coefficients and the inertia.

Here, we only analyse at the eigenfrequencies values but it is also interesting to analyse how the amplitude of the frequency response varies for different design parameters.

3.7.1.2 Amplitude of the frequency response

Figures 3.21 and 3.22 show the amplitude of the frequency response. This frequency response is in a dimensionless space. The expression will be detailed further down. Note that, the x-axis is limited to 80 Hz because nothing different happens after this value.

We have a look at the influence of the design parameters on the this frequency response.

Two different values of each design parameters are selected: a low and a high value.

From Figure 3.21 (a) and (b), we can clearly see that the peak of the secondary eigenfrequency will disappear for high value of c_1. This can explain the decrease in the torque fluctuation with the increase in the damping factor c_1 for the first scenario in Figure 3.10. Figure 3.21 (c) and (d) shows the impact of c_2 (for low and high value) on the frequency response.

Figure 3.21 (e), (f) and Figure 3.22 (a) and (b) show that the increase of k_1 and k_2 will move the peaks as we deduced from the eigenfrequencies. However, the amplitude of these peaks are also affected.

Figure 3.22 (c) and (d) shows that the increase of J_1 will reduce the width of the first peak but it will also increase the amplitude of the second one.

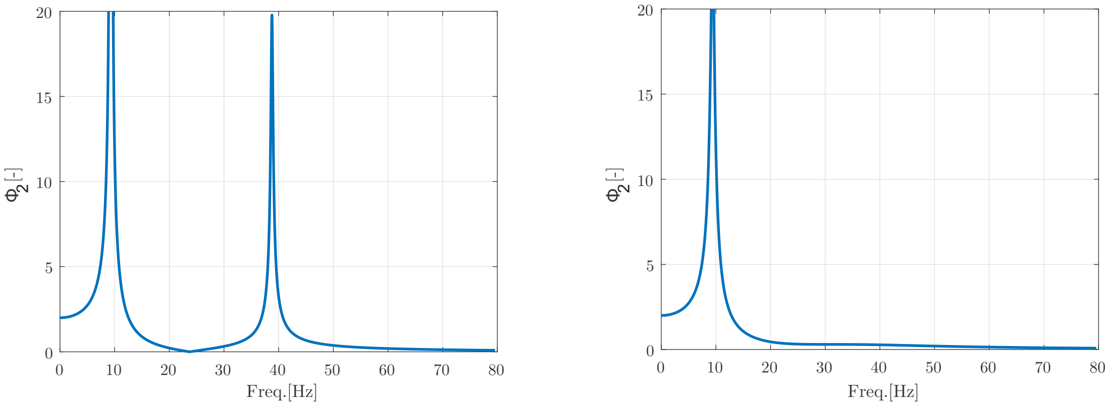

(a) For low value of c_1 ($0.1\ Nm.s/rad$)

(b) For high value of c_1 ($50\ Nm.s/rad$)

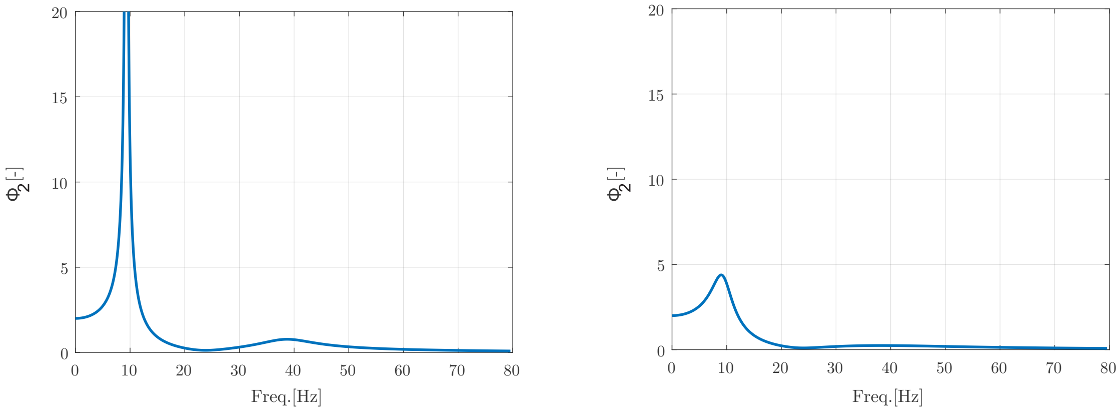

(c) For low value of c_2 ($0.1\ Nm.s/rad$)

(d) For high value of c_2 ($50\ Nm.s/rad$)

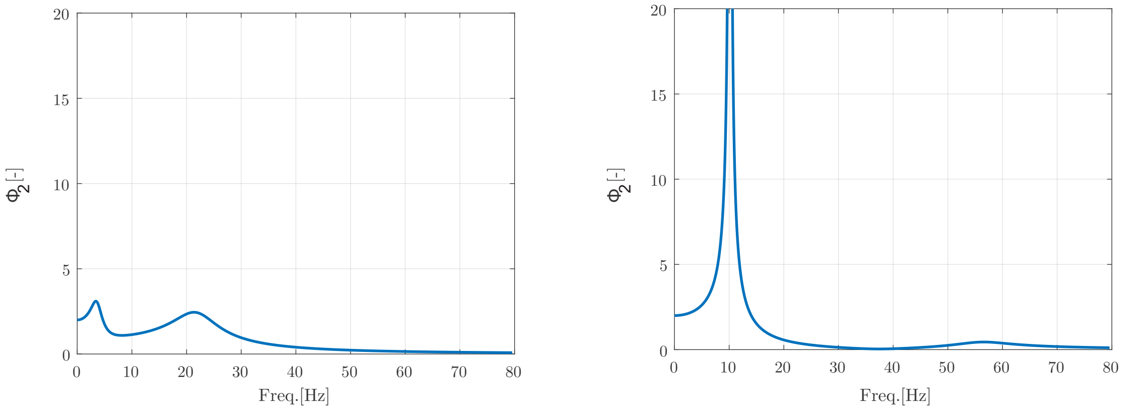

(e) For low value of k_1 ($1 \times 10^3\ Nm/rad$)

(f) For high value of k_1 ($5 \times 10^4\ Nm/rad$)

Figure 3.21 – Influence on the frequency response of the secondary flywheel .

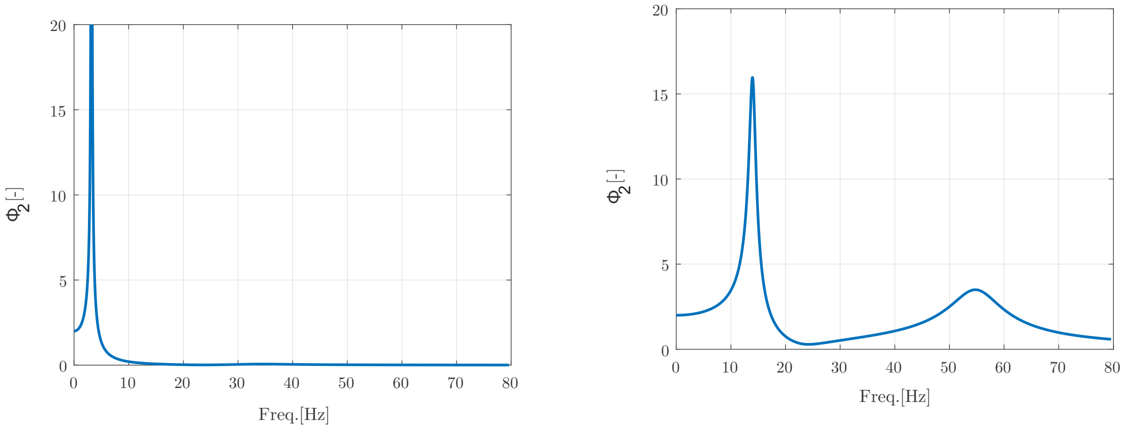

(a) For low value of k_2 (1×10^3 Nm/rad)

(b) For high value of k_2 (5×10^4 Nm/rad)

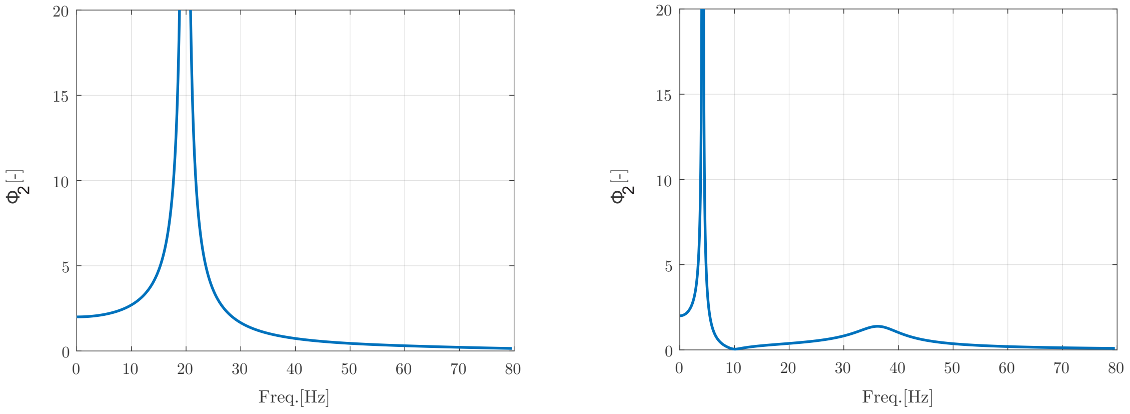

(c) For low value of J_1 (1 $kg.m^2$)

(d) For high value of J_1 (10 $kg.m^2$)

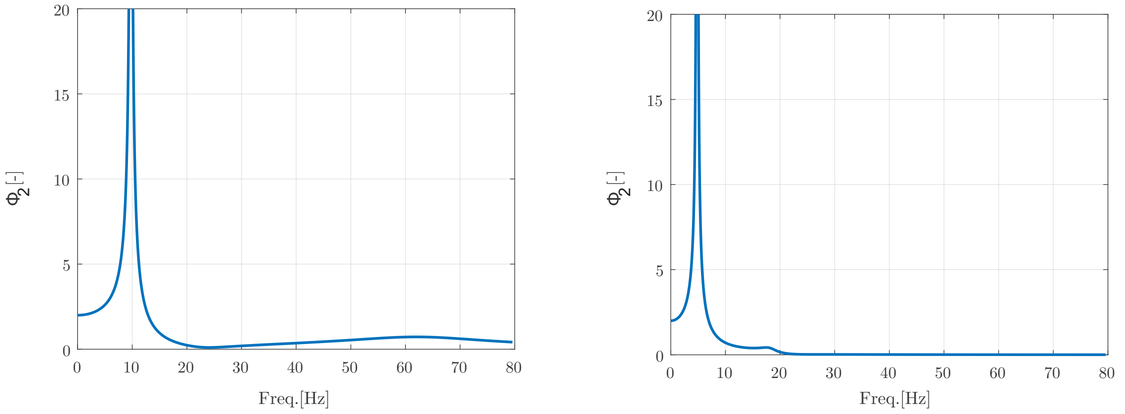

(e) For low value of J_2 (1 $kg.m^2$)

(f) For high value of J_2 (10 $kg.m^2$)

Figure 3.22 – Influence on the frequency response of the secondary flywheel .

3.7.1.3 Eigenfrequencies with the optimization of OF1 and OF2

This part will pay attention to the different values obtained from the optimization of OF1 and OF2. In fact, these values will move the eigenfrequencies, and it is important that the eigenfrequencies do not appear in the commonly used range (45 Hz to 100 Hz).

	f_{n1}[Hz]	f_{n2}[Hz]
Inital	9.33	38.74
Optimization	5.38	22.38

Table 3.3 – Eigenfrequencies obtained with the optimization

By looking at Table 3.3, the values of the eigenfrequencies are out of the used range. Moreover, the eigenfrequencies are moved to lower values, distancing the frequency range of use.

3.7.2 Frequency resolution

The equations of motion were obtained at the section 3.2 where they are solved in the time domain. The resolution in the frequency domain is approached in this subsection.

$$J_1\ddot{\varphi}_1 + c_1(\dot{\varphi}_1 - \dot{\varphi}_2) + k_1(\varphi_1 - \varphi_2) = M_e(t) \tag{3.16}$$

$$J_2\ddot{\varphi}_2 + c_1(\dot{\varphi}_2 - \dot{\varphi}_1) + k_1(\varphi_2 - \varphi_1) + c_2(\dot{\varphi}_2 - \dot{\varphi}_v) + k_2(\varphi_2 - \varphi_v) = 0 \tag{3.17}$$

with $c_2(\dot{\varphi}_2 - \dot{\varphi}_v) + k_2(\varphi_2 - \varphi_v)$, the gearbox input torque, M_v(t).
If the primary mass is excited by an external harmonic torque: $M_e(t)$=$M_e e^{j\omega t}$, the steady-state harmonic responses can be written as:

$$\varphi_1(t) = \Phi_1 e^{j\omega t} \quad and \quad \varphi_2(t) = \Phi_2 e^{j\omega t} \tag{3.18}$$

Introducing these expressions into Equations 3.16 and 3.17:

$$J_1(-\omega^2\Phi_1 e^{j\omega t}) + c_1((j\omega\Phi_1 e^{j\omega t}) - (j\omega\Phi_2 e^{j\omega t})) + k_1(\Phi_1 e^{j\omega t} - \Phi_2 e^{j\omega t}) = M_e e^{j\omega t} \tag{3.19}$$

$$\begin{aligned} &J_2(-\omega^2\Phi_2 e^{j\omega t}) + c_1((j\omega\Phi_2 e^{j\omega t}) - (j\omega\Phi_1 e^{j\omega t})) \\ &+ k_1(\Phi_2 e^{j\omega t} - \Phi_1 e^{j\omega t}) + c_2(j\omega\Phi_2 e^{j\omega t}) + k_2(\Phi_2 e^{j\omega t}) = M_{v_1} e^{j\omega t} \end{aligned} \tag{3.20}$$

These equations can then be written as:

$$\Phi_1(-\omega^2 J_1 + j\omega c_1 + k_1) - \Phi_2(j\omega c_1 + k_1) = M_e \tag{3.21}$$

$$\Phi_2(-\omega^2 J_2 + j\omega c_1 + k_1 + j\omega c_2 + k_2) - \Phi_1(j\omega c_1 + k_1) = M_{v_1} \tag{3.22}$$

This equation system can be written in a matrix format:

$$\begin{bmatrix} -J_1\omega^2 + j\omega c_1 + k_1 & -k_1 - j\omega c_1 \\ -j\omega c_1 - k_1 & -J_2\omega^2 + j\omega c_1 + k_1 + j\omega c_2 + k_2 \end{bmatrix} \begin{pmatrix} \Phi_1 \\ \Phi_2 \end{pmatrix} = \begin{pmatrix} M_e \\ M_{v_1} \end{pmatrix} \tag{3.23}$$

$$\Big[A\Big]\Big(\Phi\Big) = \Big(M\Big) \tag{3.24}$$

This system can be solved via Cramer's rule:

$$\Phi_1 = \frac{M_e(-J_2\omega^2 + j\omega c_1 + k_1 + j\omega c_2 + k_2) - M_{v_1}(-j\omega c_1 - k_1)}{Det(A)} \tag{3.25}$$

$$\Phi_2 = \frac{M_{v_1}(-J_1\omega^2 + j\omega c_1 + k_1) - M_e(-j\omega c_1 - k_1)}{Det(A)} \tag{3.26}$$

With:

$$Det(A) = (-J_1\omega^2 + c_1 j\omega + k_1)(-J_2\omega^2 + j\omega c_1 + k_1 + k_1 + j\omega c_2 + k_2) - (-j\omega c_1 - k_1)^2 \tag{3.27}$$

To come back in the time domain we just need to multiply Φ_1 and Φ_2:

- by $e^{j\omega t}$, to have the angular displacement
- by j$\omega e^{j\omega t}$, to have the angular velocity
- by - $\omega^2 e^{j\omega t}$, to have the angular acceleration

We can compare the different results from the frequency domain to the time domain from Matlab. In order to realize the comparison, the scenario 1 is taken but the mean speed and engine torque will be assumed as equal to 0. The difference of the angular displacement/velocity between the primary and secondary flywheel is compared at Figure 3.23. For both models we obtain the same curves: same peak-to-peak value is obtained as well as the mean value. We do not see a phase shift between these models.
In fact, a phase shift of 90 degrees should appear because the torque in time domain the engine torque is equal to 500 × $sin(\omega t)$. But from the frequency to the time domain, the mean torque is multiplied by $e^{j\omega t}$. At time t=0, the mean torque is equal to zero in the first case but equal to 500 in the second case. The results on Figure 3.23 are just multiply by $-i$ to have the same phase.

One of the goals of a Dual Mass Flywheel is to move the peaks in order to avoid resonance into the used range. But it is also interesting reduce the amplitude of the peaks and the area under the curve of the frequency response.

3.7.2.1 Selection of objective functions

This objective function should measure the maximum peak of the curve into the range of use. In fact the purpose is to ensure a response curve which is as flat as possible. A new objective function, called OF3 can be found:

$$OF3 = \max \text{ (peaks)} \tag{3.28}$$

This function can be easily introduced into Matlab via the *findpeaks* function.
The area under the frequency response curve can also be reduced, a fourth objective function can be found:

$$OF4 = \int_{45Hz}^{100Hz} \Phi_2 df \tag{3.29}$$

The integration will be performed by *trapz* function of Matlab.

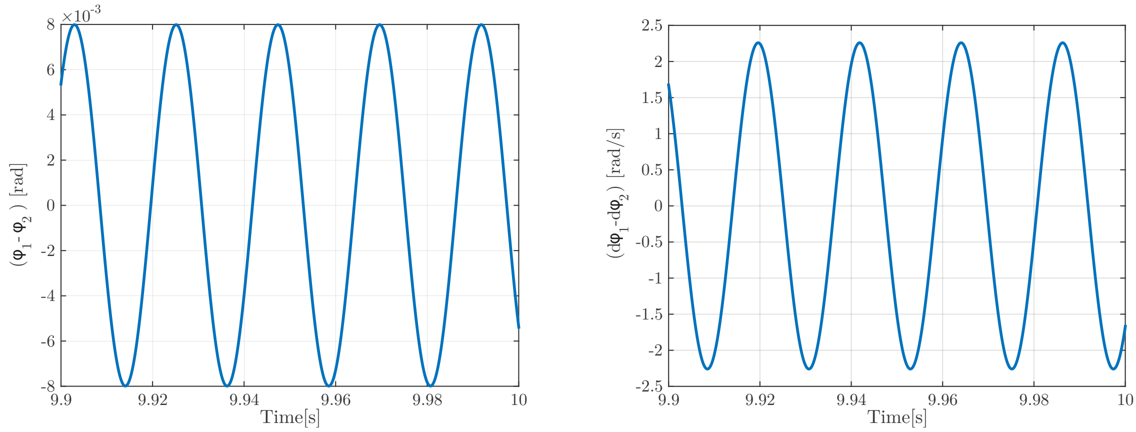

(a) $\varphi_1 - \varphi_2$ with the Matlab time domain model.

(b) $\dot{\varphi_1} - \dot{\varphi_2}$ with the Matlab time domain model.

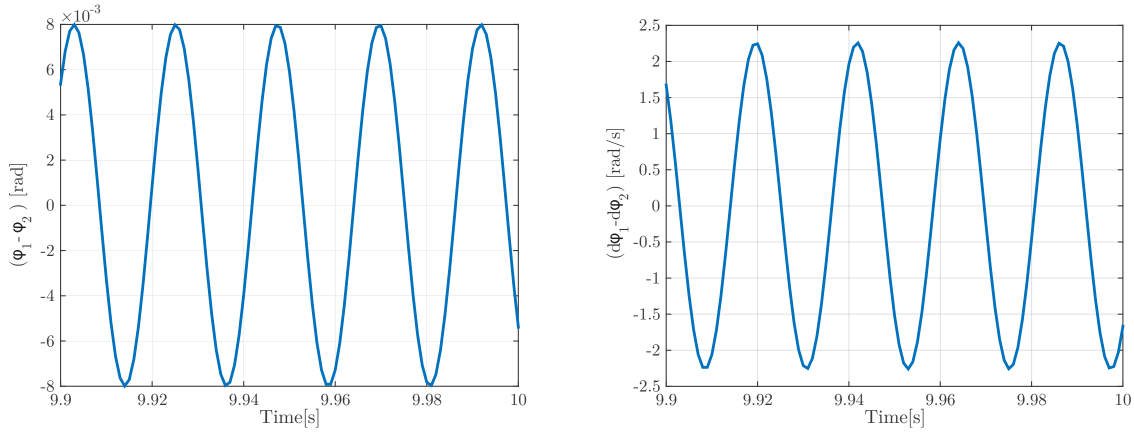

(c) $\varphi_1 - \varphi_2$ with the Matlab frequency domain model.

(d) $\dot{\varphi_1} - \dot{\varphi_2}$ with the frequency domain model.

Figure 3.23 – Comparison between the time domain and the frequency domain.

3.7.2.2 Optimization with *fminsearch*

An optimization has been performed with *fminsearch* using OF3 and OF4 as function to optimize. However, OF3 does not work in this case because no peak occurs in the used range with the initial values placed in Table 3.4. Only OF4 has thus been optimized with *fminsearch*. The lower and upper bounds used are the same as the optimization of OF1 and OF2. Table 3.4 is a summary table of the lower/upper bounds, initial values used for the optimization with *fminsearch*. Table 3.4 also gives the optimized values. Figure 3.24 shows the frequency response for the initial values of the secondary flywheel. Figure 3.24 explains the role of OF4 and shows that no peak occurs in the range of use.

3.7.2.3 Comparison with the other optimizations

A comparison of the different optimal values obtained with the optimization of OF1, OF2 and OF4 using *fminsearch* function can be easily done.

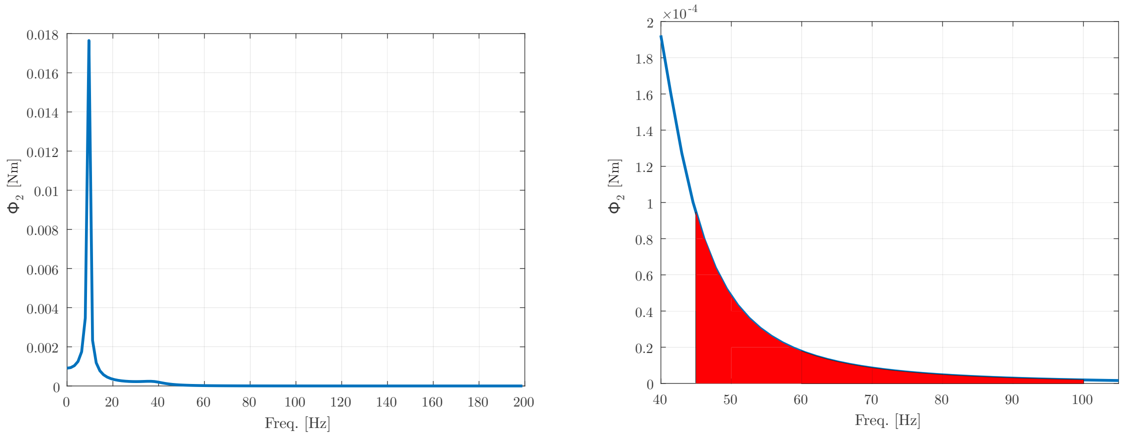

(a) Normal scale (b) Zoom in

Figure 3.24 – Frequency response of the secondary flywheel.

	J_1 $[kg.m^2]$	J_2 $[kg.m^2]$	k_1 [Nm/rad]	k_2 [Nm/rad]	c_1 [Nms/rad]	c_2 [Nms/rad]	OF4 [ ]
Lower bounds	0.9	0.3	1.00E+04	5.5E+03	15	0.5	
Initial values	1.8	0.6	2.00E+04	1.10E+04	30	1	5.5E-04
Upper bounds	2.7	0.9	3.00E+04	1.65E+04	45	1.5	
Returned Values	2.7	0.9	1.0E+04	5.5E+03	15	0.5	7.6E-05

Table 3.4 – Optimization of OF4 with $fminsearch$

The great thing is that all the optimizations return approximately the same values of the design parameters. It could be possible to have objective functions which are opposite to each other but fortunately this is not the case.

The optimization of the time domain has the same effect as the optimization of frequency domain:

- Increase the inertia
- Reduce the stiffness coefficients
- Reduce the damping coefficients

3.7.3 Dimensional analysis

A dimensional analysis is performed in this part. This analysis allows to avoid a choice of the order of magnitude of the different parameters of the mechanical system. From Equation 3.26, Φ_2 can be split in 2 parts:

$$\Phi_2 = \Phi_{2_1} + \Phi_{2_2} \tag{3.30}$$

$$\Phi_{2_1} = \frac{M_{v_1}(-J_1\omega^2 + j\omega c_1 + k_1)}{Det(A)} \tag{3.31}$$

$$\Phi_{2_2} = \frac{-M_e(-j\omega c_1 - k_1)}{Det(A)} = \frac{M_e(j\omega c_1 + k_1)}{Det(A)} \tag{3.32}$$

The same applies for Φ_1, which can be split in 2 parts:

$$\Phi_1 = \frac{M_e(-J_2\omega^2 + j\omega c_1 + k_1 + j\omega c_2 + k_2) + M_{v_1}(k_1 + j\omega c_1)}{Det(A)} \tag{3.33}$$

$$\Phi_{=}\Phi_{1_1}+\Phi_{1_2} \tag{3.34}$$

$$\Phi_{1_1}=\frac{M_e(-J_2\omega^2+j\omega c_1+k_1+j\omega c_2+k_2)}{Det(A)} \tag{3.35}$$

$$\Phi_{1_2}=\frac{M_{v_1}(k_1+j\omega c_1)}{Det(A)} \tag{3.36}$$

The objective is to improve the output performance. The **frequency amplitude of the secondary flywheel** (Φ_2) will be treated. For the interested reader, the dimensional analysis is performed for the first flywheel at Appendix .

$$\frac{\Phi_{2_1}}{\frac{M_{v_1}}{k_2}}=\frac{-\omega^2J_1+c_1j\omega+k_1}{(-J_1\omega^2+c_1j\omega+k_1)(-\frac{J_2}{k_2}\omega^2+j\omega\frac{c_1}{k_2}+\frac{k_1}{k_2}+j\omega\frac{c_2}{k_2}+\frac{k_2}{k_2})-\frac{(k_1+j\omega c_1)^2}{k_2}} \tag{3.37}$$

If, the numerator and denominator are divided by J_1:

$$\frac{\Phi_{2_1}}{\frac{M_{v_1}}{k_2}}=\frac{-\omega^2+\frac{c_1j\omega}{J_1}+\frac{k_1}{J_1}}{(-\omega^2+\frac{c_1j\omega}{J_1}+\frac{k_1}{J_1})(-\frac{J_2}{k_2}\omega^2+j\omega\frac{c_1}{k_2}+\frac{k_1}{k_2}+j\omega\frac{c_2}{k_2}+\frac{k_2}{k_2})-\frac{(k_1+j\omega c_1)^2}{k_2J_1}} \tag{3.38}$$

These following dimensionless variable will be assumed:

$$\omega_1=\sqrt{\frac{k_1}{J_1}} \tag{3.39}$$

$$\omega_2=\sqrt{\frac{k_2}{J_2}} \tag{3.40}$$

$$\psi=\frac{\omega_1}{\omega_2} \tag{3.41}$$

$$\Omega=\frac{\omega}{\omega_2} \tag{3.42}$$

$$\mu=\frac{J_1}{J_2} \tag{3.43}$$

$$\xi_1=\frac{c_1}{2J_1\omega_1} \tag{3.44}$$

$$\xi_2=\frac{c_2}{2J_2\omega_2} \tag{3.45}$$

The numerator can be written as:

$$-\omega^2+\frac{c_1j\omega\boldsymbol{2\omega_1}}{J_1\boldsymbol{2\omega_1}}+\frac{k_1}{J_1}=-\omega^2+2\xi_1\omega_1j\omega+{\omega_1}^2 \tag{3.46}$$

Regarding the denominator:

$$(-\omega^2+\frac{c_1j\omega}{J_1}+\frac{k_1}{J_1})(-\frac{J_2}{k_2}\omega^2+j\omega\frac{c_1}{k_2}+\frac{k_1}{k_2}+j\omega\frac{c_2}{k_2}+\frac{k_2}{k_2})-\frac{(k_1+j\omega c_1)^2}{k_2J_1}=ab-c \tag{3.47}$$

a can be written as:

$$(-\omega^2 + \frac{c_1 j\omega}{J_1} + \frac{k_1}{J_1}) = (-\omega^2 + \frac{c_1 j\omega \mathbf{2}\boldsymbol{\omega_1}}{J_1 \mathbf{2}\boldsymbol{\omega_1}} + \omega_1^2) = (-\omega^2 + 2j\omega\xi_1\omega_1 + \omega_1^2) \tag{3.48}$$

b can be written as:

$$(-\frac{J_2}{k_2}\omega^2 + j\omega\frac{c_1}{k_2} + \frac{k_1}{k_2} + j\omega\frac{c_2\mathbf{2}}{k_2\mathbf{2}} + \frac{k_2}{k_2}) = (-\frac{\omega^2}{{\omega_2}^2} + j\omega\frac{c_1\mathbf{2}\boldsymbol{J_1\omega_1}}{{\omega_2}^2 J_2\mathbf{2}\boldsymbol{J_1\omega_1}} + \frac{k_1}{k_2} + j\omega\frac{c_2\mathbf{2}}{{\omega_2}^2 J_2\mathbf{2}} + 1) \tag{3.49}$$

$$= (-\Omega^2 + 2j\Omega\mu\xi_1\psi + \psi^2\mu + 2j\Omega\xi_2 + 1) \tag{3.50}$$

And c can be written as:

$$\frac{(k_1 + j\omega c_1)^2}{k_2 J_1} = \frac{1}{k_2 J_1}(k_1^2 + 2k_1 j\omega c_1 - \omega^2 c_1^2) \tag{3.51}$$

$$= \frac{k_1^2}{k_2 J_1} + \frac{2k_1 j\omega c_1\mathbf{2}\boldsymbol{\omega_1}}{k_2 J_1\mathbf{2}\boldsymbol{\omega_1}} - \frac{\omega^2 c_1^2\mathbf{2}\boldsymbol{\omega_1}}{k_2 J_1\mathbf{2}\boldsymbol{\omega_1}} = \psi^2\mu\omega_1^2 + 4\psi^2\mu j\omega\omega_1\xi_1 - \frac{2\xi c_1\omega^2}{k_2} \tag{3.52}$$

$$= \psi^2\mu\omega_1^2 + 4\psi^2\mu j\omega\omega_1\xi_1 - 4\xi_1^2\omega^2\mu\psi^2 \tag{3.53}$$

Finally, equation 3.37 can be written as:

$$\frac{\frac{\Phi_{2_1}}{M_{v_1}}}{k_2} = \frac{-\omega^2 + 2\xi_1\omega_1 j\omega + {\omega_1}^2}{(-\omega^2 + 2j\omega\xi_1\omega_1 + \omega_1^2)(-\Omega^2 + 2j\Omega\mu\xi_1\psi + \psi^2\mu + 2j\Omega\xi_2 + 1) - \psi^2\mu\omega_1^2 - 4\psi^2\mu j\omega\omega_1\xi_1 + 4\xi_1^2\omega^2\mu\psi^2} \tag{3.54}$$

If, the numerator and denominator of equation 3.54 are divided by ω_2, the expression can be reduced as:

$$\frac{\frac{\Phi_{2_1}}{M_{v_1}}}{k_2} = \frac{-\Omega^2 + 2j\xi_1\Omega\psi + \psi^2}{(-\Omega^2 + 2j\Omega\xi_1\psi + \psi^2)(-\Omega^2 + 2j\Omega\mu\xi_1\psi + \psi^2\mu + 2j\Omega\xi_2 + 1) - \psi^4\mu - 4\psi^2\mu j\Omega\xi_1\psi + 4\xi_1^2\Omega^2\mu\psi^2} \tag{3.55}$$

By identification, $\frac{\frac{\Phi_{2_2}}{M_e}}{k_2}$ can easily be found:

$$\frac{\frac{\Phi_{2_2}}{M_e}}{k_2} = \frac{2j\xi_1\Omega\psi + \psi^2}{(-\Omega^2 + 2j\Omega\xi_1\psi + \psi^2)(-\Omega^2 + 2j\Omega\mu\xi_1\psi + \psi^2\mu + 2j\Omega\xi_2 + 1) - \psi^4\mu - 4\psi^2\mu j\Omega\xi_1\psi + 4\xi_1^2\Omega^2\mu\psi^2} \tag{3.56}$$

Finally, introducing equation 3.55 and 3.56 into equation 3.34, the following expression can be obtained:

$$\Phi_2[\,] = \Phi_{2_1}[\,] + \Phi_{2_2}[\,]$$

$$= \frac{-\Omega^2 + 4j\xi_1\Omega + 2\psi^2}{(-\Omega^2 + 2j\Omega\xi_1\psi + \psi^2)(-\Omega^2 + 2j\Omega\mu\xi_1\psi + \psi^2\mu + 2j\Omega\xi_2 + 1) - \psi^4\mu - 4\psi^2\mu j\Omega\xi_1\psi + 4\xi_1^2\Omega^2\mu\psi^2} \tag{3.57}$$

This equation 3.57 represents the response Φ_2 of the secondary flywheel.
An example is applied to Equation 3.57 with the initial values included in Table 3.5. The attentive reader can see that they are the same values used in the section 3.6. Figure 3.25 shows the plot of this example. The two eigenfrequencies can be refounded: two peaks occur at each eigenfrequencies.

Parameters	Values
k_1	20000 [Nm/rad]
k_2	11000 [Nm/rad]
c_1	30 [Nm.s/rad]
c_2	1 [Nm.s/rad]
J_1	1.8 [kg.m^2]
J_2	0.6 [kg.m^2]

Table 3.5 – Values used for the example

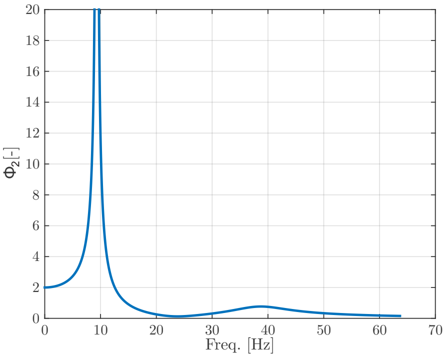

Figure 3.25 – Frequency response of the secondary flywheel.

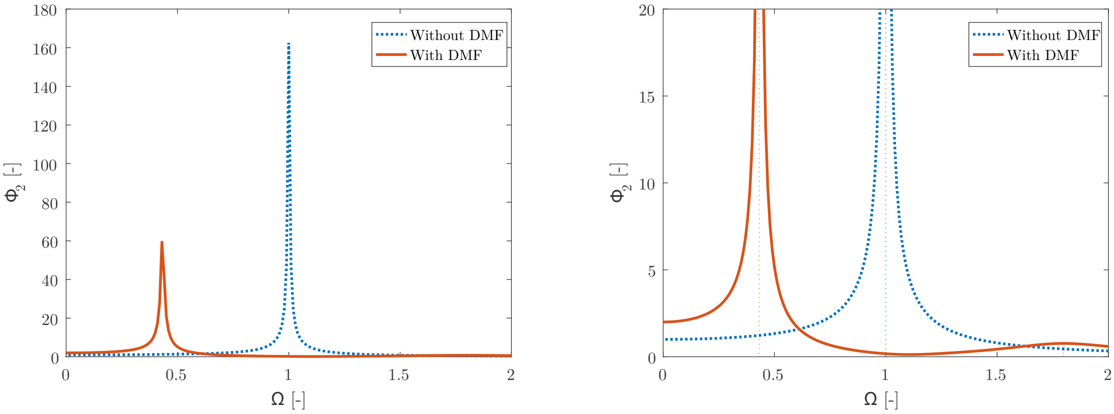

Figure 3.26 – Impact of the Dual Mass flywheel (normal and large scale).

It is also interesting to show the impact of the DMF on the frequency response. Without the Dual Mass flywheel, the engineering model is composed of one inertia and one spring and damper between the single flywheel and the gearbox which represent the property of the output shaft. This model is shown at Figure 3.27.
Figure 3.26 shows the impact of the DMF: with the single flywheel only one peak occurs while the DMF creates two resonance peaks on both sides of the initial peak (in our case, they have a lower amplitude).

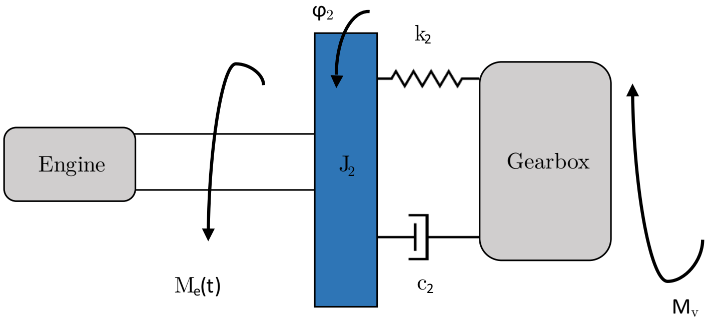

Figure 3.27 – Single Mass flywheel

3.7.3.1 Sensitivity analysis on the response of the secondary flywheel

This part analyses the sensitivity of the dimensionless parameters. The response of the secondary flywheel depends only on the following parameters:

- Ω, ξ_1, ξ_2, μ, ψ

Three different cases are choosing to show their influence on the frequency response:

- Initial values, the values from the tables 3.5 are replaced in the different dimensionless parameters.
- Maximum values, the maximum of the dimensionless parameters are taken by choosing the parameters of the tables 3.5 multiplied or divided by 0.5 with the aim of having a maximum value of the dimensionless parameters.
- Minimum values, the minimum of the dimensionless parameters are taken by choosing the parameters of the tables 3.5 multiplied or divided by 0.5 with the aim of having a minimum value of the dimensionless parameters.

According to Figure 3.28 we can conclude that:

- The increase of the inertia ratio μ moves the peaks towards smaller Ω values.
- The increase of ψ will significantly increase the amplitude frequency response, φ_2.
- The damping factors ξ_1 and ξ_2 have the same impact on the response of the secondary flywheel, when they increase the peaks are decreased. But ξ_1 has a higher impact than the second damping factor.

Actually, we have a contradiction between the previous conclusions. In fact, we saw that increasing the damping coefficient is beneficial for the frequency response amplitude. Whereas previously, the optimization reduced the damping coefficient. In fact, the damping coefficients have no effect when the eigenfrequencies are far from the frequency excitation. But the system has to go through low frequencies to reach high frequencies. Therefore it is important to reduce as well as possible the peaks at low frequencies.

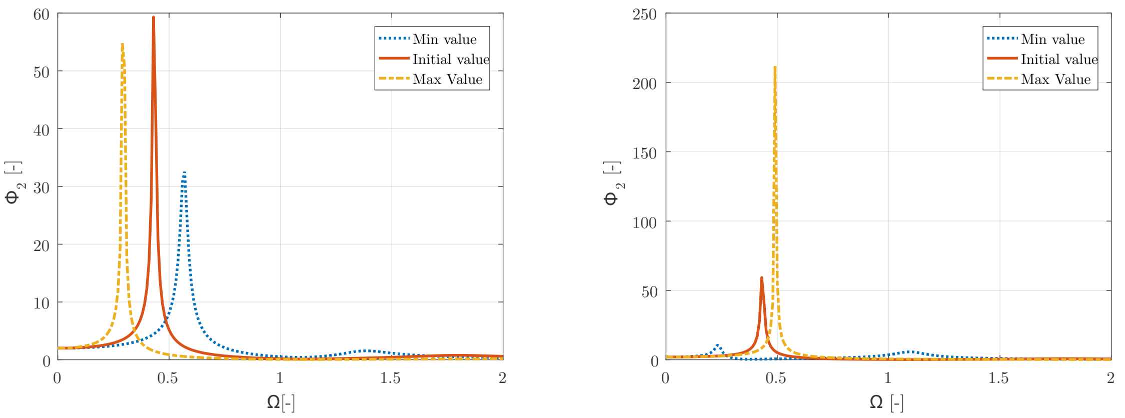

(a) Influence of μ.

(b) Influence of ψ

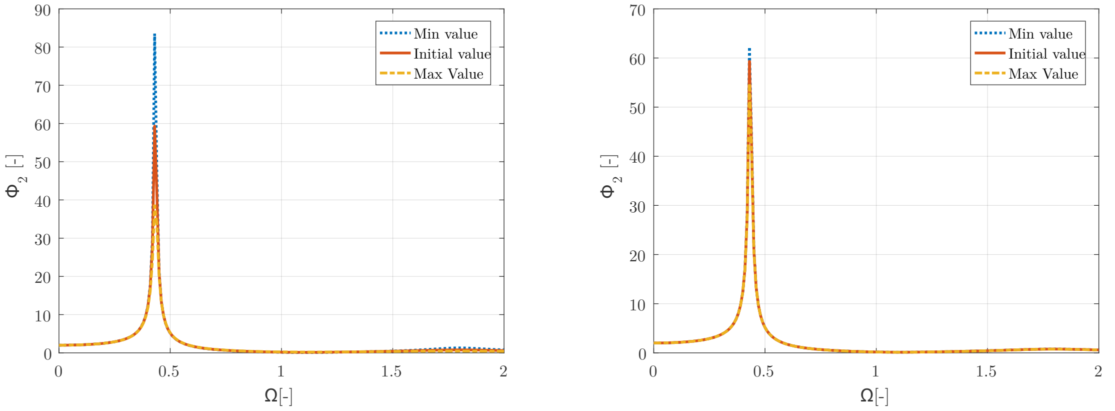

(c) Influence of ξ_1

(d) Influence of ξ_2

Figure 3.28 – Influence of the dimensionless parameters on the response of the secondary flywheel

3.7.3.2 Optimization of the dimensionless expression

The optimization uses another way, $fmincon$ is not used anymore.
The objective functions OF3 and OF4 depend only on the following parameters:

- Ω, ξ_1, ξ_2, μ, ψ

The frequency response depends only on these five parameters. It is necessary to constrain different parameters.
According to the paper [25], the inertia ratio μ is imposed to 3 and the secondary damping factor, ξ_2, is assumed as equal to 0.0062.
ψ and ξ_1 were varied from 0 to 1 and 0 to 2, respectively (increment of 0.01). Ω is varied from 0 to 2. A plot of the frequency response can be obtained for the increment of each ψ and ξ_1.
The maximum of the peaks (OF3) and the area under each curve (OF4) are recorded. The variation of OF3 and OF4 according to ψ and ξ_1 can be obtained on Figure 3.29 and 3.30, respectively.
The minimum value of each plot can be calculated, an optimal value of ψ and ξ_1 is therefore obtained for OF3 and OF4.

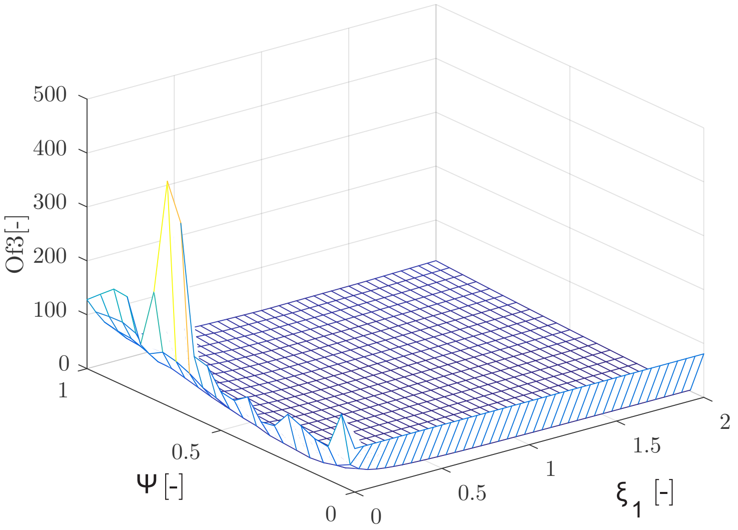

Figure 3.29 – Influence of ψ and ξ_1 on OF3

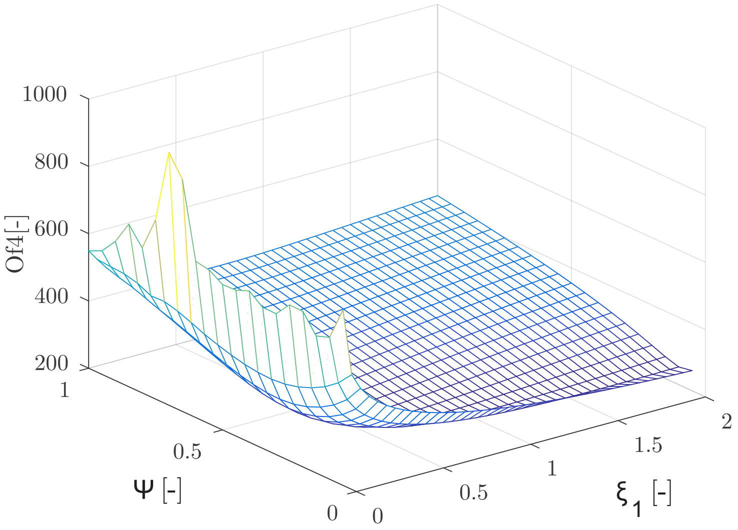

Figure 3.30 – Influence of ψ and ξ_1 on OF4

For the optimization of OF3, the following values are obtained:

- $\xi_{1opt_{OF3}} = 2$
- $\psi_{opt_{OF3}} = 0.05$

For the optimization of OF4, the following values are obtained:

- $\xi_{1opt_{OF4}} = 0.6$
- $\psi_{opt_{OF4}} = 0.25$

If these optimized values are introduced into Equation 3.57, the benefits of the optimization can be observed. Figure 3.31 demonstrates the good effect: the peak and the area of the frequency response are well reduced.

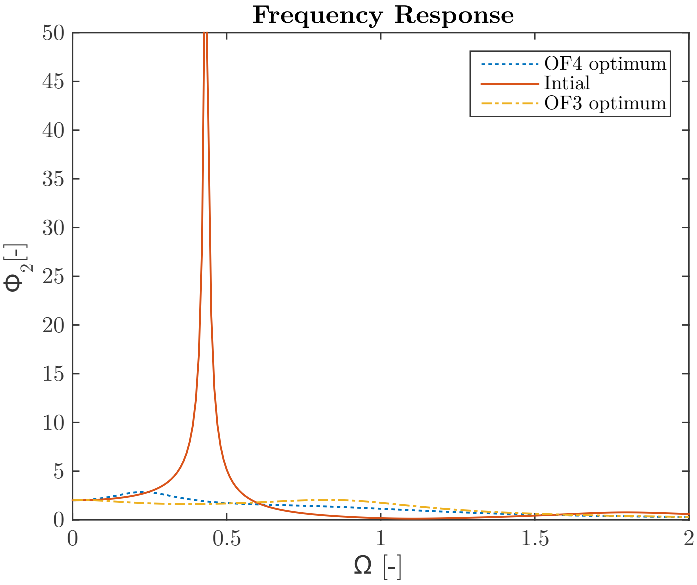

Figure 3.31 – Frequency response with optimal values deduced from OF3 and OF4 optimization.

4

Engine Dynamics

Until now, a simple sine function has been used to represent the input torque. But in reality, the input torque has a more complex expression. This part will study the engine dynamics to deduce its expression and show its impact on the output response.

4.1 Assumptions

In this chapter we will assume that :

- The engine is running at constant speed
- The crankshaft is rigid
- The inertias of the conrod and the crank are neglected
- The friction forces are neglected

4.2 Piston motions

The position of the piston can be described by $x = x_1 + x_2$.

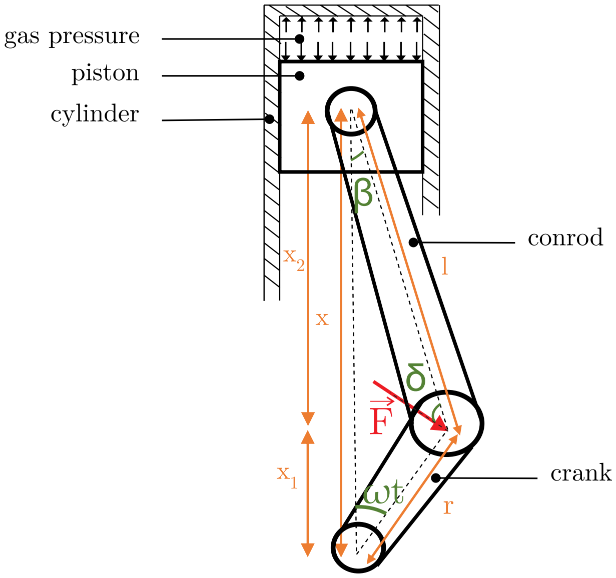

Figure 4.1 – Silder-crank mechanism

Where $x_1 = r \times cos(\omega t)$
Moreover, $x_2^2 + (r \times sin(\omega t))^2 = l^2$ by Pythagoras.
That means that $x_2 = \sqrt{l^2 - (r \times sin(\omega t))^2}$.
Finally, the expression of the position of the piston can be deduced:

$$x = r \times cos(\omega t) + l\sqrt{1 - \frac{r^2}{l^2} \times sin^2(\omega t)} \tag{4.1}$$

If the Taylor expansion of $\sqrt{1-x}$ is used, the second term of the right-hand side of this equation becomes:

$$l\sqrt{1 - \frac{r^2}{l^2} \times sin^2(\omega t)} = l\left(1 + \frac{1}{2} \times (-\frac{r^2}{l^2} \times sin^2(\omega t))\right) \tag{4.2}$$

Using the Simpson formulas $sin^2(\omega t) = \dfrac{1 - cos(2\omega t)}{2}$, the expression of x becomes:

$$x = r \times cos(\omega t) + l \times \left(1 + \frac{1}{2}\frac{-r^2}{l^2}\frac{1 - cos(2\omega t)}{2}\right) \tag{4.3}$$

$$x = r \times \left(cos(\omega t) + \frac{r}{4l}cos(2\omega t)\right) + l - \frac{r^2}{4l} \tag{4.4}$$

Assuming that ω is constant, we can obtain the following expression for the velocity and acceleration of the piston.

$$\dot{x} = -r\omega\left(sin(\omega t) + \frac{r}{2l}sin(2\omega t)\right) \tag{4.5}$$

$$\ddot{x} = -r\omega^2\left(cos(\omega t) + \frac{r}{l}cos(2\omega t)\right) \tag{4.6}$$

4.3 Forces acting on the piston

Four forces action on the piston can be enumerated:

1. The inertia force: $F_{inertia} = m\ddot{x}$
2. The force due the gas pressure: $F_{gas} = \frac{1}{4}\pi D^2 \times p_{cyl}$
   - with D, the bore diameter
   - with p_{cyl}, the pressure inside the cylinder
3. The friction force: $F_{friction}$. In our case the friction force will be neglected.
4. The force from rod: F_{rod}.

Balance of forces in vertical direction:

$$F_{inertia} + F_{gas} + F_{friction} + F_{rod} \times cos(\beta) = 0 \tag{4.7}$$

$$F_{rod} = \frac{1}{cos(\beta)}\left(-m\ddot{x} - \frac{1}{4}\pi D^2 p_{cyl} - F_{friction}\right) \tag{4.8}$$

Torque acting on the crankshaft is given by Torque $= r \times F$.

$$F = cos(\delta) \times F_{rod} = \frac{cos(\delta)}{cos(\beta)}\left(-m\ddot{x} - \frac{1}{4}\pi D^2 p_{cyl} - F_{friction}\right) \tag{4.9}$$

where:

- $\delta = 180 - 90 - \omega t - \beta = 90 - \omega t - \beta$
- $\beta = arcsin(\frac{r}{l}sin(\omega t))$

Knowing that $lsin(\beta) = asin(\omega t)$, the following expression can be deduced:

$$Torque = r \times (A \times B) \tag{4.10}$$

Where:

- A = $\dfrac{cos\left(90 - (\omega t) - arcsin\dfrac{sin(\omega t)}{R}\right)}{cos\left(arcsin(\frac{asin(\omega t)}{l})\right)}$
- B = $\left(0.25\pi D^2 p_{cyl} - m \times r \times \omega^2 \left[cos(\omega t) + \frac{1}{R}cos2(\omega t)\right]\right)$

Assuming that R is the rod ratio which is equal to: $\dfrac{l}{r}$.
The previous equation becomes for 6-cylinder engine:

$$Torque = r \times \sum_{i=1}^{6}(A_i \times B_i) \tag{4.11}$$

Where:

- $A_i = \dfrac{cos\left(90 - (\omega t - \alpha_i) - arcsin\dfrac{sin(\omega t - \alpha_i)}{R}\right)}{cos\left(arcsin(\frac{asin(\omega t - \alpha_i)}{l})\right)}$
- $B_i = \left(0.25\pi D^2 p_{cyl} - m \times r \times \omega^2 \left[cos(\omega t - \alpha_i) + \frac{1}{R}cos2(\omega t - \alpha_i)\right]\right)$

  Where α_i is the phase angle,
  - α_1= 0 °
  - α_2= 120 °
  - α_3= 240 °
  - α_4= 360 °
  - α_5= 480 °
  - α_6= 600 °

In fact the crankshaft of a 4-stroke engine has to turn through 720° to complete a 4-stroke cycle. Considering that a 6-cylinder engine is analysed, the phase angle between each force is given by 720/6.
Some characteristics of a Volvo truck engine have been obtained, they are placed in Table 4.1. Moreover, the evolution of the pressure with the crank angle is necessary. The cylinder pressure as a function of crankangle has been assumed to have the shape shwon in Figure 4.2.

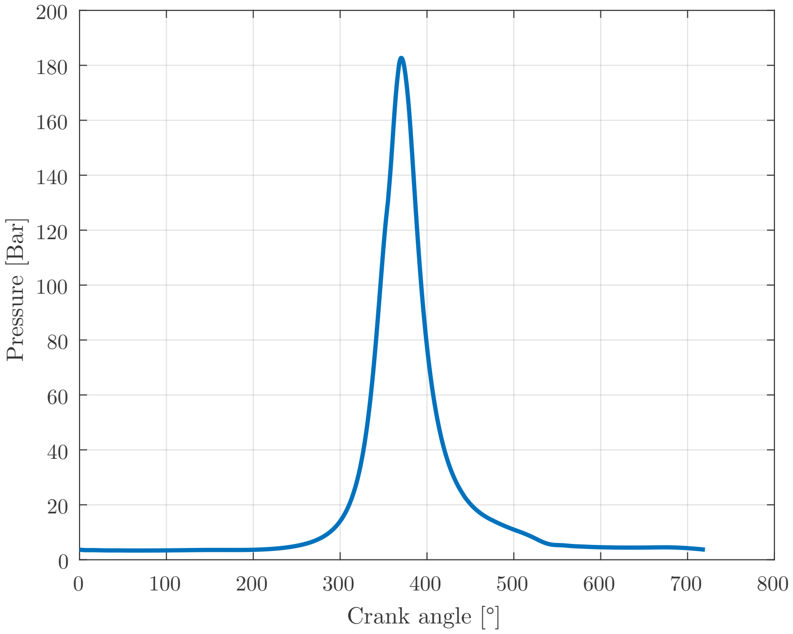

Figure 4.2 – Crank angle evolution of the pressure inside a cylinder

Characteristics	Values
Diameter of the bore	130 mm
Length of the crank	80 mm
Length of the conrod	270 mm
Weight of the piston assembly	5 kg

Table 4.1 – Main characteristics of the piston

Equation 4.3 is plotted on Figure 4.3 for 3 different scenario. This figure also compares the different contributions of the torque.

- Torque from the gas pressure
- Torque from the inertia

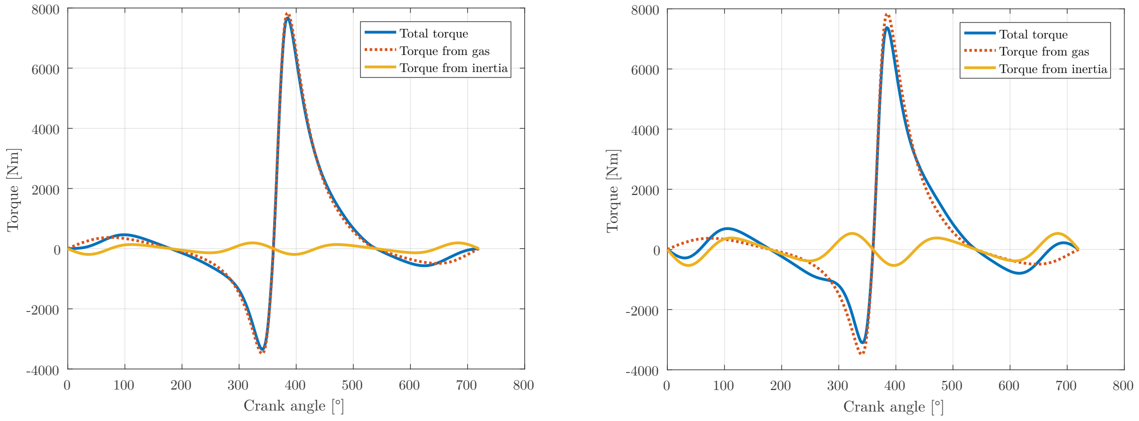

(a) 900 RPM. (b) 1500 RPM.

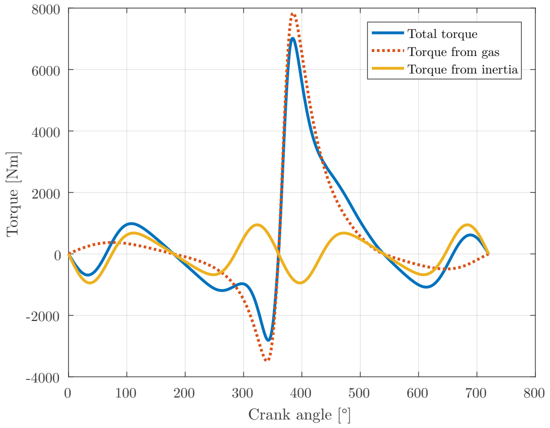

(c) 2000 RPM.

Figure 4.3 – Crank angle history of the torque for 3 different scenarios.

Regarding to Figure 4.3 we can observe that the main contribution of the engine torque comes from the gas torque but increasing the input velocity will increase the contribution of the inertia torque.

Figure 4.4 shows the crank angle history of the torque for a 6-cylinder engine for the first scenario. Six peaks can be observed. They correspond to the power of each cylinder.

The behaviour of the dynamic output responses of the system with a more accurate expression of the engine torque is analysed. The initial and optimized values of the design parameters obtained in the previous chapter have been used. A comparison of the dynamics responses for the initial and optimized case have been realized. Results for the engine speed of 900 RPM are plotted from Figure 4.5 to 4.7. For the engine speed of 1500 and 2000 RPM, the reader may refer to Appendix F.

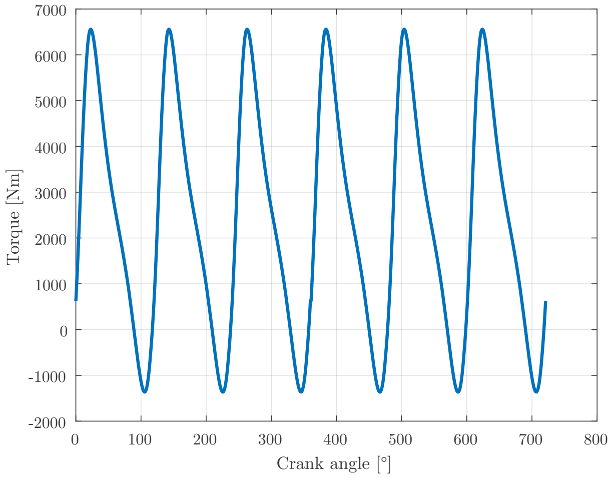

Figure 4.4 – Torque produce by a 6-cylinder engine.

First of all, we can see that the shape of the curves is very similar to the shape of the curves obtained in the previous chapter at subsection 3.6.1. Same conclusions can be deduced from these figure. Actually, the optimization reduces all the fluctuations:

- from the deflection angle (and its time derivative) between the flywheels
- from the deflection angle (and its time derivative) between the secondary flywheel and the gearbox side
- from the gearbox input torque

The average of the deflection angle between the flywheels for the optimization case is different from the one of the initial case. We also observe this difference for the deflection angle between the secondary flywheel and the gearbox side. There is still a phase shift between the initial and optimized case.

For this first scenario we can thus observe that a more accurate expression of the engine torque does not add much information in our model. In fact, even if the engine torque is not exactly a sine function the output response looks like a simple sine function.

However, the shape of the curve of the time history of the time derivative deflection angle between the secondary flywheel and the gearbox side for the second and third scenario looks different.

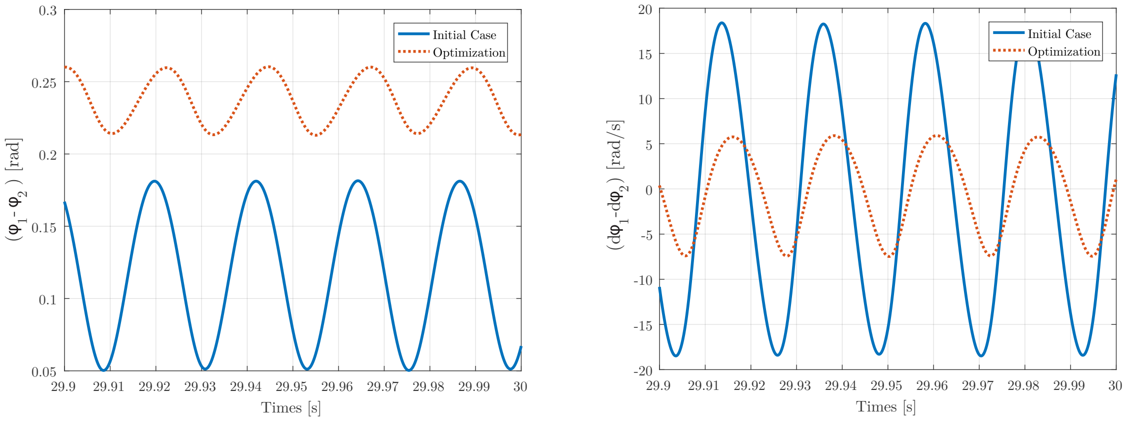

(a) Time history of $(\varphi_1 - \varphi_2)$.

(b) Time history of $(\dot{\varphi}_1 - \dot{\varphi}_2)$.

Figure 4.5 – Time history of the deflection angle and its time derivative between the flywheels.

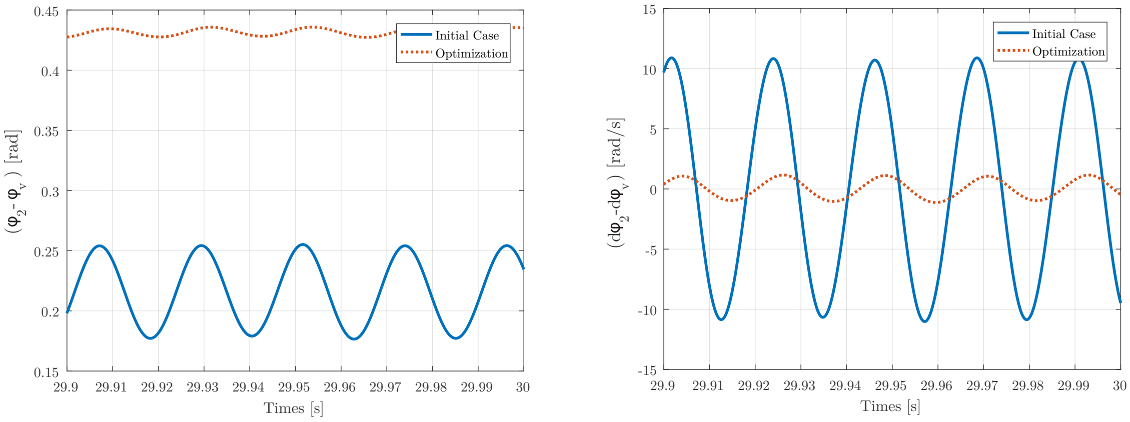

(a) Time history of $(\varphi_2 - \varphi_v)$.

(b) Time history of $(\dot{\varphi}_2 - \dot{\varphi}_v)$.

Figure 4.6 – Time history of the deflection angle and its time derivative between the primary flywheel and the gearbox.

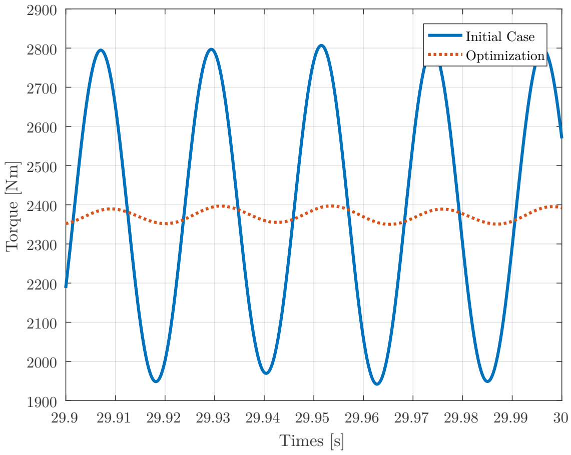

Figure 4.7 – Time history of the gearbox input torque.

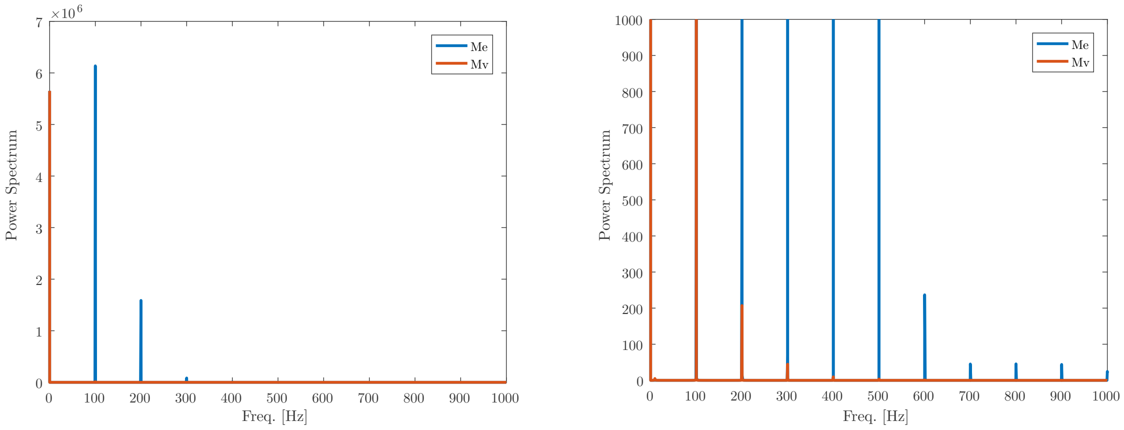

(a) Normal scale.

(b) Large scale.

Figure 4.8 – DFT diagram comparing the engine and the gearbox input torque.

To assure that we have a similarity between the engine torque and the gearbox input torque a representation of vibration has been done with the help of DFT.
The use of the power spectrum (PS) is chosen given that a periodic signal is used. The power spectrum corresponds to twice the squared magnitude of the Fourier series coefficients versus frequencies. In fact, the most suitable spectral representation for periodic signals in terms of signal power is the power spectrum. The interested reader can find more details on this reference [20]. The DFT diagram in Figure 4.8 compares the engine torque and gearbox input torque for the 1500 RPM scenario. Figure 4.8 shows the link between the engine torque and gearbox input torque. In fact each peak of the gearbox input torque corresponds to a peak of the engine torque. Note that, a new peak for the gearbox input torque appears at very low frequencies which probably due to the fact that the steady state was not totally reached. To avoid this effect a longer simulation time should be used but this time could be very long which causes a longer calculation time. Regarding Figure 4.8, the magnitude of the other peaks are reduced significantly. This DFT analysis allows to assure the similarity of between the engine and gearbox input torque.

Conclusion and Future Work

One solution to reduce **torsional vibration** is the Dual Mass flywheel.
A simplified model of a Dual Mass flywheel has been developed in **Matlab** and in the open-source software **EasyDyn**. Both models give **similar** results. Three different engine scenarios (900, 1500 and 2000 RPM) have been chosen for the analysis.

A distinction between the frequency and temporal domains has also been done:

- **Time domain**:
  Two objective functions (OFs) have been defined with the aim of having better damping properties at the crankshaft output. In fact, in the best case, the vibration induced by the engine should be cancelled at the output of the DMF.
  The first OF is OF1 which estimates the gearbox input **torque fluctuations**.
  With the first objective function optimization, good results can be obtained: the torque fluctuation is reduced to 5% of the initial case.
  The secondary OF is OF2 and estimates the **power losses**.
- **Frequency domain**:
  Two objective functions have been proposed in order to estimate the peak amplitude of the secondary flywheel response .
  OF3, the third OF of our study, will calculate the maximum of the **peaks**.
  A fourth OF, OF4 will calculate the **area** under the curve of the amplitude response of the secondary flywheel.

The optimization for the different OFs return the same results. Decreasing stiffness and increasing the moment of inertia improve the output response. Finally we can also conclude that increasing the damping reduce the peaks of the eigenfrequencies which benefits the output behaviour.

The use of a simplified input torque (sinusoidal) is enough to understand the dynamic output response. Nevertheless the differences observed at higher speed (1500 and 2000 RPM), highlight the importance of including **more realistic input torque expression**.

Some suggestions for future work:

- Extend this model to a full powertrain model
- Validation of the model by comparison of measured data
- Study the fatigue life of the components
- Take into consideration the non-linearity effects

Bibliography

[1] Mein-Autolexikon. `http://www.mein-autolexikon.de`. Accessed: 2016-05-13.

[2] Volvo truck. `http://www.volvotrucks.com`. Accessed: 2016-05-13.

[3] Daniel Lorenz, Thomas Weigand, and Tobias Höche. Torsional vibration damping arrangement with power splitting, September 23 2013. US Patent App. 14/438,535.

[4] Schaeffler Automotive Aftermarket. Dual mass flywheel : Technology/failure diagnosis, special tool/user instructions. Technical report, 2013.

[5] Hermann Pflaum Georg Johann Meingaßner and Karsten Stahl. Innovative torsional vibration reduction devices - vehicle-related design and component strength analysis. Technical report, SAE International, 2014.

[6] Guangming Zhao, Zhengfeng Jiang, and Lei Chen. Linear analysis for performance of dual mass flywheel with centrifugal pendulum vibration absorbers system. TELKOMNIKA Indonesian Journal of Electrical Engineering, 11(5):2371–2376, 2013.

[7] W.S. Oh, H.S. Lee, Y.W. Jin, and J.W. Hwang. Apparatus for damping of flywheel.

[8] CDX Automotive. Fundamentals of Automotive Technology. Jones & Bartlett Learning, 2013.

[9] Zf friedrichshafen ag. `http://zf.com`. Accessed: 2016-05-13.

[10] DQ Truong and KK Ahn. MR fluid damper and its application to force sensorless damping control system. INTECH Open Access Publisher, 2012.

[11] Charles Hill. Guidelines for preventing torsional vibration problems in reciprocating machinery. 2002.

[12] Ing Hartmut Faust. Powertrain systems of the future. In Engine, transmission and damper systems for downspeeding, downsizing and cylinder deactivation. Schaeffler Symposium Book (Steinhagen: Schaeffler Technologies GmbH & Co., 2014), pages 25–41, 2014.

[13] Alan G Haddow and Steven W Shaw. Centrifugal pendulum vibration absorbers: An experimental and theoretical investigation. Nonlinear Dynamics, 34(3-4):293–307, 2003.

[14] Anoop Surynarayana. Engine dynamics and torsion vibration reduction. Master's thesis, Chalmers University of Technology, 2015.

[15] Yulan Sun, Marc Thomas, and Jacques Masounave. Amortissement des vibrations de torsion de rotors à l'aide de fluides électro-rhéologiques.

[16] Dirk Güth, Markus Schamoni, and Jürgen Maas. Energy-efficient mrf clutch avoiding no-load losses. In SPIE Smart Structures and Materials+

Nondestructive Evaluation and Health Monitoring, pages 86881D–86881D. International Society for Optics and Photonics, 2013.

[17] Ehab Abouobaia, Rama Bhat, and Ramin Sedaghati. Development of a new torsional vibration damper incorporating conventional centrifugal pendulum absorber and magnetorheological damper. Journal of Intelligent Material Systems and Structures, page 1045389X15590275, 2015.

[18] RA Shannan. Torsional vibration damper selection–high-powered performance boat engine. Orbit, pages 12–17, 1997.

[19] Seyed Mohammad Shojaalsadati. Torsional Vibration Attenuation in V-Type Locomotive Diesel Engine Crankshaft using Centrifugal Pendulum Absorber. PhD thesis, Concordia University, 2014.

[20] Techniques in vibration engineering. Prof. Dr. Ir. Georges Kouroussis, Mutuelle d'édition de la FPMs.

[21] BHJ Dynamics INC. Crankshaft torsion and dampers. Technical report.

[22] Structural Dynamics Control, Second edition. Prof. Dr. Ir. Viktor Berbyuk, Department of Applied Mechanics, Chalmers University of Technology, 2014.

[23] Matlab. `http://www.mathworks.com`. Accessed: 2016-05-13.

[24] EasyDyn. `http://hosting.umons.ac.be/html/mecara/EasyDyn/index.html`. Accessed: 2016-05-13.

[25] Payam Bighal. High efficiency heavy duty truck engine. 2012.

[26] Jeffrey C Lagarias, James A Reeds, Margaret H Wright, and Paul E Wright. Convergence properties of the nelder–mead simplex method in low dimensions. SIAM Journal on optimization, 9(1):112–147, 1998.

[27] Matlab fminsearch description. `http://nl.mathworks.com/help/matlab/ref/fminsearch.html`. Accessed: 2016-05-13.

A

Dimensional analysis Φ_1 case

The same procedure is applied to Φ_1

$$\frac{\Phi_{1_1}}{\frac{M_e}{k_2}} = \frac{(-J_2\omega^2 + j\omega c_1 + k_1 + j\omega c_2 + k_2)}{(-J_1\omega^2 + c_1 j\omega + k_1)(-\frac{J_2}{k_2}\omega^2 + j\omega\frac{c_1}{k_2} + \frac{k_1}{k_2} + j\omega\frac{c_2}{k_2} + \frac{k_2}{k_2}) - \frac{(k_1 + j\omega c_1)^2}{k_2}} \tag{A.1}$$

Equation A.1 has the same denominator as Equation 3.37. The flowing equations will focus on the numerator (N) of Equation A.1, if the numerator and denominator are divided by J_1, the numerator can be written as:

$$N = \frac{-J_2\omega}{J_1} + \frac{k_2}{\boldsymbol{J_1}} + \frac{\boldsymbol{c_2} j\omega}{J_1} + \frac{k_1}{J_1} + \frac{j\omega c_1}{J_1} = -\frac{\omega^2}{\mu} + \frac{\omega_2^2 J_2 \boldsymbol{\xi_1 2\omega_1}}{\boldsymbol{c_1}} + \frac{\boldsymbol{J_2\xi_2 2\omega_2} j\omega}{J_1} + \omega_1^2 + \frac{j\omega c_1 \boldsymbol{2\omega_1}}{J_1 \boldsymbol{2\omega_1}}$$

$$= -\frac{\omega^2}{\mu} + \frac{\omega_2^2\xi_1^2}{\mu} + \frac{\xi_2 2\omega_2 j\omega}{\mu} + \omega_1^2 + j\omega\xi_1 2\omega_1 \tag{A.2}$$

As done for Φ_2, the expression will be divided by ω_2^2. In this case, the previous equation becomes:

$$N = -\frac{\Omega^2}{\mu} + \frac{\xi_1^2}{\mu} + + \frac{2\xi_2\Omega}{\mu} + \psi^2 + 2j\Omega\xi_1\psi \tag{A.3}$$

Equation A.1 can thus be reduced as:

$$\frac{\Phi_{1_1}}{\frac{M_e}{k_2}} = \frac{\frac{\Omega^2}{\mu} + \frac{\xi_1^2}{\mu} + + \frac{2\xi_2\Omega}{\mu} + \psi^2 + 2j\Omega\xi_1\psi}{(-\Omega^2 + j\Omega\xi_1 + \xi^2)(-\Omega^2 + 2j\Omega\mu\xi_1 + \psi^2\mu + 2j\Omega\xi_2 + 1) - \psi^4\mu - 4\psi^2\mu j\Omega\xi_1 + 4\xi_1^2\Omega^2\mu} \tag{A.4}$$

Φ_{1_2} can be found by identification to Equation 3.32:

$$\frac{\Phi_{1_2}}{\frac{M_{output_1}}{k_2}} = \frac{2j\xi_1\Omega\psi + \psi^2}{(-\Omega^2 + j\Omega\xi_1 + \xi^2)(-\Omega^2 + 2j\Omega\mu\xi_1 + \psi^2\mu + 2j\Omega\xi_2 + 1) - \psi^4\mu - 4\psi^2\mu j\Omega\xi_1 + 4\xi_1^2\Omega^2\mu} \tag{A.5}$$

Finally, the dimensionless equation of Φ_1 can be obtained:

$$\Phi_1[\,] = \Phi_{1_1}[\,] + \Phi_{1_2}[\,]$$

$$= \frac{\frac{\Omega^2}{\mu} + \frac{\xi_1^2}{\mu} + \frac{2\xi_2\Omega}{\mu} + 2\psi^2 + 4j\Omega\xi_1\psi}{(-\Omega^2 + j\Omega\xi_1 + \xi^2)(-\Omega^2 + 2j\Omega\mu\xi_1 + \psi^2\mu + 2j\Omega\xi_2 + 1) - \psi^4\mu - 4\psi^2\mu j\Omega\xi_1 + 4\xi_1^2\Omega^2\mu} \tag{A.6}$$

B

Design parameters in dimensionless space

J_1, J_2, k_1, k_2, c_1, c_1 are called design parameters. As these parameters are dimensional, that requires to decide the magnitude of the different element of the system. It is interesting to have a mathematical model in dimensionless form in order to have a more general model.
The chosen dimensionless parameters are ξ_1, ξ_1, μ :

$$\omega_1 = \sqrt{\frac{k_1}{J_1}} \quad \text{and} \quad \omega_2 = \sqrt{\frac{k_2}{J_2}} \tag{B.1}$$

$$\xi_1 = \frac{c_1}{2J_1\omega_1} \quad \text{and} \quad \xi_2 = \frac{c_2}{2J_2\omega_2} \tag{B.2}$$

$$\mu = \frac{J_1}{J_2} \tag{B.3}$$

Equation 3.1 can be written as:

$$\ddot{\varphi}_1 + 2\xi_1\omega_1(\dot{\varphi}_1 - \dot{\varphi}_2) + \omega_1^2(\varphi_1 - \varphi_2) = \frac{M_e(t)}{J_1} \tag{B.4}$$

In the same way Equation 3.2 can be written as:

$$\ddot{\varphi}_2 + \mu 2\xi_1\omega_1(\dot{\varphi}_2 - \dot{\varphi}_1) + \mu\omega_1^2(\varphi_2 - \varphi_1) + 2\xi_2\omega_2(\dot{\varphi}_2 - \dot{\varphi}_v) + \omega_2^2(\varphi_2 - \varphi_v) = 0 \tag{B.5}$$

A matrix form can again be obtained:

$$\begin{bmatrix} 1 & 0 \\ 0 & 1 \end{bmatrix} \begin{pmatrix} \ddot{\phi}_1 \\ \ddot{\phi}_2 \end{pmatrix} + \begin{bmatrix} 2\xi_1\omega_1 & -2\xi_1\omega_1 \\ -2\xi_1\omega_1\mu & 2\xi_1\omega_1\mu + 2\xi_2\omega_2 \end{bmatrix} \begin{pmatrix} \dot{\phi}_1 \\ \dot{\phi}_2 \end{pmatrix} + \begin{bmatrix} \omega_1^2 & -\omega_1^2 \\ -\omega_1^2\mu & \omega_1^2\mu + \omega_2^2 \end{bmatrix} \begin{pmatrix} \phi_1 \\ \phi_2 \end{pmatrix} = \begin{pmatrix} \frac{M_e(t)}{J_1} \\ \omega_2^2\varphi_v + 2\xi_2\omega_2\dot{\varphi}_v \end{pmatrix} \tag{B.6}$$

$$\begin{bmatrix} M \end{bmatrix} \begin{pmatrix} \ddot{\phi}_1 \\ \ddot{\phi}_2 \end{pmatrix} + \begin{bmatrix} C \end{bmatrix} \begin{pmatrix} \dot{\phi}_1 \\ \dot{\phi}_2 \end{pmatrix} + \begin{bmatrix} K \end{bmatrix} \begin{pmatrix} \phi_1 \\ \phi_2 \end{pmatrix} = \begin{pmatrix} \frac{M_e(t)}{J_1} \\ \omega_2^2\varphi_v + 2\xi_2\omega_2\dot{\varphi}_v \end{pmatrix} \tag{B.7}$$

with :
M , the inertia matrix;
C , the damping matrix;
K , the stiffness matrix.

C

Matlab code

C.1 Integration file

C.1.1 Main

```
clear all
close all
clc
%%%%%%%%%%%%%%%%%%%%%%%%
%%%   Global Values  %%%
%%%%%%%%%%%%%%%%%%%%%%%%
global A
global C
global K
global B
global M
global xi_2
global omega_2
global J1
global c2
global k2

%%%%%%%%%%%%%%%%%%%%%%%%
%%% Time parameters  %%%
%%%%%%%%%%%%%%%%%%%%%%%%
t_end=150;
space=1000001;
t=linspace(0,t_end,space);
%%%%%%%%%%%%%%%%%%%%%%%%%
OF_index=round(0.5*space):space; % specify the beginning of the measurement of the Objectives functions

%%%%%%%%%%%%%%%%%%%%%%%%%%
%%% Engine parameters  %%%
%%%%%%%%%%%%%%%%%%%%%%%%%%

M_0=300;
M_1=500;
w_1=100*2*pi;
phi_1=0;
M_e=@(t) (M_0+M_1*sin(w_1*t+phi_1));
```

```matlab
%%%%%%%%%%%%%%%%%%%%%%%%%
%%% Load parameters  %%%
%%%%%%%%%%%%%%%%%%%%%%%%%

w_2=w_1/3;
phiV=@(t) w_2*t;
d_phiV= w_2;

%%%%%%%%%%%%%%%%%%%%%%%%%%%%%%%%%%%
%%%%  Choice of the study      %%%%
%%%%%%%%%%%%%%%%%%%%%%%%%%%%%%%%%%%

choice=1;  % 1 = Dimension Space   2 = Dimension less Space

%%%%%%%%%%%%%%%%%%%%%%%%%%%%%%%%%%%%%%%%%%%%%%%%%%%%%
%%%%%%%%%%%%%%%%%%%%%%%%%%%%%%%%%%%%%%%%%%%%%%%%%%%%%
if choice==1
%Dimension space


%Parameters
k1=2e4;% N.m/rad
J1=1.8;%Kg.m^2
k2=1.1e4;% N.m/rad
J2=0.6;%Kg.m^2
c1=30;%N.m/(rad/s)
c2=20;%N.m/(rad/s)
% To enter en vector :
% x=[2.69999999998828 0.899999999994571 10000.0000002360
   5500.00000001733 15.0000000005116 0.885053281818175]
% J1=x(1);
% J2=x(2);
% k1=x(3);
% k2=x(4);
% c1=x(5);
% c2=x(6);
% Definition of the intertia, damping and  stiffness matrix
M=[J1 0;
    0 J2];
C=[c1 -c1;
    -c1 c1+c2];
K=[k1 -k1;
    -k1 k1+k2];
end

%%%%%%%%%%%%%%%%%%%%%%%%%%%%%%%%%%%%%%%%%%%%%%%%%%%%%%%%%%
%%%%%%%%%%%%%%%%%%%%%%%%%%%%%%%%%%%%%%%%%%%%%%%%%%%%%%%%%%
if choice==2
% Dimension less space

%Parameters
xi_1=0.079057;%c1/(2*J1*omega_1);%0.2 ; %c1/(2*J1*omega_1);%
xi_2=0.006155;%c2/(2*J2*omega_2);%;%0.3;%c2/(2*J2*omega_2);%
omega_1=105.4093;%sqrt(k1/J1);%0.0137;%sqrt(k1/J1);%0.5; %sqrt(k1/J1);%
omega_2=135.40;%sqrt(k2/J2);%0.0484;%sqrt(k2/J2);%0.3; %sqrt(k2/J2);%
mu=3;%5.3598;%0.0102;%J1/J2;%0.05;%J1/J2;%
```

```
J1=1.8;

% Definition of the intertia, damping and  Stiffness matrix
 M=[1 0;
    0 1];
 C=[2*xi_1*omega_1 -2*xi_1*omega_1;
    -2*xi_1*omega_1*mu 2*xi_1*omega_1*mu+2*xi_2*omega_2];
 K=[omega_1^2 -omega_1^2;
     -omega_1^2*mu omega_1^2*mu+omega_2^2];
end
%%%%%%%%%%%%%%%%%%%%%%%%%%%%%%%%%%%%%%%%%%%%%%%%%%%%%%%%%%

%%%%%%%%%%%%%%%%%%%%%%%%%%%%%%%%%%%%%%%%%%%%%%%%%%%%%%%%%
%%%%  Rewrite the second order differential equations  %%
%%%%  into a first order  differential equations       %%
%%%%%%%%%%%%%%%%%%%%%%%%%%%%%%%%%%%%%%%%%%%%%%%%%%%%%%%%%
A= [zeros(2) eye(2);
    -M\K -M\C];
B= [zeros(2); M^(-1)];

%%%%%%%%%%%%%%%%%%%%%%%%%%%%%%%%%%%
%%%%  Integration with ODE45   %%%%
%%%%%%%%%%%%%%%%%%%%%%%%%%%%%%%%%%%
% Specify tolerance
options = odeset ( 'Abstol ' ,1e-6, 'Reltol ' ,1e-6) ;
% Start of integration with ODE45
[t,X] = ode45(@(t,y) funoptim(t,y,choice,M_e,phiV,d_phiV),t,[0;0;d_phiV
   ;d_phiV],options);

% With X :
% X(:,1) = phi1
% X(:,2) = phi2
% X(:,3) = dphi1
% X(:,4) = dphi2

%%%%%%%%%%%%%%%%%%%%%%%%%%%%%%%%%%%%%%%%%%
%%%%  To have the acceleration values %%%%
%%%%%%%%%%%%%%%%%%%%%%%%%%%%%%%%%%%%%%%%%%

  for i = 1:length(t)
    tmp =  fun(t(i),X(i,:)',choice,M_e,phiV,d_phiV);
    acc(i,:) = tmp(3:4);
  end
%%%%%%%%%%%%%%%%%%%%%%%%%%%%%%%%%%%%%%%%%%%%%
%%%%  Calculation of the vehicle torque  %%%%
%%%%%%%%%%%%%%%%%%%%%%%%%%%%%%%%%%%%%%%%%%%%%
for i=1:length(t)
if choice==1
Mv1(i)=c2*(X(i,4)-d_phiV);
Mv2(i)=k2*(X(i,2)-phiV(t(i)));
end
if choice==2
Mv1(i)=2*xi_2*omega_2*J1/mu*(X(i,4)-d_phiV);
Mv2(i)=omega_2^2*J1/mu*(X(i,2)-phiV(t(i)));
end
Mv(i)=Mv1(i)+Mv2(i);
```

```
%%%%%%%%%%%%%%%%%%%%%%%%%%%%%%%%%%%%%%%%%%%%%
%%%%        Calculation of power         %%%%
%%%%%%%%%%%%%%%%%%%%%%%%%%%%%%%%%%%%%%%%%%%%%
power_a(i)=(M_e(t(i))*X(i,3));
power_b(i)=(Mv(i)*d_phiV);
vec_Me(i)=M_e(t(i));
vec_phiV(i)=phiV(t(i));
dphiV(i)=w_2;
relativepower_a(i)=M_e(t(i))*(X(i,4)-X(i,3));
relativepower_b(i)=Mv(i)*(dphiV(i)-X(i,4));
end

%%%%%%%%%%%%%%%%%%%%%%%%%%%%%%%%%%%%%%%%%%%%%%%%%%%%%%%%
%%%%%%   Objective Function 1  Torque variation   %%%%%%
%%%%%%%%%%%%%%%%%%%%%%%%%%%%%%%%%%%%%%%%%%%%%%%%%%%%%%%%
%Old function
% Mv_average=mean(Mv);
% for i=1:length(t)
%       Mv_temp(i)=Mv(i)-Mv_average;
% end
%       Mv_squared= Mv_temp.*Mv_temp;
%       OF1= sqrt(1/t_end*(trapz(Mv_squared)));
% OF1  ( Standard deviation )
OF1=std(Mv(OF_index));
%%%%%%%%%%%%%%%%%%%%%%%%%%%%%%%%%%%%%%%%%%%%%%%%%%%%%%%%
%%%%%%      Objective Function 2  Losses         %%%%%%
%%%%%%%%%%%%%%%%%%%%%%%%%%%%%%%%%%%%%%%%%%%%%%%%%%%%%%%%
%%% Calculation of the dissipations due to the damping
if choice==1
OF2=mean(1/2*c1*(X(OF_index,4)-X(OF_index,3)).^2+1/2*c2*(X(OF_index,4)-
   d_phiV).^2);
end
if choice==2
OF2= mean(J1/mu*mu*xi_1*omega_1*(X(OF_index,4)-X(OF_index,3)).^2+J1/mu*
   xi_2*omega_2*(X(OF_index,4)-dphiV').^2);
end


%%%%%%%%%%%%%%%%%%%%%%%%%%%%%%%%%%%%%%%%%%%%%%%%%%%%%%%%%%%%%%%%%%%%%%%
%%%%%      Objective Function:   Losses + torque Fluctuations     %%%%%
%%%%%%%%%%%%%%%%%%%%%%%%%%%%%%%%%%%%%%%%%%%%%%%%%%%%%%%%%%%%%%%%%%%%%%%
% Choice of a coefficient alpha
alpha=0.5;
OF=alpha*OF1+(1-alpha)*OF2;
```

C.1.2 Function used

```
function dy = funoptim(t,y,choice,M_e,phiV,d_phiV)
%syms omega_1 omega_2 xi_1 xi_2 mu
global A;
global B;
global xi_2;
global omega_2;
global J1;
global c2
global k2

% Definition of the force vector
if choice==1
F=[M_e(t); c2*d_phiV+k2*phiV(t)];
end
if choice==2
F=[M_e(t)/J1; 2*xi_2*omega_2*d_phiV+omega_2^2*phiV(t)];
end

%%% First order differential equations system
dy=A*y+B*F;
```

C.2 Optimization file

C.2.1 Main file

```
clear all
close all
clc %clear out old variables


OFchoice=2;%1 = OF1   %2 =  OF2
iteration=0;
tic
for frequency= 0:1:100
    iteration= iteration+1;
xopt1(iteration,:)=fminsearchbnd(@(x) OFdimension(x,OFchoice,frequency)
    ,[1.8,0.6,2e4,1.1e4,30,1],[0.9,0.3,1e4,5500,15,0.5],[2.7,0.9,3e4
    ,16500,45,1.5]);
end
toc
```

C.2.2 Function used

```
function optimization= OFdimension(x,Optimization_choice,frequency)

%%%%%%%%%%%%%%%%%%%%%%%%
global A
global B

J1=x(1);
J2=x(2);
k1=x(3);
k2=x(4);
c1=x(5);
c2=x(6);


%%%%%%%%%%%%%%%%%%%%%%%%
```

```
%%% Time parameters  %%%
%%%%%%%%%%%%%%%%%%%%%%%%
t_end=30;
space=30001;
t=linspace(0,t_end,space);
%%%%%%%%%%%%%%%%%%%%%%%%%
OF_index=round(0.9*space):space;

%%%%%%%%%%%%%%%%%%%%%%%%%%
%%% Engine parameters  %%%
%%%%%%%%%%%%%%%%%%%%%%%%%%

M_0=300;
M_1=500;
w_1=frequency*2*pi;

phi_1=0;
M_e=@(t) (M_0+M_1*sin(w_1*t+phi_1));
%%%%%%%%%%%%%%%%%%%%%%%%%
%%% Load parameters  %%%
%%%%%%%%%%%%%%%%%%%%%%%%%

%%%% Variation of the load

w_2=w_1/3;
phiV=@(t) w_2*t;
d_phiV= w_2;

%%%%%%%%%%%%%%%%%%%%
% Definition of the intertia, damping and  Stiffness matrix
M=[J1 0;
    0 J2];
C=[c1 -c1;
    -c1 c1+c2];
K=[k1 -k1;
    -k1 k1+k2];

%%%%%%%%%%%%%%%%%%%%%%%%%%%%%%%%%%%%%%%%%%%%%%%%%%%%%%%%%
%%%%%%%%%%%%%%%%%%%%%%%%%%%%%%%%%%%%%%%%%%%%%%%%%%%%%%%%%
%%%%  Rewrite the second order differential equations  %%
%%%%  into a first order  differential equations       %%
%%%%%%%%%%%%%%%%%%%%%%%%%%%%%%%%%%%%%%%%%%%%%%%%%%%%%%%%%
A= [zeros(2) eye(2);
    -M\K -M\C];
B= [zeros(2); M^(-1)];

%%%%%%%%%%%%%%%%%%%%%%%%%%%%%%%%%%%
%%%%  Integration with ODE45   %%%%
%%%%%%%%%%%%%%%%%%%%%%%%%%%%%%%%%%%
options = odeset ( 'Abstol ' ,1e-6, 'Reltol ' ,1e-6) ;
[t,X] = ode45(@(t,y) funOFdimension(t,y,M_e,phiV,d_phiV,c2,k2),t,[0;0;
   d_phiV;d_phiV],options);

% With X :
% X(:,1) = phi1
% X(:,2) = phi2
% X(:,3) = dphi1
% X(:,4) = dphi2



% %%%%%%%%%% Vehicle torque + Losses calculation
%%%%%%%%%%%%%%%%%%%%%%%%%%%%%%%%%%%%%%%%%%%%%
%%%%  Calculation of the vehicle torque  %%%%
%%%%%%%%%%%%%%%%%%%%%%%%%%%%%%%%%%%%%%%%%%%%%

for i=1:length(t)
Mv1(i)=c2*(X(i,4)-d_phiV);
Mv2(i)=k2*(X(i,2)-phiV(t(i)));
Mv(i)=Mv1(i)+Mv2(i);
vec_Me(i)=M_e(t(i));
vec_phiV(i)=phiV(t(i));
dphiV(i)=w_2;
end

%%%%%%%%%%%%%%%%%%%%%%%%%%%%%%%%%%%%%%%%%%%%%%%%%%%%%%%%
%%%%%%   Objective Function 1  Torque variation   %%%%%%
%%%%%%%%%%%%%%%%%%%%%%%%%%%%%%%%%%%%%%%%%%%%%%%%%%%%%%%%
% Calculation of OF1 for each value of the parameter

if Optimization_choice==1
optimization=std(Mv(OF_index))
end
Optimization_choice=2;
%%%%%%%%%%%%%%%%%%%%%%%%%%%%%%%%%%%%%%%%%%%%%%%%%%%%%%%%
%%%%%%       Objective Function 2  Losses         %%%%%%
%%%%%%%%%%%%%%%%%%%%%%%%%%%%%%%%%%%%%%%%%%%%%%%%%%%%%%%%
% Calculation of OF2 for each value of the parameter
if Optimization_choice==2
optimization=mean(1/2*c1*(X(OF_index,4)-X(OF_index,3)).^2+1/2*c2*(X(
    OF_index,4)-d_phiV).^2)
end
```

C.3 Real Torque expression

```
clear all
close all
clc

%pressure
crankangledegree=load('crankangle.mat');
pressurebar=load('pressure.mat');

PressureCrankangle(:,1)=pressurebar.pressure;
PressureCrankangle(:,2)=crankangledegree.crankangle;

Pressurecrankangle2(:,1)=pressurebar.pressure(1:end-1);
Pressurecrankangle2(:,2)=crankangledegree.crankangle(1:end-1);
Longpressurecrankangle = repmat(Pressurecrankangle2,2,1);
```

```
%Bore
Bore=130*10^-3;%82*10^-3;%130*10^-3;%m
%Weight of piston assembly
m=5;%0.75;%5;%kg
%Crank
a=80*10^-3;%46.6*10^-3; %80*10^-3;%m
%Conrod
l=270*10^-3;%m
%Rod ratio
R=l/a;%3.15;%l/a;%
%l=a*R;
RPM=1500;
f=RPM/60;
omega=f*2*pi;

friction=0;
z=0;
phi=[0 120 240 360 480 600];
for theta=0:1:720
z=z+1;
vec(z)=theta;
Torque6cylinder=0;
for i=1:6
beta=asin(a/l*sin(degtorad(theta+phi(i))));
delta=degtorad(90-(theta+phi(i))-radtodeg(beta));
acceleration=a*omega^2*(cos(degtorad(theta+phi(i)))+a/l*cos(2*degtorad(
    theta+phi(i)))-(a/l)^3*cos(4*degtorad(theta+phi(i))));
pressure=Longpressurecrankangle(1+theta+phi(i),1)*10^5;
part1=1/4*pi*Bore^2*pressure;
part2=-m*acceleration;
part3=-friction;
Frod=1/cos(beta)*(part1+part2+part3);
F=cos(delta)*Frod;
Torque=a*F;

Torque6cylinder = Torque6cylinder + Torque;

end
Torquereal(z)=Torque6cylinder;
end


repeat=1000;
Torquelongtime = repmat(Torquereal,1,repeat);
Thetalong=0:length(Torquelongtime)-1;
plot(Thetalong,Torquelongtime,'LineWidth',2)
xlabel('Crank angle [degree]')
    ylabel('Torque [Nm]')
     grid on


mean(Torquelongtime)

vectortime=Thetalong*60/(RPM*360);
for i=1:length(vectortime)-1
dt(i)= vectortime(i+1)-vectortime(i);
```

```
end
```

D

EasyDyn model

D.1 General data of the studied mechanism

The system comprises 2 bodies (defined by the global variable `nbrbody`). Each body is called S_j (j from 0 to 1). The number of degrees of freedom of the system is 2 (`nbrdof`). The configuration parameters are denoted by q_i (i from 0 to 1).

The inertial data, given by the user, consist of the inertia tensor $\Phi_{G,Si}$ of each body i expressed with respect to the center of gravity.

$$\Phi_{G,S0} = \begin{pmatrix} 1.79985 & 0 & 0 \\ 0 & 0.899925 & 0 \\ 0 & 0 & 0.899925 \end{pmatrix} \quad \text{, in } kg.m^2$$

$$\Phi_{G,S1} = \begin{pmatrix} 0.59995 & 0 & 0 \\ 0 & 0.299975 & 0 \\ 0 & 0 & 0.299975 \end{pmatrix} \quad \text{, in } kg.m^2$$

D.2 Complete kinematics calculed by CAGeM

The following parameters have been calculated from the user's file `DMF.mu` and with a CPU time of 0 second.

Homogeneous transformation matrix of each body

$$T_{0G,S0} = \begin{pmatrix} 1 & 0 & 0 & 0 \\ 0 & \cos(q_0) & -\sin(q_0) & 0 \\ 0 & \sin(q_0) & \cos(q_0) & 0 \\ 0 & 0 & 0 & 1 \end{pmatrix}$$

$$T_{0G,S1} = \begin{pmatrix} 1 & 0 & 0 & 0.05 \\ 0 & \cos(q_1) & -\sin(q_1) & 0 \\ 0 & \sin(q_1) & \cos(q_1) & 0 \\ 0 & 0 & 0 & 1 \end{pmatrix}$$

The time derivative of these matrices

$$\dot{T}_{0G,S0} = \begin{pmatrix} 0 & 0 & 0 & 0 \\ 0 & -\dot{q}_0 \sin(q_0) & -\dot{q}_0 \cos(q_0) & 0 \\ 0 & \dot{q}_0 \cos(q_0) & -\dot{q}_0 \sin(q_0) & 0 \\ 0 & 0 & 0 & 0 \end{pmatrix}$$

$$\dot{T}_{0G,S1} = \begin{pmatrix} 0 & 0 & 0 & 0 \\ 0 & -\dot{q}_1 \sin(q_1) & -\dot{q}_1 \cos(q_1) & 0 \\ 0 & \dot{q}_1 \cos(q_1) & -\dot{q}_1 \sin(q_1) & 0 \\ 0 & 0 & 0 & 0 \end{pmatrix}$$

The velocity of the center of gravity of each body

$$\vec{v}_{G,S0} = \begin{pmatrix} 0 \\ 0 \\ 0 \end{pmatrix}$$

$$\vec{v}_{G,S1} = \begin{pmatrix} 0 \\ 0 \\ 0 \end{pmatrix}$$

The acceleration of the center of gravity of each body

$$\vec{a}_{G,S0} = \begin{pmatrix} 0 \\ 0 \\ 0 \end{pmatrix}$$

$$\vec{a}_{G,S1} = \begin{pmatrix} 0 \\ 0 \\ 0 \end{pmatrix}$$

The rotation velocity of each body

$$\vec{\omega}_{S0} = \begin{pmatrix} \dot{q}_0 \\ 0 \\ 0 \end{pmatrix}$$

$$\vec{\omega}_{S1} = \begin{pmatrix} \dot{q}_1 \\ 0 \\ 0 \end{pmatrix}$$

The rotation acceleration of each body

$$\dot{\vec{\omega}}_{S0} = \begin{pmatrix} \ddot{q}_0 \\ 0 \\ 0 \end{pmatrix}$$

$$\dot{\vec{\omega}}_{S1} = \begin{pmatrix} \ddot{q}_1 \\ 0 \\ 0 \end{pmatrix}$$

D.3 Definition of external efforts

External efforts different from gravity have been defined in the file `DMF.AppEff.cpp`, automatically included in `DMF.cpp` (procedure `AddAppliedEfforts()`), and listed below

```
//constants
double k1=2e4, c1=30, k2=1.1e4, c2=1, ve=2*3.141592653589793*100, vv=ve/3 ;

//Torque
body[0].MG+=body[0].TOG.R.ux()*(300+500*sin(ve*t));
body[1].MG-=body[1].TOG.R.ux()*(c2*(qd[1]-vv)+k2*(q[1]-vv*t));

// Torsional spring
body[0].MG+=body[0].TOG.R.ux()*(-k1*(q[0]-q[1]));
body[1].MG-=body[1].TOG.R.ux()*(-k1*(q[0]-q[1]));

// Torsional damping
```

```
body[0].MG+=body[0].TOG.R.ux()*(-c1*(qd[0]-qd[1]));
body[1].MG-=body[1].TOG.R.ux()*(-c1*(qd[0]-qd[1]));
```

D.4 Simulation

The routine `NewmarkIntegration` performs the integration of the equations of motion up to time FinalTime by regular time intervals equal to StepSave and with the maximum allowed time step StepMax defined in the file `dp3.cpp`. The following values are used:

- FinalTime equal to 30 s,
- StepSave to 0.0001 s,
- StepMax to 0.0001 s.,

The initial conditions are $qd_0 = \frac{w_e}{3}$, $qd_1 = \frac{w_e}{3}$, the others being equal to zero. Where $w_e = 2\pi \times frequency$, $frequency$= 45,75 or 100 Hz depending of the scenario of study.

D.5 Visualization

An animation is available via EasyAnim. Figure D.1 represent a print screen of the visualization.

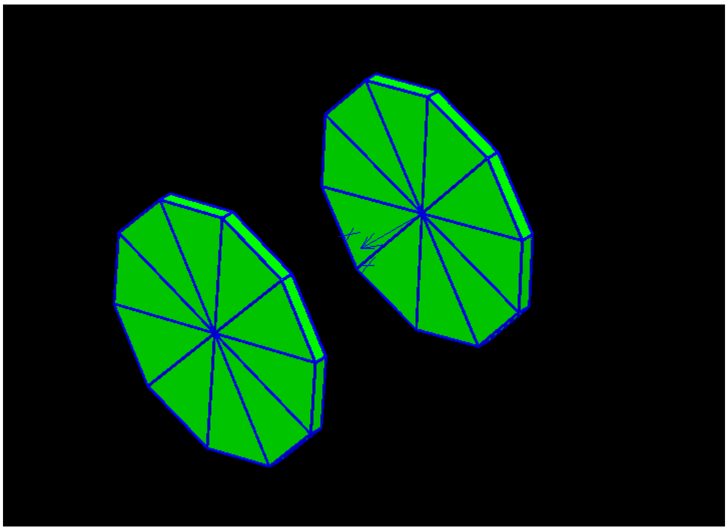

Figure D.1 – Visualization via EasyAnim

D.6 User's MuPAD code

```
//

// Copyright (C) 2003 Olivier VERLINDEN
//     Service de Mecanique rationnelle, Dynamique et Vibrations
//     Faculte Polytechnique de Mons
//     31, Bd Dolez, 7000 MONS (Belgium)
//     Olivier.Verlinden@fpms.ac.be

// This file is part of EasyDyn

// EasyDyn is free software; you can redistribute it and/or modify it
// under the terms of the GNU General Public License as published by the
// Free Software Foundation; either version 2, or (at your option) any
// later version.

// EasyDyn is distributed in the hope that it will be useful, but WITHOUT
// ANY WARRANTY; without even the implied warranty of MERCHANTABILITY or
// FITNESS FOR A PARTICULAR PURPOSE.  See the GNU General Public License
// for more details.

// You should have received a copy of the GNU General Public License
// along with EasyDyn; see the file COPYING.  If not, write to the Free
// Software Foundation, 59 Temple Place - Suite 330, Boston, MA  02111-1307, USA.
//
//                              FACULTE POLYTECHNIQUE DE MONS
//
//                service de Mecanique Rationnelle, Dynamique et Vibrations
//
//
//                     -----------------------------------------------
//                                 fichier utilisateur
//                              (ecrit en language MuPAD)
//
//
//                   Ir. Georges KOUROUSSIS - mars 2003
// Modification : Bourgois Geremy Juin 2016
//
//

// Title of the application
title:="Simulation of a Dual Mass Flywheel":

// Definition of nbrdof  : Number of degrees of freedom
//               nbrbody : Number of bodies
//               nbrcont : Number of constraints (unused in this version).
nbrdof:= 2:
nbrbody:= 2:

// Gravity vector
gravity[1]:=0:
gravity[2]:=0:
gravity[3]:=0:

// Eventual constants
r:=0.13:
l:=0.05:

// Inertia characteristics

mass[0]:=213:
```

```
mass[1]:=71:

Ixx[0]:=1/2*mass[0]*r^2:
Ixx[1]:=1/2*mass[1]*r^2:

Iyy[0]:=1/4*mass[0]*r^2:
Iyy[1]:=1/4*mass[1]*r^2:
Izz[0]:=1/4*mass[0]*r^2:
Izz[1]:=1/4*mass[1]*r^2:

// Definition of the position matrices

TOG[0]:=Trotx(q[0]):
TOG[1] := Trotx(q[1])*Tdisp(l,0,0):
// Initial conditions
qi[0]:=0:
qi[1]:=0:
qdi[0]:= vv:
qdi[1]:= vv:
// Simulation parameters
FinalTime:=10:
StepSave:=0.0001:
StepMax:=0.0001:

SIMPLIFY:=1:
// Set FORCES to 1 in case you want to include *.AppEff.cpp into procedure
// AddAppliedEfforts() to define forces other than gravity
FORCES:=1:
// Set ANIM to 1 in case you want CaGEM to generate the skeleton code
// for visualization and animation of the system
ANIM:=1:
// Set STATIC to 1 in case you want CaGEM to generate the code
// to search for static equilibrium before integration
STATIC:=0:
// Set PLOT to 1 in case you want CaGEM to generate the GNUPLOT code
// to plot the evolution of position, velocity and acceeration
PLOT:=1:
// SET LATEX_FR to 1 if you want the LaTeX report in French
LATEX_FR:=1:
// SET LATEX_EN to 1 if you want the LaTeX report in English
LATEX_EN:=1:
```

E

Optimization results

E.1 1500 RPM scenario

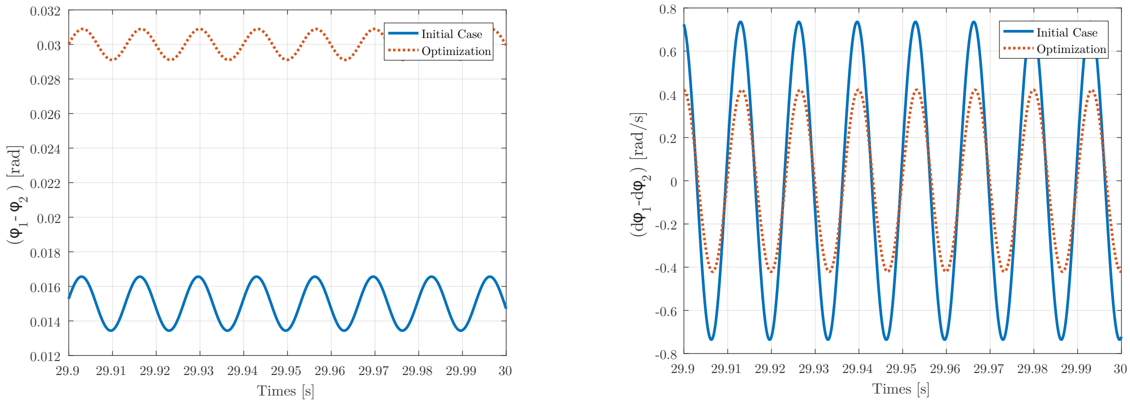

(a) $\varphi_1 - \varphi_2$ (b) $\dot{\varphi}_1 - \dot{\varphi}_2$

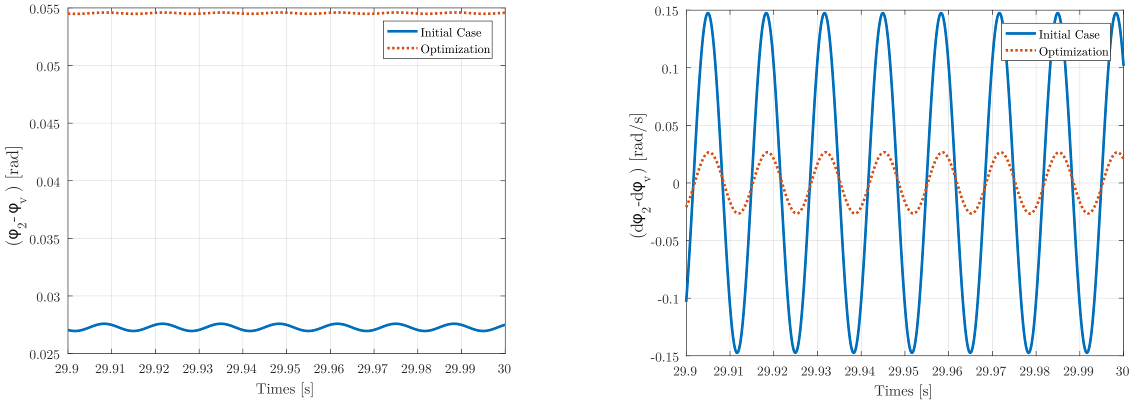

(c) $\varphi_2 - \varphi_v$ (d) $\dot{\varphi}_2 - \dot{\varphi}_v$

Figure E.1 – Benefits of the optimization on the different deflection angles and their time derivatives. (1500 RPM scenario)

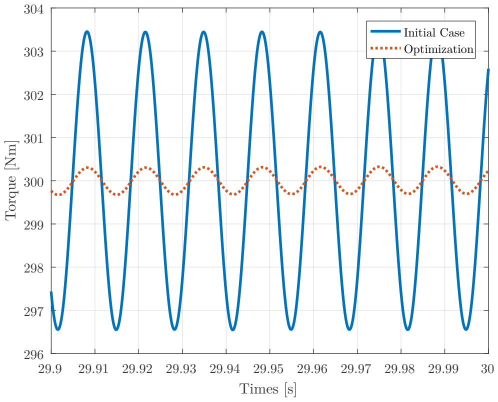

Figure E.2 – Benefits of the optimization of the output torque (1500 RPM scenario).

E.2 2000 RPM scenario

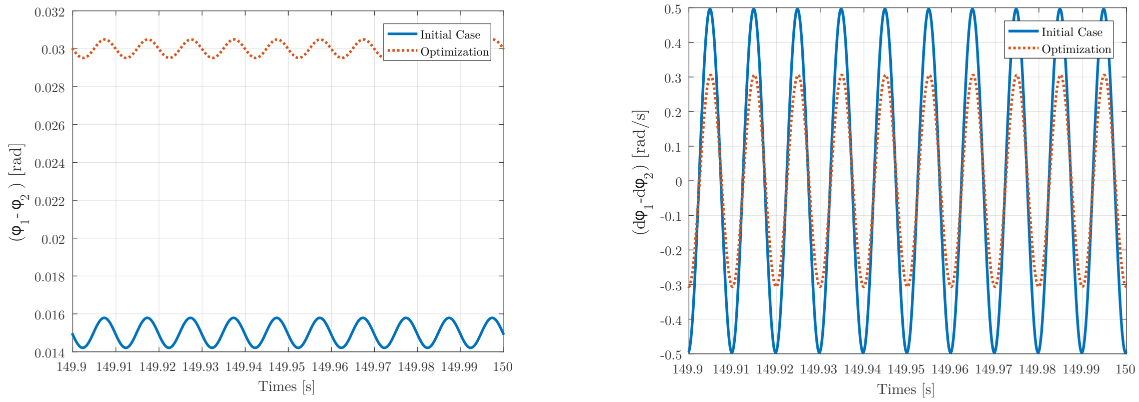

(a) $\varphi_1 - \varphi_2$

(b) $\dot{\varphi}_1 - \dot{\varphi}_2$

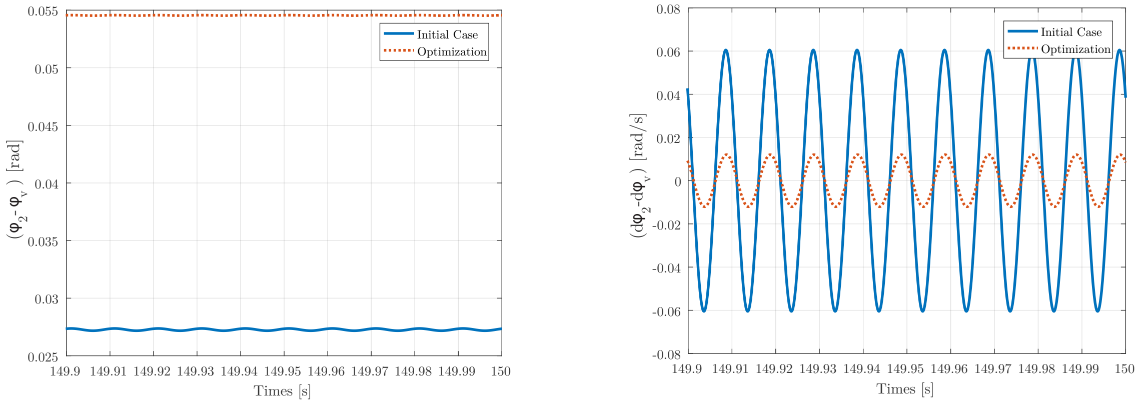

(c) $\varphi_2 - \varphi_v$

(d) $\dot{\varphi}_2 - \dot{\varphi}_v$

Figure E.3 – Benefits of the optimization on the different deflection angles and their time derivatives.(2000 RPM scenario)

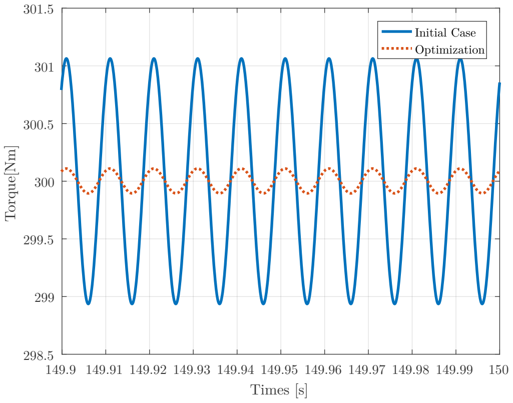

Figure E.4 – Benefits of the optimization of the output torque. (2000 RPM scenario)

F

Optimization results with a real expression of the Torque

F.1 1500 RPM scenario

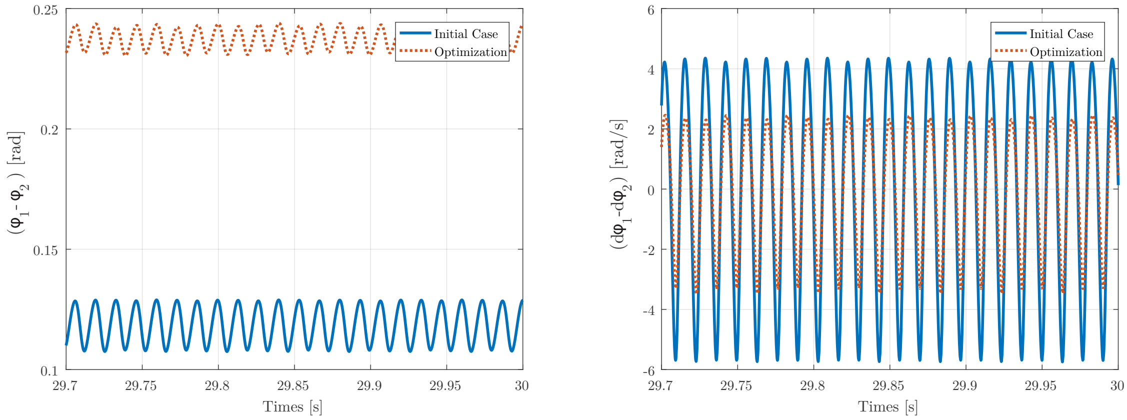

(a) Time history of $(\varphi_1 - \varphi_2)$.

(b) Time history of $(\dot{\varphi}_1 - \dot{\varphi}_2)$.

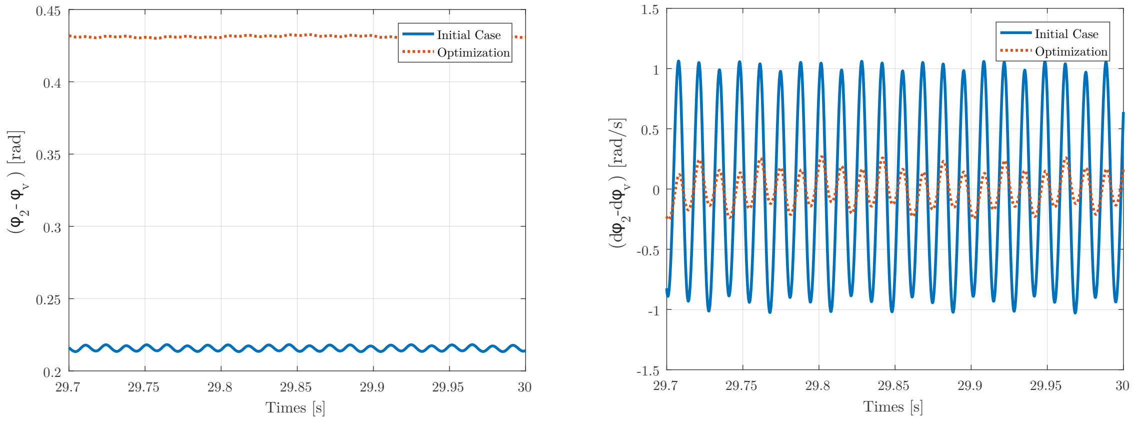

(c) Time history of $(\varphi_2 - \varphi_v)$.

(d) Time history of $(\dot{\varphi}_2 - \dot{\varphi}_v)$.

Figure F.1 – Benefits of the optimization on the different deflection angles and their time derivatives. (1500 RPM scenario)

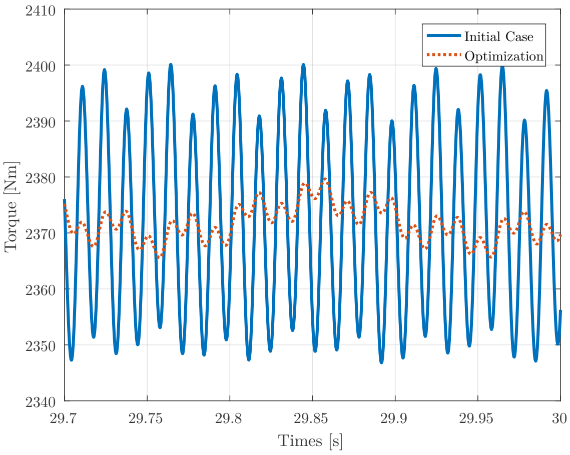

Figure F.2 – Benefits of the optimization of the output torque (1500 RPM scenario).

F.2 2000 RPM scenario

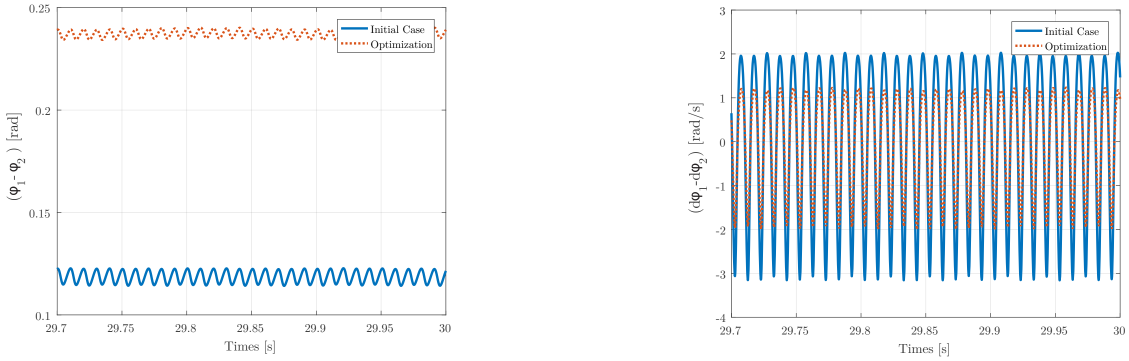

(a) Time history of $(\varphi_1 - \varphi_2)$.

(b) Time history of $(\dot{\varphi}_1 - \dot{\varphi}_2)$.

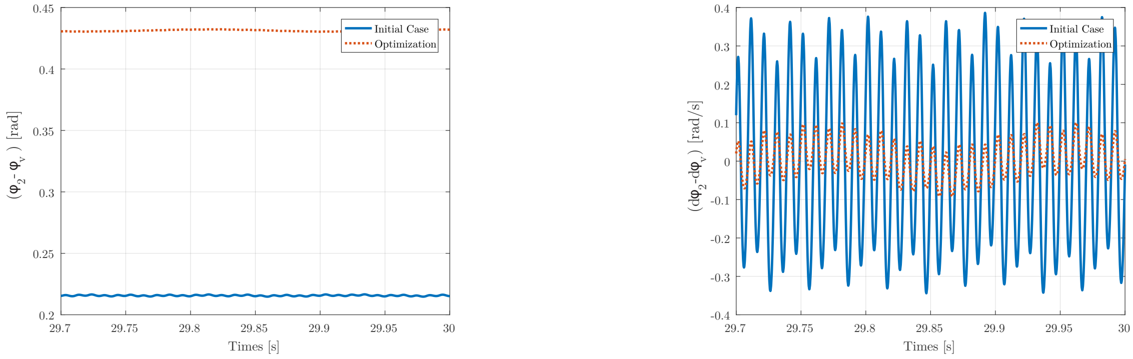

(c) Time history of $(\varphi_2 - \varphi_v)$.

(d) Time history of $(\dot{\varphi}_2 - \dot{\varphi}_v)$.

Figure F.3 – Benefits of the optimization on the different deflection angles and their time derivatives. (1500 RPM scenario)

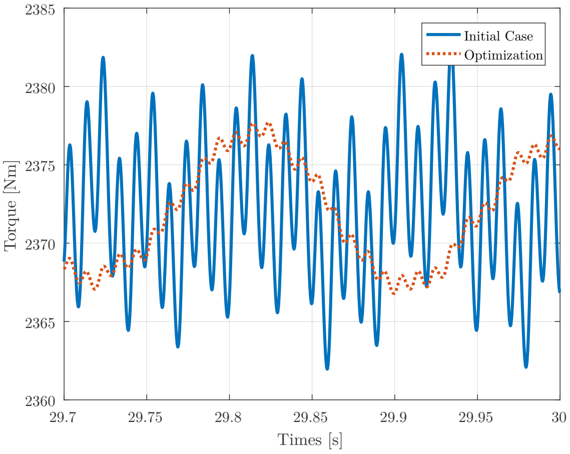

Figure F.4 – Benefits of the optimization of the output torque (20000 RPM scenario).